

A COMPARATIVE ANALYSIS BETWEEN RECYCLED CARBON FIBRE AND RANDOMLY ORIENTED GLASS FIBRE SANDWICH PANELS UNDER THREE-POINT AND IMPACT LOADING

By

Temitope Omisore

A thesis submission in partial fulfilment of the requirements of the University of Derby for the award of Master of Philosophy

College of Science and Engineering

April 2023

Acknowledgement

This thesis would not have come to completion without the kind support and encouragement from many individuals of whom I would like to extend my sincerest appreciation towards.

First and foremost, I would like to thank God almighty for giving me the inspiration and strength that was required to push through and complete my research.

I would like to express my heartfelt appreciation towards my family and particularly my parents for their constant encouragement and support. I also want to extend my appreciation towards my brothers for their well wishes towards my academic endeavour.

I also wish to express my many thanks to my programme leader Dr. Tahir Sharif and my project supervisor Dr. Rizwan Choudhry for their guidance, patience, thoughtful suggestions, and valuable feedback helping me keep on top of the project objectives.

Immeasurable thanks are extended towards the University of Derby for allowing me to do my Master of Philosophy degree at the university.

Lastly, I would like to thank my fellow colleagues from the composite's lab at the University of Derby, particularly Daniel Odiyi, Marzena Pawlik and Wong Yung Liang as their thoughtfulness, patience and kind words of encouragement helped me push forward in the project.

Abstract

The increased industrial use of fibre reinforced composites structures such as sandwich panels is a result of their lightweight, flexible, and high strength capabilities. Sandwich panels are generally assembled by placing a lightweight core in between two facesheets. The core provides the required thickness without increase in weight while the facesheets provide the required strength at less than half the cores thickness. Whilst the material choice for both vary, carbon and glass fibre reinforced polymers are predominantly the two main composite materials commonly utilised in the fabrication of sandwich panel facesheets. New developments in the application of fibre reinforced structures have raised an environmental and economic awareness for the necessity to recycle and repurpose fibre cut-off waste. The UK is the first major economy to pioneer a “green industrial revolution” by passing legislative laws, backed with funding, to bring industries such as the composite industry up to speed to achieve product sustainability and recyclability.

With focus in the composite industry shifting towards zero waste production cycles, it becomes a necessity to investigate the mechanical behaviour of fibre cut-off waste in structures such as sandwich panels. This thesis aims to contribute towards the issue by presenting an experimental comparison of sandwich panels fabricated using recycled carbon fibre (RCF) and chopped strand matt glass (CSMG). The experimental work undertaken are three-point bending and low-velocity impact. Across all industry that utilise sandwich panels, the two phenomena mentioned are observed to contribute significantly to panel degradation during its working life. For fair comparison, the sandwich panels for both fibres consist of the same areal density and same manufacturing methods.

Novelty in the thesis is granted through the comparative study between the mechanical behaviour of RCF and CSMG sandwich panels as this has not been investigated for industrial application. Obtained experimental data show that the RCF panels are stronger than the CSMG panels which could be an alternative to sandwich panels made with CSMG.

Table of Contents

1	INTRODUCTION	1-11
1.1	Research Background	1-11
1.2	Research Gap.....	1-13
1.3	Aim and Objectives.....	1-13
1.4	Thesis Layout	1-13
2	LITERATURE REVIEW	2-16
2.1	Fibre Reinforced Polymers	2-16
2.1.1	Carbon Fibre Reinforced Polymers.....	2-17
2.1.2	Recycled Carbon Fibre	2-18
2.1.3	Glass Fibre Reinforced Polymers.....	2-20
2.1.4	Chopped Strand Mat Glass Fibre.....	2-21
2.2	Sandwich Panels	2-23
2.3	Three-Point Bending on Sandwich Panels	2-25
2.4	Impact Damage of Sandwich Panels.....	2-29
2.5	Literature Summary and Gap.....	2-34
3	PANEL FABRICATION AND EXPERIMENTAL METHODS.....	3-37
3.1	Materials	3-37
3.2	Panel Fabrication.....	3-38
3.3	Experimental Methods	3-40
3.3.1	Fibre Content	3-42
3.3.2	Three-Point Bending Tests.....	3-44
3.3.3	Low-velocity Impact Tests.....	3-45
4	RESULTS AND ANALYSIS	4-49
4.1	Fibre Content.....	4-49
4.2	Three-point Bending Tests	4-50
4.2.1	RCF Panels.....	4-52
4.2.2	CSMG Panels	4-55

4.2.3	Comparative Summary	4-57
4.3	Impact Tests	4-59
4.3.1	Samples Tested at 10 J	4-59
4.3.2	Samples Tested at 20 J	4-63
4.3.3	Samples Tested at 30 J	4-67
4.3.4	Comparative Summary	4-72
4.4	Chapter Summary.....	4-74
5	GUIDELINE FOR FATIGUE AFTER IMPACT TEST	5-76
5.1	Impact Tests at 4.5 J	5-77
5.1.1	RCF Panels.....	5-77
5.1.2	CSMG Panels	5-81
5.1.3	Comparative Summary	5-83
5.2	Load Levels for Fatigue Test	5-85
5.3	Chapter Summary.....	5-86
6	CONCLUSION AND RECOMMENDATIONS	6-89
7	REFERENCES	7-91

List of Figures

Figure 1.1 Schematic illustration of sandwich panel	1-11
Figure 1.2 Example of sandwich panel applications in a.) a wind turbine blades and in b.) a trailer of a truck [4]	1-12
Figure 2.1 Tensile properties of FDM-fabricated 20 wt.% CF/ABS and GF/ABS FRPs (data from [8]–[10]))	2-16
Figure 2.2 Summary of process to produce PAN carbon fibres properties [11]	2-17
Figure 2.3 a.) Gen2Carbon G-TEX M non-woven mat [14], b.) SigmaRF fabrics [15]	2-18
Figure 2.4 Chopped strand mat glass [18]	2-22
Figure 2.5 Illustration of a.) corrugated, b.) foam and c.) honeycomb panels [25]	2-24
Figure 2.6 failure modes of sandwich panels in three-point bending [36]	2-27
Figure 2.7 Impact support fixture [47]	2-31
Figure 2.8 Drop-weight impact test specimen [47]	2-31
Figure 2.9 Energy conversion history [48]	2-32
Figure 2.10 Typical energy-time curve of sandwich panel under impact [43]	2-33
Figure 2.11 Commonly Observed Damage Modes during impact testing [47]	2-34
Figure 3.1 Image of both RCF (a i., a ii.) and CSMG (b i., b ii.) matts alongside their microscopic images	3-37
Figure 3.2 Sandwich panel layup sequence	3-38
Figure 3.3 Sandwich panel undergoing infusion.	3-39
Figure 3.4 a.) Brilliant ATAI 420 cutting machine, b.) RCF, and c.) CSMG sandwich panels ready for cutting.	3-41
Figure 3.5 Gridlines on cores of a.) RCF and b.) CSMG sandwich panels	3-42
Figure 3.6 a.) High performance microwave digestion system, b.) tubes containing samples.	3-42
Figure 3.7 a.) Yellow liquid indicating the fibre requiring more washing, b.) clear liquid indicating the fibre is fully clean.	3-43
Figure 3.8 a.) Tinius Olsen H50KT Universal Testing Machine, b i.) Load Cell, b ii.) Crosshead b iii.) Sandwich panel placed on supports, c.) Control keys.....	3-45
Figure 3.9 Instron CEAST 9340 drop tower impact system	3-46
Figure 4.1 fibre volume fraction VS spacing ratio (R/r) [52]	4-49
Figure 4.2 Parameters required for calculating sandwich panel stress.....	4-50
Figure 4.3 RCF samples post-loading.....	4-52

Figure 4.4 a.) Force-deflection curves for RCF samples, b.) Elastic region of RCF panels	4-53
Figure 4.5 CSMG samples post bending	4-55
Figure 4.6 a.) Force-deflection curves for CSMG samples, b.) Elastic region of CSMG panels	4-56
Figure 4.7 Average comparison of a.) force and b.) deflection c.) facesheet stress and d.) core shear stress	4-58
Figure 4.8 a.) Top facesheet view with microscopic image and b.) cross sectional view with microscopic image of impacted RCF panel at 10 J	4-59
Figure 4.9 Impacted CFRP sample exhibiting fibre fracture at 10 J[55]	4-60
Figure 4.10 Top facesheet view with microscopic image and b.) cross sectional view with microscopic image of impacted CSMG panel at 10 J	4-60
Figure 4.11 Force-displacement curve for RCF-SI-1 and CSMG-SI-1 at 10 J	4-61
Figure 4.12 Force-time curve for RCF-SI-1 and CSMG-SI-1 at 10 J	4-61
Figure 4.13 Energy-time curve for RCF-SI-1 and CSMG-SI-1 samples at 10 J	4-62
Figure 4.14 Top facesheet view and b.) cross sectional view of impacted RCF specimen at 20 J	4-63
Figure 4.15 a.) Top facesheet view and b.) cross sectional view of impacted CSMG specimen at 20J	4-64
Figure 4.16 Force-displacement curve for RCF-SI-2 and CSMG-SI-2 at 20 J	4-65
Figure 4.17 Force-time curve for RCF-SI-2 and CSMG-SI-2 at 20 J	4-65
Figure 4.18 Energy-time curve for RCF-SI-2 and CSMG-SI-2 at 20 J	4-66
Figure 4.19 Top facesheet view and b.) cross sectional view of impacted RCF specimen at 30 J	4-67
Figure 4.20 Top facesheet view and b.) cross sectional view of impacted CSMG specimen at 30 J	4-68
Figure 4.21 Force-displacement curve for RCF-SI-3 and CSMG-SI-3 samples at 30 J	4-69
Figure 4.22 Typical force deflection responses of foam core sandwich composites under low-velocity impact loading [57].	4-69
Figure 4.23 Force-time curve for RCF-SI-3 and CSMG-SI-3 samples at 30 J	4-70
Figure 4.24 Comparison of experimental and analytical load-time curve for penetrated panel [56]	4-70
Figure 4.25 Energy-time curve for RCF-SI-3 and CSMG-SI-3 samples at 30 J	4-71
Figure 4.26 Comparison between a.) average peak force, b.) average displacement c.) average absorbed energy of standard impact RCF and CSMG panels	4-73

Figure 5.1 Impacted RCF specimens alongside microscopic images.	5-77
Figure 5.2 Force-displacement curve for RCF samples at 4.5 J	5-78
Figure 5.3 Force-time curve for RCF samples at 4.5 J	5-79
Figure 5.4 Energy-time curve for RCF samples at 4.5 J	5-79
Figure 5.5 a.) impact force history, b.) impact force-displacement curve and c.) energy absorption [59]	5-80
Figure 5.6 Impacted RCF specimens alongside microscopic images.	5-81
Figure 5.7 Force-displacement curve for CSMG samples at 4.5 J.....	5-82
Figure 5.8 Force-Time curve for CSMG samples at 4.5 J.....	5-82
Figure 5.9 Force-time curve for CSMG samples at 4.5 J	5-83
Figure 5.10 Comparison between a.) average peak force, b.) average displacement c.) average absorbed energy of non-standard impact RCF and CSMG panels.....	5-84
Figure 5.11 Deflection and Force standard deviation for RCF (a, b) and CSMG (c, d) panels.	5-86

List of Tables

Table 2.1 Mechanical properties of carbon and glass fibres [7]	2-17
Table 2.2 Mechanical properties of Gen2Carbon recycled carbon fibre [14]	2-19
Table 2.3 Mechanical properties of sigmaRF [15].....	2-20
Table 2.4 Compositions (wt%), density and mechanical properties of glasses used in fibre reinforcement production [11].	2-21
Table 2.5 Example of structural efficiency of sandwich panels with regards to weight [25]	2-23
Table 2.6 Test results [33]	2-26
Table 2.7 Theoretical equations for maximum core shear stress.....	2-29
Table 3.1 CSMG and RCF properties	3-37
Table 3.2 Amount of resin used per panel. (ns: non – standard)	3-39
Table 3.3 Sample size of cut-out samples for tests	3-40
Table 3.4 Parameters used for low velocity impact tests.	3-47
Table 4.1 Average fibre volume content for RCF and CSMG panels.....	4-49
Table 4.2 Results for: maximum deflection (δ_{max}), ultimate force (F_{ult}), facesheet stress (F_{1u} & F_{2u}) and core shear stress (τ_{max}) for RCF panels.....	4-54
Table 4.3 Results for: maximum deflection (δ_{max}), ultimate force (F_{ult}), facesheet stress (F_{1u} & F_{2u}) and core shear stress (τ_{max}) for CSMG panels.....	4-57
Table 4.4 normalised three-point bending data.....	4-58
Table 4.5 Impact data for standard size RCF and CSMG panels	4-71
Table 4.6 Observable failure per energy level for standard RCF and CSMG samples ...	4-72
Table 4.7 Normalised impact data F_{peak} - peak force, E_a - absorbed energy	4-73
Table 5.1 Obtained RCF data form impact tests.....	5-80
Table 5.2 Obtained CSMG data form impact tests.	5-83
Table 5.3 Normalised impact data F_{peak} - peak force, E_a - absorbed energy	5-84
Table 5.4 Three-point bending data for RCF and CSGM specimen's elastic region. (F – force, D – deflection, Avg. Average, S.D – Standard deviation).....	5-85

List of Abbreviations

Abbreviation	Definition
ABS	Acrylonitrile–butadiene–styrene
AM	Additive manufacturing
CFRP	Carbon fibres reinforced Polymers
CF	Carbon fibre
CSMG	Chopped strand mat glass
FRP	Fibre reinforced polymers
GF	Glass fibre
PAN	Polyacrylonitrile
PVC	Poly(vinyl chloride)
RCF	Recycled carbon fibre

CHAPTER 1: INTRODUCTION

1 INTRODUCTION

1.1 Research Background

The advantages of using sandwich panels are the high stiffness and lightweight features they offer. Sandwich panels are made by placing a core in between two face sheets, as seen in Figure 1.1, with the help of an adhesive. A wide variety of materials can be used for facesheets and they typically range between metals and fibre reinforced polymers (FRP). As for the core, just three configurations are commonly used which are corrugated, foam and honeycomb, all of which a variety of materials that can be used to achieve. The core is the component that gives sandwich panels their desired high strength-to-weight and stiffness-to-weight ratios allowing for versatility in their application [1].

For example, in the automotive industry, sandwich panels have become very crucial to manufacturers who seek to produce lighter cars which in turn increases fuel efficiency. A study by Deniz Hara and Gokhan O. Ozgen on the use of sandwich panels in automobile body panels showed that foam core sandwich structures at 50% less weight than steel sheet metal panels have the same bending stiffness performance [2]. A. Pavolic et al. [3] carried out a study on optimising the stiffness to weight ratio of an ultralight photovoltaic roof of a solar sport car using carbon fibre sandwich panels. The aim was to present a design that would be suitable for durability under low modal vibrations that lead to the panel failure. Experimental work in agreement with numerical simulation supported the design to have very good performance under such scenario.

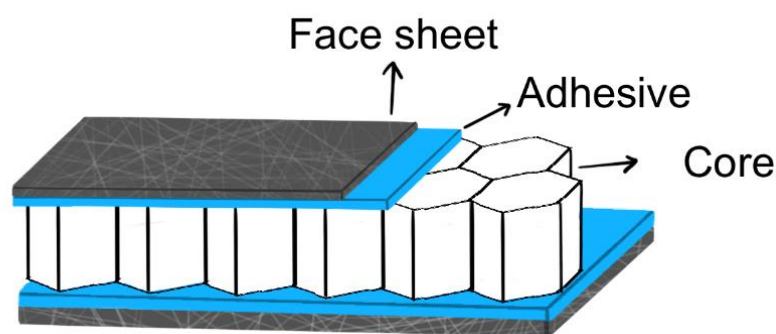


Figure 1.1 Schematic illustration of sandwich panel



Figure 1.2 Example of sandwich panel applications in a.) a wind turbine blades and in b.) a trailer of a truck [4]

Although the materials used to fabricate sandwich panels vary with application, fibre reinforced sandwich panels are typically fabricated with either glass fibre or carbon fibre. This is due to the high strength the carbon fibre provides and the ductility provided by the glass fibre. However, as shown in Figure 1.2, their diverse application across industries equate to exposure to conditions that can cause severe damage to them. The wind turbine in Figure 1.2a would be prone to low-velocity impact damage from debris that is carried along by the wind and the trailer of the truck in Figure 1.2b can undergo three-point (flexural) loading when a heavy crate is placed onto its surface.

Three-point bending and low-velocity impact on sandwich panels have been studied extensively by researchers who have done so using a range of experimental parameters and material configurations. Zhou et al. [5] investigated the effect of facesheet thickness, impactor shape and core density on the impact failure mechanisms of sandwich panels made with carbon fibre reinforced panels with honeycomb cores. They concluded that the tip of the impactor was a significant parameter affecting both failure modes and energy absorption of the panels. The effects of poly(vinyl chloride) (PVC) foam core density on the flexural properties sandwich panels with woven glass fibre facesheets was studied in detail by Steeves and Fleck. They were able to derive analytical expressions for sandwich panel failure modes under flexural loading which are: core shear, indentation, face wrinkling and buckling [6].

1.2 Research Gap

The lightweight and high strength features carbon and glass fibre reinforced sandwich panels offer have attracted more research towards their optimisation for better mechanical performance and damage resistance. However, growing environmental concerns on increasing amounts of fibre cut-off waste has brought attention to the need to experimentally evaluate how such materials can be re-used in sandwich panels. As there is very little to no information from previous literature addressing such an issue, this thesis aims to present experimental data on sandwich panels fabricated with recycled carbon fibre and chopped strand mat glass under three-point bending and low-velocity impact.

The aim and objectives are outlined in section 1.3.

1.3 Aim and Objectives

This thesis aims to investigate the three-point bending behaviour and impact response of sandwich panels manufactured with recycled carbon fibre (RCF) and chopped strand mat glass (CSMG).

Objectives:

- Manufacture sandwich panels using recycled carbon fibre and chopped strand mat glass fibre of the same areal density by using a guideline from ASTM standards.
- Investigate the mechanical characterisation of both sandwich panels (RCF and CSMG) under three-point bending and impact loading.
- Analyse microscopic imaging to identify the damage behaviour of sandwich panels.
- Provide a fatigue after impact testing guideline on sandwich panels made of RCF and CSMG.

1.4 Thesis Layout

The structure at which this thesis will follow is listed below:

Chapter 1: Introduction:

This chapter entails a brief introduction of sandwich panels, areas of application, three-point bending, low-velocity impact, research gap and lastly presents aims and objectives for this thesis.

Chapter 2: Literature Review:

This chapter contains a summary of previous literature on fibre reinforced composites, sandwich panels, three-point bending on sandwich panels and low-velocity impact on sandwich panels. This section also includes details of theoretical expressions for sandwich

panels under loading, experimental parameters and, observed failure modes for sandwich panels. The chapter concludes with a literature summary and gap.

Chapter 3: Panel Fabrication and Experimental Methods:

Contains descriptions of the materials and process used for fabricating the sandwich panels in this thesis. The methodology and equipment used for carrying out all experimental work on the panels are discussed. Experimental work carried out are acid digestion, three-point bending and low-velocity impact test.

Chapter 4: Results and Analysis:

Analysis of the results obtained from each experiment is described in this section. This includes data for the fibre content, three-point bending and low-velocity impact tests. Each experimental analysis is based on obtained data and visual analysis of the samples.

Chapter 5: Guideline for Fatigue After Impact Test:

Firstly, this chapter begins by highlighting the importance of carrying out fatigue after impact tests on sandwich panels. Secondly, it presents experimental findings of samples tested at a low impact energy. The low energy is selected not to cause too much panel damage. Thirdly, data from three-point bending tests in chapter 4 are used to generate fatigue load levels. The chapter then concludes with a guideline using parameters from the impact test and three-point bending data.

Chapter 6: Conclusion and Recommendations:

Proceeds to conclude the thesis by giving a general overview of the experimental work carried out alongside a discussion of experimental findings for the RCF and CSMG panels. It then proceeds to give recommendations for future works on sandwich panels fabricated with RCF and CSMG.

CHAPTER 2: LITERATURE REVIEW

2 LITERATURE REVIEW

2.1 Fibre Reinforced Polymers

Fibre-reinforced polymers (FRP) offer attributes such as high strength to weight ratio, low thermal expansion coefficient, anti-corrosion, and high thermal conductivity. They are categorised into two groups: discontinuous and continuous fibre reinforced composites. The several traditional techniques required to produce such composites are now being replaced with recently developed additive manufacturing (AM) as the process is a more cost effective and efficient method. This development has also contributed to their industrial application. For Example, most Boeing 787 Dreamliner aircrafts are reported to have approximately 80% of composites by volume comprising of 32 tons of carbon fibre-reinforced composites [7].

The two most popular reinforced fibres produced through AM are carbon fibre (CF) and glass fibre (GF). Carbon fibre polymers are generally observed to be stronger than glass fibre polymers when using the same resin system. Duty et al. [8] found that 20 wt.% carbon fibre combined with acrylonitrile–butadiene–styrene (ABS) filament can give a tensile modulus and strength of 11.9 GPa and 66 MPa respectively, while the tensile modulus and strength of the 20 wt.% glass fibre with the same filament were 5.7 GPa and 54 MPa respectively. H. L. Tekinaip et al. [9] reported similar findings for the tensile modulus at 11.5 GPa and strength of 60 MPa for 20 wt.% carbon fibre/ABS Hill et al. [10] used the same fibre/matrix configuration, 20 wt.% carbon fibre, and achieved 8.4 GPa in tensile modulus and 67 MPa in tensile strength. A graphical comparison is presented in Figure 2.1

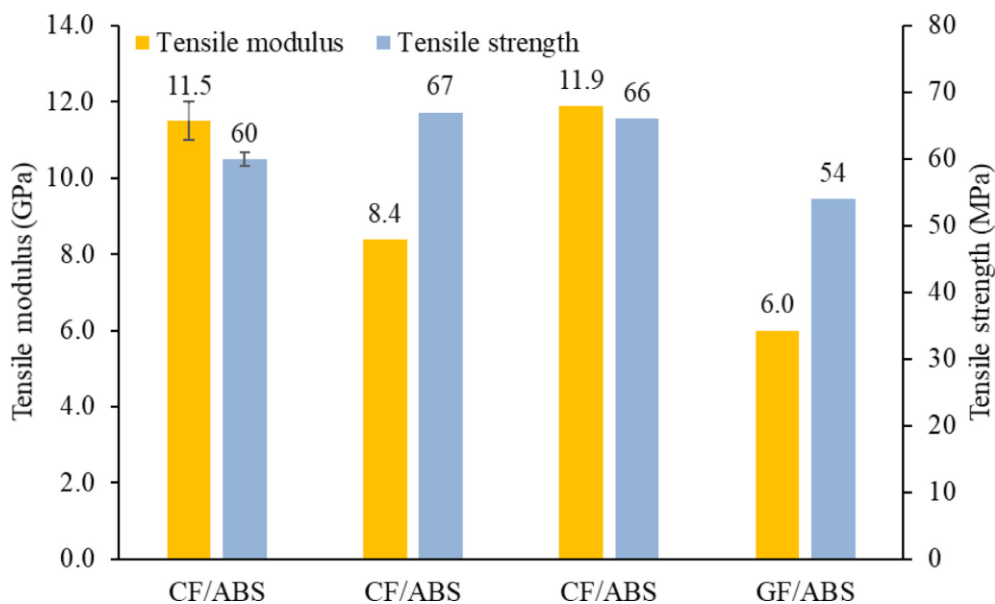


Figure 2.1 Tensile properties of FDM-fabricated 20 wt.% CF/ABS and GF/ABS FRPs (data from [8]–[10])

Table 2.1 contains the mechanical properties of a single carbon and glass fibre strand [7].

Table 2.1 Mechanical properties of carbon and glass fibres [7]

Fibre type	Young's modulus (GPa)	Tensile strength (MPa)	Specific strength (kN.m/kg)
Carbon fibre	120 - 180	1600 – 4127	2457 – 3919
Glass fibre	30 – 40	1500 – 3450	1307 – 3300

The tensile strength is defined as the maximum stress in a material before it yields whilst being pulled and the specific strength is defined material strength divided by its density. It is expressed as kilo newtons per kilogram. Sections 2.1.1 to 2.1.4 gives brief description of both fibres production well as the reclaimed fibres from them.

2.1.1 Carbon Fibre Reinforced Polymers

As show in Table 2.1, Carbon fibres reinforced Polymers (CFRP) are high modulus and high strength fibres. They can meet demands of structural systems that require higher values of modulus and strength than those values which can be provided by the glass fibres. Carbon fibres are produced from polyacrylonitrile (PAN), a fossil-based polymer, that gets wet spun into a precursor fibre before being turned into carbon fibre. The PAN has 49% yield of carbon. The transformation into carbon fibres is then done in a series of steps heating the air (pyrolysis) around the fibre to 275°C causing the fibre to turn black due to oxygen interacting with the PAN. This causes cross-linking, producing a three-dimensional infusible atomic network. Further heating is then applied at the fibres at 1000 °C to produce carbon fibre [11].

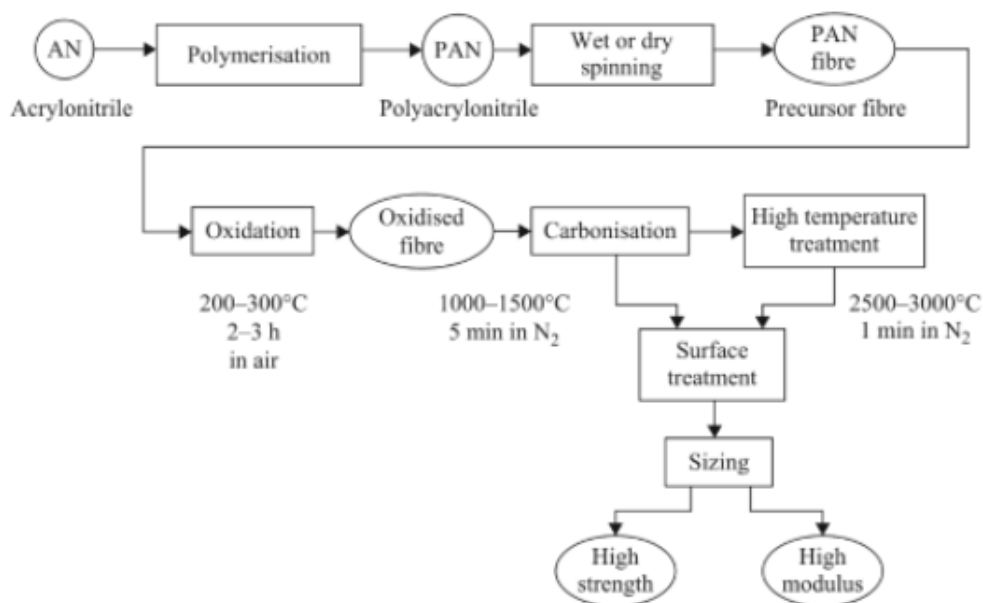


Figure 2.2 Summary of process to produce PAN carbon fibres properties [11]

The properties of carbon fibres made from PAN can be modified according to the pyrolysis temperature as illustrated in Figure 2.2. CFRPs are presently being used in sports and recreational equipment (fishing rods and golf clubs), pressure vessels, filament-wound rocket motor cases, and aircraft structural components (body, stabiliser, wing, and rudder components), in both military and commercial, helicopters and fixed wing [12].

2.1.2 Recycled Carbon Fibre

The production of recycled carbon fibre from used virgin carbon fibre is seen as a breakthrough in waste management for the composite industry. As the global production volume of carbon fibre reinforced plastics keeps increasing at a significant rate – from 46,000 tonnes in 2011 to 140,000 tonnes in 2020 it has been predicted that over 30% of the produced carbon fibre will end up wasted at some point in the process. Gen2Carbon (formally known as ELG Carbon Fibre) and Sigmatech are two companies in the UK that have developed cost-effective means of recovering carbon fibres from manufacturing waste and end-of-life components without significant degradation to the fibre properties [13].

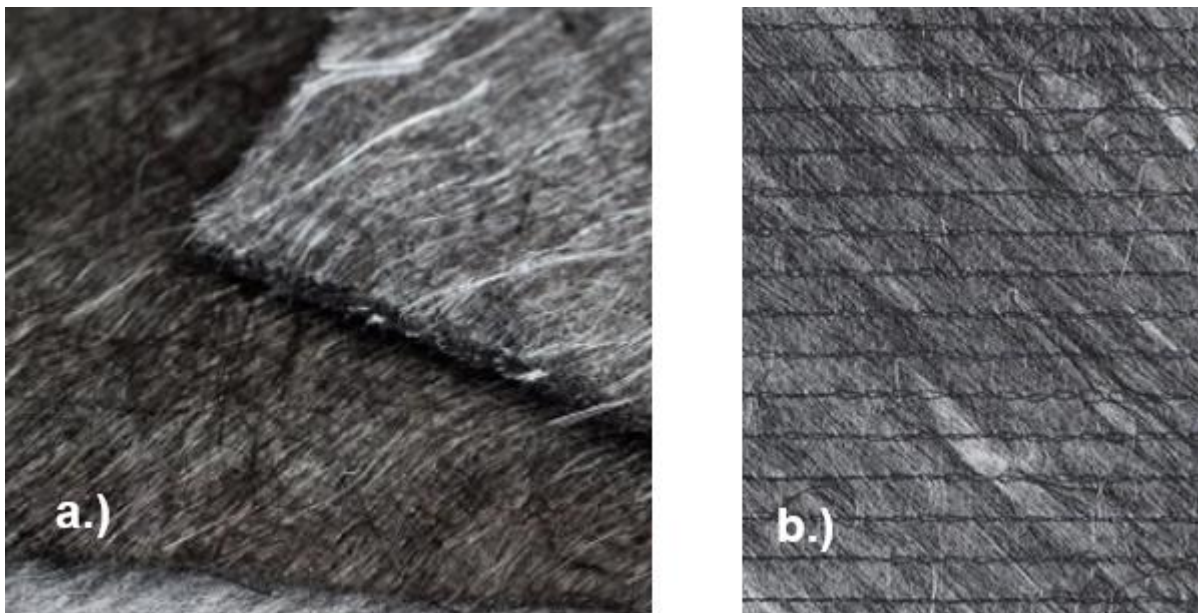


Figure 2.3 a.) Gen2Carbon G-TEX M non-woven mat [14], b.) SigmaRF fabrics [15]

As shown in Figure 2.3a, the orientation of the Gen2Carbon mat orientation is random from the production techniques used to produce it. In Figure 2.3b the fibres of the SigmaRF are oriented at 45°. The following analysis contains information for costs difference between the recycled carbon fibre and virgin carbon fibre:

- In the automotive industry carbon fibre costs \$5-\$7/ lb whereas recycled carbon fibre is cheaper.

- The low cost of conversion techniques for recycled carbon fibre makes it suitable for use in injection moulding and composite manufacturing.
- It leaves a very low carbon footprint at 10% of the global warming potential of virgin carbon fibre.
- The products for reinforcement cost \$8-\$12/ lb.


Mechanical properties of recycled carbon fibre from Gen2Carbon and Sigmatech are presented in Table 2.2 and Table 2.3.

Table 2.2 Mechanical properties of Gen2Carbon recycled carbon fibre [14]

PROPERTY	UNIT	TRANSVERSE	LONGITUDINAL
Tensile Strength	MPa	300	200
Tensile Modulus	GPa	30	20
Compression Strength	MPa	190	170
Compression Modulus	GPa	25	20
Flexural Strength	MPa	300	210
Density	g/m ³	1.06	

In Table 2.2 the tensile modulus is a measure of an object's stiffness or resistance to pulling forces. The compressive modulus is the capacity of a material to withstand axially directed pushing forces. When the limit of compressive strength is reached, materials are crushed.

Table 2.3 Mechanical properties of sigmaRF [15]

DMC5271265			
Sigmatex Fabric Test Sheet			
Description	365GSM/-45°+45°/RecycledCF:PP/45:55/1265mm/Low-Med Consolidation tapes		
Property	Test Method	Units	Nominal Value
Flexural Strength	ISO 14125	N/mm ²	302
Flexural Modulus	ISO 14125	kN/mm ²	27
Tensile Strength	ISO 527-5	N/mm ²	360
Tensile chord Modulus @ 0.05-0.25% Strain	ISO 527-5	kN/mm ²	27
Tensile chord Modulus @ 0.05-0.5% Strain	ISO 527-5	kN/mm ²	27
Elongation at Break	ISO 527-5	%	1.3
Heat Deflection Temperature	ISO 75	°C	165
Charpy Impact @ 23°C	ISO 179-1/1eA	kJ/m ²	47
Charpy Impact @ -30°C	ISO 179-1/1eA	kJ/m ²	40
Shore D Hardness	ISO 62	N/A	86
Density	ISO 10119	g/cm ³	1.15

In Table 2.3 the flexural modulus is defined as a mechanical property that measures a material's stiffness or resistance to a bending action. The flexural strength, also known as bending strength, or transverse rupture strength, is a material property, defined as the maximum stress in a material just before it yields in a bending test.

Gen2Fibre keeps discovering new applications for recycled carbon fibre by collaborating with several companies. One of these is automotive injection moulding company, Sanko Gosei. The company replaced 30% glass fibre polypropylene compound with recycled carbon fibre in an injection moulded headlamp support in. This allowed for an increase in rigidity and a reduction in weight of 8%.

2.1.3 Glass Fibre Reinforced Polymers

Glass fibre reinforced polymers (GFRP) are produced through the extrusion of molten glass at around 1250°C through holes with diameters of one or two millimetres in a spinneret. The filaments are then drawn to produce fibres with diameters usually between 5 and 15 µm [16].

The spinnerets typically contain several hundred holes to allow for a strand of glass fibre to be produced, most of which are chemically based on silica (SiO₂). E-glass fibre are the most widely used glass for fibre reinforced composites whilst glass fibres with superior mechanical properties are referred to as S-glass. C-glass is a chemically resistant variant of glass fibre. Glass fibres are often coated with a protective coating known as size as they are easily damaged through abrasion either because of contact with other fibres or machinery. Simply put, the purpose of the size is to protect the fibre as well as hold the strand together [11]. The properties and compositions of the most common types of glass fibres are shown in Table 2.4.

Table 2.4 Compositions (wt%), density and mechanical properties of glasses used in fibre reinforcement production [11].

Glass type	E	S	C
SiO ₂	54	65	65
Al ₂ O ₃	15	25	4
CaO	18		14
MgO	4	10	3
B ₂ O ₃	8		5.5
F	0.3		
Fe ₂ O ₃	0.3		
TiO ₂			
Na ₂ O			8
K ₂ O	0.4		0.5
Density	2.54	2.49	2.49
Strength at 20°C (GPa)	3.5	4.65	2.8
Elastic modulus at 20°C (GPa)	73.5	86.5	70
Failure strain at 20°C (%)	4.5	5.3	4.0

The wide adoption of glass fibre reinforcements is due to low cost and ease of production as they do not require any extra specialised techniques to handle them. However, as highlighted in Table 2.1 and Table 2.4, their low mechanical properties prevent them from being used in components that require light weight and high strength features. Thus, it becomes important to tailor the material properties for suitable applications [11].

2.1.4 Chopped Strand Mat Glass Fibre

Much like the recycled fibre, short strands of E-glass are randomly oriented and bound to create a mat which can then be wetted out with resin. This allows them to be used for general reinforcements for traditional fibreglass moulds as they provide excellent strand integrity and display even strength consideration throughout all directions. Chopped strand fibres are

comparatively less expensive and exhibit low potency compared to plain weave. Their applications can be found in small mould and pattern making and partition boards [17].

S. Heckadka et al. [17] investigated the tensile, flexural, impact and inter-laminar shear strength of chopped strand E-glass composites. Samples were fabricated using three layers of chopped strand. Experimental results indicated that the three-layer arrangement resulted in inferior impact strengths. However, maximum tensile strengths of 415 MPa was observed alongside flexural strengths of 237 MPa was noticed. This was done at an achievable average fibre content of 30%.



Figure 2.4 Chopped strand mat glass [18]

Figure 2.4 shows the random orientation of the CSMG fibre. In-plane shear failure properties of chopped glass fibre-reinforced polyester by means of traction-compression biaxial testing were experimentally investigated by Serna Moreno et al. [19]. Specimens with different geometries and loading conditions were utilised to estimate failure modes. Results revealed that loading conditions and composite geometry influenced stress strain failure fields. Dolati et al. [20] compared impact strengths of composites fabricated with epoxy glass fibres in three different forms, namely, unidirectional, plain weave, and chopped strand mat. They observed that composites with chopped strand mat displayed superior resistance to damage

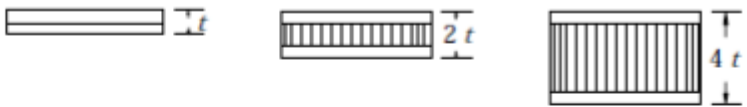
extension when subjected to single and repeated high velocity impact test with ice projectiles. A technical data sheet is not presented for the chopped strand mat glass as it is not provided by suppliers.

The applications of carbon and glass fibre in composite structures known as sandwich panels will be expressed in more detail throughout sections 2.2 to 2.4.

2.2 Sandwich Panels

Sandwich panels share the same features of being lightweight, and high strength with fibre reinforced polymers as explained in section 2.1. They are assembled by placing a lightweight core in between two fibre reinforced facesheet. The facesheets carry most of the bending and in-plane loads while the core provides flexural stiffness and the out of-plane shear and compressive strength [21]. Sandwich panels also possess additional features that allows for application for a variety of purposes, among them are high flexural strength and stiffness, high impact strengths and high resistance to corrosion [22]–[24]. The separation the core provides in between the facesheets allow for increase in moment of inertia of the panels with little increase in weight. This in turn produces a component that is efficient in resisting flexural, and impact loads. As illustrated in Figure 2.5, the configuration of a sandwich panel core materials can vary between a.) corrugated core, b.) foam core and c.) honeycomb core [25].

Table 2.5 Example of structural efficiency of sandwich panels with regards to weight [25]



Relative Bending Stiffness	1	7.0	37
Relative Bending Strength	1	3.5	9.2
Relative Weight	1	1.03	1.06

Table 2.5 illustrates the advantageous effect of sandwich panel for flexural strength and stiffness compared to solid panels using typical beam theory, expressed with typical value for facesheet core density. Researchers have observed that the overall strength and stiffness of sandwich panels could be improved by increasing the thickness or density of the core.

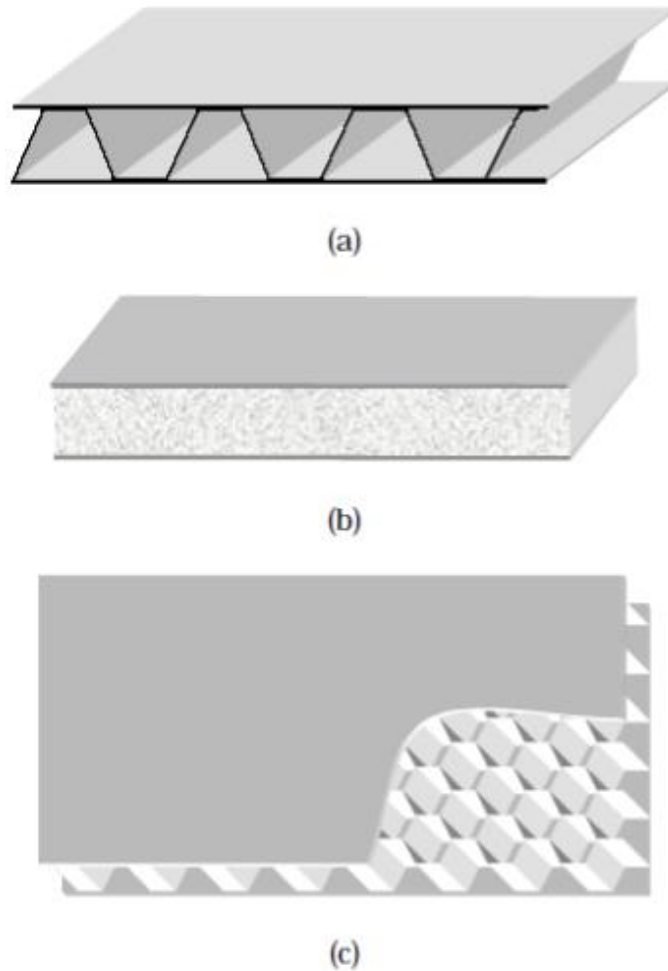


Figure 2.5 Illustration of a.) corrugated, b.) foam and c.) honeycomb panels [25]

The connection between the facesheet and core, particularly foam cores, is often an area of focus amongst researchers since the dominant failure mode of sandwich panels is face sheet-core delamination [26]. Zenkert et al. [27] discovered that soft cores, rather than the facesheets, contribute significantly to the working life of a panel through shear failure. Y. M. Jen & Li. Y. Chang [28] confirmed this while carrying out flexural tests on three types of aluminium honeycomb sandwich beams with different facesheet thicknesses. The experimental results showed that there are no apparent relationships between the facesheet thickness and the working life of the specimens. In the various applications sandwich panels are used in, sandwich panels usually suffer from three-point bending failure, and impact damage which causes a reduction in their load-bearing capacity and working life. For this reason, the mechanical response of sandwich panels under three-point bending and low-velocity impact damage has attracted extensive investigations over the last few years. As a result, a variety of facesheet and core materials have been explored to enhance the damage resistance of sandwich panels under both phenomena [29]. Sections 2.3 and 2.4 explain further in detail.

2.3 Three-Point Bending on Sandwich Panels

Previous literature from researchers have stated that the overall mechanical response of sandwich panels during three-point bending is dependent on the properties of the face sheets stiffness, and strength properties of the core, as well as the adhesion between the facesheet and core.

Compression and three-point bending performances of carbon fibre reinforced lattice-core sandwich composites were investigated by H. Fan et al. [30] The three-point bending tests were carried out at a loading rate of 2 mm/min. Experimental results revealed that debonding failure dominated the mechanical behaviour of the sandwich structures due to their stiff facesheets. After the rapid global debonding of one facesheet, the strength failure of the other facesheets controls the final failure of the structure. Similar observations of facesheet core debond were reported by H. E Balcioglu [31].The researcher studied the flexural behaviours of natural sandwich composites produced using vehicle tires and natural jute fibre woven fabric under three-point bending. The tests samples were dimensioned according to ASTM C393 standards to determine facesheet bending stress, core shear stress and facesheet bending. In context, the effect of granule diameter and core thickness were experimentally investigated. Observations revealed that similar damage mechanisms occurred in natural sandwich composites for the same type of load. Damage mechanisms such as facesheet-core interface separation, facesheet material crack and core material breakage in the samples progressed, respectively under the three-point loading.

The effect of span length and core composition on a panel's performance under three-point bending has been reported. B.Wang et al. [32] investigated the failure mechanism of Polymethacrylimide (PMI) foam core sandwich panel in bending. The sandwich panels had span lengths of 140 mm and 500 mm. Experimental work in agreement with theoretical analysis showed that the PMI foam core sandwich panels failed by core shear for the samples with 140 mm span length and face wrinkling turned out to be the principal failure of the 500 mm span length panels. K. Toradmal et al. [33] carried out three-point bending analysis on honeycomb structures fabricated with three different facesheets for application in the railway industry. The facesheets used were stainless steel (SS-304), Aluminium (A 3003 H19) and Glass fibre reinforced polymer. Specimen geometry was in line with the ASTM C393 standard with dimensions for the width 100 mm, is twice the total thickness 32 mm, and a length of 300 mm. At least three specimens were tested, and span length used was 240 mm. The results revealed that the GFRP honeycomb structure would be more suitable for application than the stainless-steel panel as it has a higher value for the ultimate

failure load. Although the aluminium still had a relatively higher load, the 14.28% weight reduction offered by the GFRP sandwich panel made it a better choice. The test results can be found in Table 2.6.

Table 2.6 Test results [33]

Panel	Ultimate load (N)	Average Ultimate Load (N)
SS-I	2240	2080
SS-II	2040	
SS-III	1960	
AL-I	2480	2427
AL-II	2560	
AL-III	2240	
GFRP-I	2280	2147
GFRP-II	2080	
GFRP-III	2080	

On the effects of core composition, C. Kaboglu et al. [34] investigated the effects of varied core density on the three-point bending and high-velocity impact loading properties on sandwich structures. The sandwich panel consisted of three layers of closed cell poly(vinyl chloride) (PVC) foam to form the core and the facesheets were GFRP composites. Each cell had a density ranging from 60 to 100 kg/m³. Experimental findings revealed that under three-point bending, the use of low-density cores decreases the likelihood of failure of sandwich structures by sudden force drop. An experimental study by I. M. Daniel et al. [35] was conducted on the behaviour of composite sandwich beams under four-point and three-point bending. The sandwich beams were manufactured using unidirectional carbon/epoxy facesheets and aluminium honeycomb/foam cores. Experimental findings revealed that the bending behaviour of the was governed by the facesheets. However, when shear failure was present, failure of the honeycomb was governed by the low core strength. In the case of the foam core beams, indentation failures were controlled by the flexural stiffness of the facing and compressive core strength.

The four main observed modes of collapse identified for sandwich beams under three-point bending are: (i) face yield or face microbuckling, (ii) wrinkling of the compressive facesheet, (iii) core shear, and (iv) indentation beneath the loading rollers, are illustrated in Figure 2.6 [36].

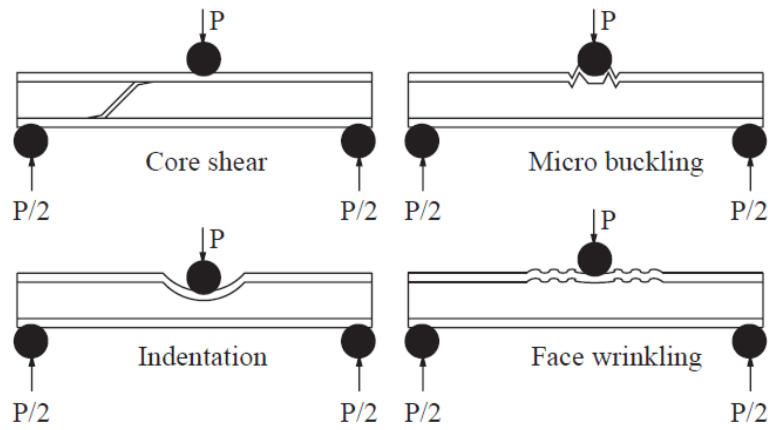


Figure 2.6 failure modes of sandwich panels in three-point bending [36]

Analytical expressions for each collapse mode have also been established by previous researchers to be used to predict sandwich panel three-point bending collapse loads [36]. They are expressed as:

Microbuckling:

$$P = \frac{4\sigma_f b t_f d}{L} \quad \text{Eq(2.1)}$$

Where P is the applied load, L is the span length, σ_f is the microbuckling strength due to compressive stress, t_f is the facesheet thickness, b is the sandwich width and d is the sandwich thickness.

Core shear:

$$\tau_c = \frac{P}{2(bd)} \quad \text{Eq(2.2)}$$

Where τ_c is core shear.

Face wrinkling:

$$P = \frac{2b t_f d}{L} \sqrt[3]{E_c E_f G_c} \quad \text{Eq(2.3)}$$

Where E_c the cores axial moduli, E_f is the facesheets young modulus and G_c is the cores shear moduli.

Indentation:

$$P = b t_f \left(\frac{\pi^2 \sigma_c^2 E_f d}{3L} \right)^{1/3} \quad \text{Eq(2.4)}$$

Where σ_c is the compressive shear strength.

Theoretical expressions have been proposed to determine the mid-span deflection of sandwich panels during bending. This has been done through a modification of the equation used for a beam under loading at its centre given in Eq(2.5):

$$\delta = \frac{PL^3}{48EI} \quad \text{Eq(2.5)}$$

Where δ is the deflection, P is the applied load, L is the span length of the beam, EI (otherwise known as D) is the flexural rigidity of the beam.

In the case of a sandwich panel under three-point bending, the sum of mid-point deflection is due to the bending of the face sheets and the shear of the core:

$$\delta = \frac{PL^3}{48D} + \frac{PL}{4AG} \quad \text{Eq(2.6)}$$

Where A is the area of the core, and G is the shear modulus of the core.

The flexural rigidity of the facesheets can be found using the parallel axis theorem and is combined with the rigidity of the core in Eq(2.7).

$$D = \frac{E_f b t_f d^2}{2} + \frac{E_f b t_f^3}{6} + \frac{E_c b c^3}{12} \quad \text{Eq(2.7)}$$

Where E_f is face sheet youngs modulus, E_c is the cores young modulus, b is the width of the panel, d is the distance between the centroids of the face sheets, c is the thickness of the core.

The core shear rigidity AG is given in Eq(2.8).

$$AG = \frac{bd^2G}{c} \quad \text{Eq(2.8)}$$

The first term in Eq(2.7) is the stiffness of the facesheets about the centroid. The second term is the stiffness of the facesheets about their centroid. The third is the stiffness of the facesheets about the centroid of the beam [36].

The theoretical expression to calculate the maximum core shear stress in sandwich panels during three-point bending have been discussed in different papers. J. Arabaoui et al [37] investigated the effect of the core thickness and intermediate layers on the mechanical properties of a polypropylene honeycomb sandwich panel. The investigation led to the formulation of a method to calculate the shear stress of a core during bending. The method alongside the utilised ASTM standard for three-point bending (ASTM C393/C393 M) are presented in Table 2.7.

J. Mei et al [38] carried out three-point loading tests on empty and foam filled CFRP X-core sandwich panels with three different thicknesses. A rectangular crosshead of width 16 mm was used to apply load onto the sandwich panels at a rate of 2 mm/min. The theoretical expressions in Eq(2.6), Eq(2.7), Eq(2.8) were used for the prediction of the bending stiffness, initial failure load and were found to be in good agreement with finite element models as well as experimental outcomes.

Table 2.7 Theoretical equations for maximum core shear stress

Paper	Maximum core shear stress
(Arbaoui, 2014)	$\tau_{max} = \frac{P}{2(bd)}$
(ASTM- ASTM C393/C393 M)	$\tau_{max} = \frac{P}{(d + c)b}$

Where τ is the core shear, P is the maximum applied load, b is the sandwich width, d is the sandwich thickness, and c is core thickness.

In summary of chapter, the key factors influencing a panels behaviour under three-point bending are facesheet stiffness, core strength, span length and core composition. Theoretical expressions have been developed for three aspects of a panel under three-point bending: the four main failure modes, the determination of the mid-span deflection of a panel and the maximum core shear stress. It is therefore important to select suitable panel materials that satisfies each factor according to its final application.

2.4 Impact Damage of Sandwich Panels

Impact damage can occur during all phases of a panel's life cycle, e.g., during production, service, and use [39]. The purpose of an impact tests is to simulate the damage resistance of a sandwich panel under various conditions such as hailstorms, dropped work tools or even the floors of transport vehicles. Previous studies have indicated that impact damage initiation is not just dependent on the panel support conditions but the material properties and geometry of the core [40]. It is also noted that when a sandwich panel undergoes impact damage, the core provides necessary traverse shear resistance, separation and fixing of the facesheets, as well providing other features such as carrying in-plane loads, heat insulation and impact energy absorption [41]. Kim and Jun [42] investigated the effects face layup and core density on the delamination area. The sandwich panel was made of graphite/epoxy facesheets and Nomex honeycomb core. The observations revealed that the higher the core

density the smaller the delamination area other than a lower density core for the same level of absorbed impact energy.

Generally, during impact loading, the core is responsible for majority of the impact energy absorption. R. Ouadday et al. [43] combined an experimental and numerical approach to characterising the behaviour of dual core sandwich panels composed of glass fibre reinforced epoxy facesheets and alumina trihydrate-filled epoxy and extruded polystyrene foam core. For all impact energies applied, the dual core sandwich panel was found to absorb 50% of all energies. More so, foam compression was found to be the main impact energy absorption mechanism. Y. Zhang et al. [44] investigated the dynamic mechanical behaviour and energy absorption characteristics of aluminium honeycomb sandwich panels (AHSPs) under repeated impact loading. With the increase in repeated impact, the integral folds of the honeycomb core increased as well as the buckling areas which led to the honeycomb core compression and finally densification. This proved that the energy absorption performance of AHSPs under repeated impact can be efficiently regulated by the wall thickness as well as length of honeycomb.

The damages observed on a panel under low-velocity impact can range from barely visible damage to full panel penetration. Therefore, to carry out full investigation of sandwich panels, key impact data such as maximum contact force, contact time, deflection at peak load, energy absorbed, and impact velocity are used to analyse the impact damage characteristics of sandwich panels. K.B. Shin et al. [45] observed these parameters rise with impact energy when carrying out experimental study of low-velocity impact response on sandwich panels that are prime candidates for the structural materials of body-shell and floor of the Korean low floor bus. J.A Artero-Guerrero et al. [46] states that Peak force, coefficient of restitution, maximum displacement and residual stiffness plots are a function of impact energy alone and neither impact velocity or impact or mass.

To carry out low-velocity impact tests, the ASTM D7136/7136M – 12 standard is often referenced in previous works as it specifies the specimen geometry alongside the ideal fixture for the test. Figure 2.7 and Figure 2.8 illustrates the required fixture support for the test as well as sample size.

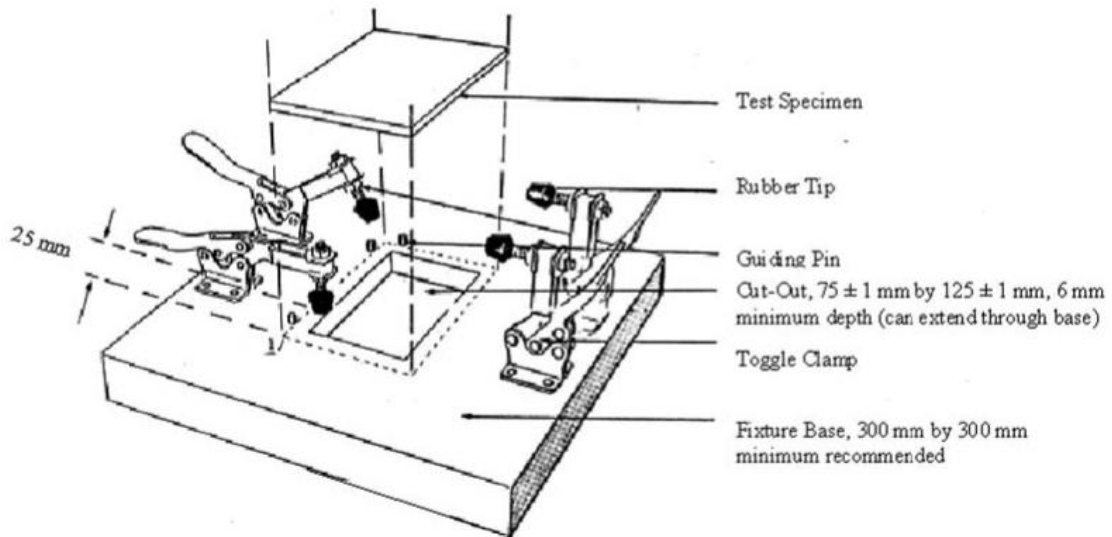


Figure 2.7 Impact support fixture [47]

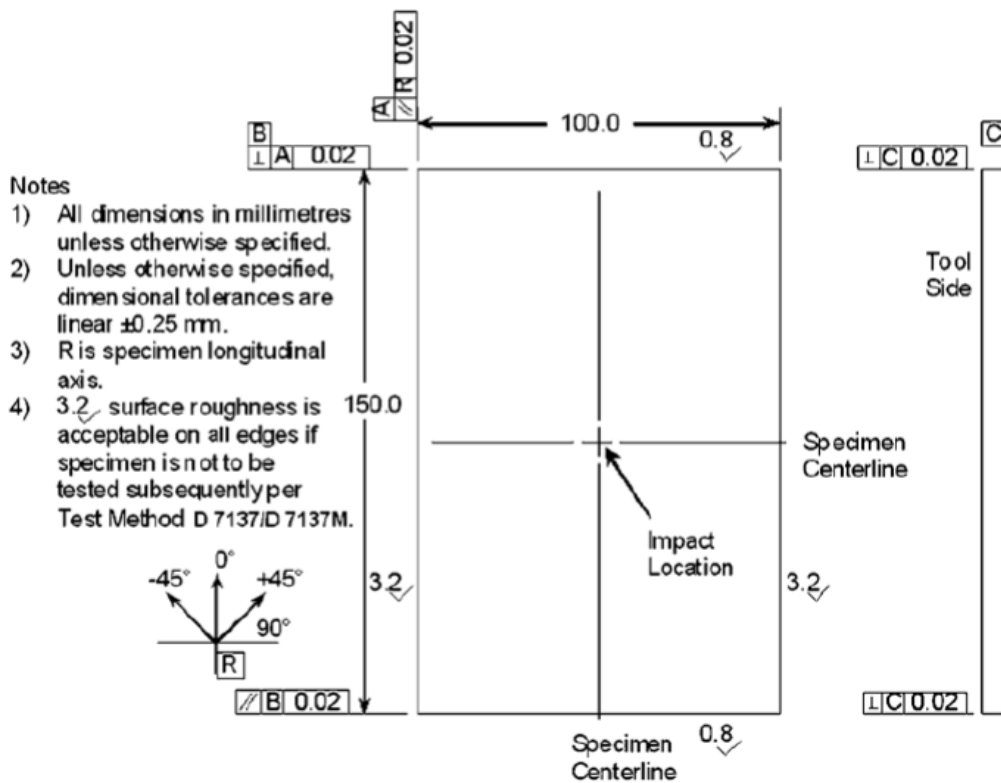


Figure 2.8 Drop-weight impact test specimen [47]

Following the law of conservation of energy, the total energy during an impact event is constant, which is the kinetic energy of the impactor. At the start of the test the gravitational energy is converted into kinetic energy and then reduces as it being absorbed by the panel. Theoretical expressions for the energy absorption are describes as [48]:

$$E_A = E_k^1 - E_k^R = Mg\Delta H = Mg(H_1 - H_R) \quad \text{Eq(2.9)}$$

Where E_A is the absorbed energy, E_k^1 is the kinetic energy of the impactor, E_k^R is the impact rebound kinetic energy of the impactor, M is the impactor mass, g is the acceleration due to gravity, H_1, H_R are the initial and rebound heights of the impactor respectively and ΔH is the gap height of the impactor [48].

The formula for the kinetic energy E_K , based on the mass of the striker is expressed as:

$$E_k^1 = \frac{1}{2}mv_1^2 = MgH_1 \quad \text{Eq(2.10)}$$

$$E_k^R = \frac{1}{2}mv_R^2 = MgH_R \quad \text{Eq(2.11)}$$

Where v is the impactor velocity, and m is the impactor mass.

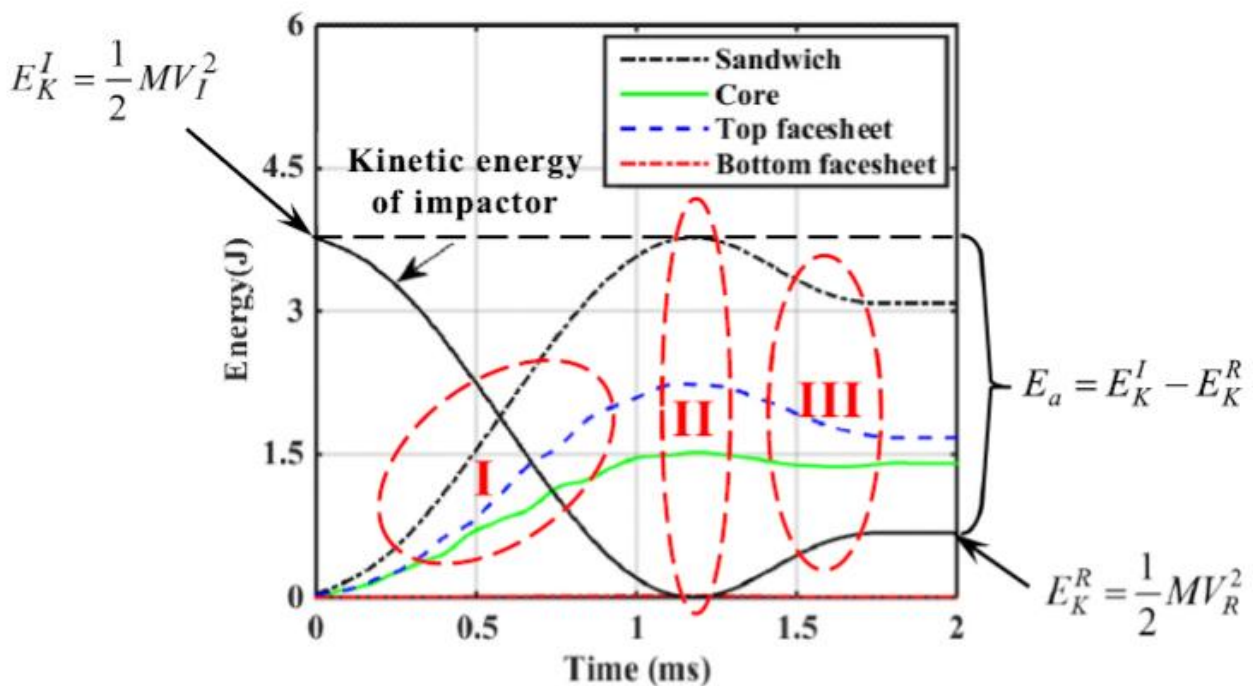


Figure 2.9 Energy conversion history [48]

An illustration of Eq(2.9), Eq(2.10), and Eq(2.11) for the energy conversion history during impact has been presented in Figure 2.9, for an experiment carried out by D. Zhang et al. at impact energy of 3.81 J [48]. An illustration of elastic and dissipated energy during an impact even is given in Figure 2.10 [43].

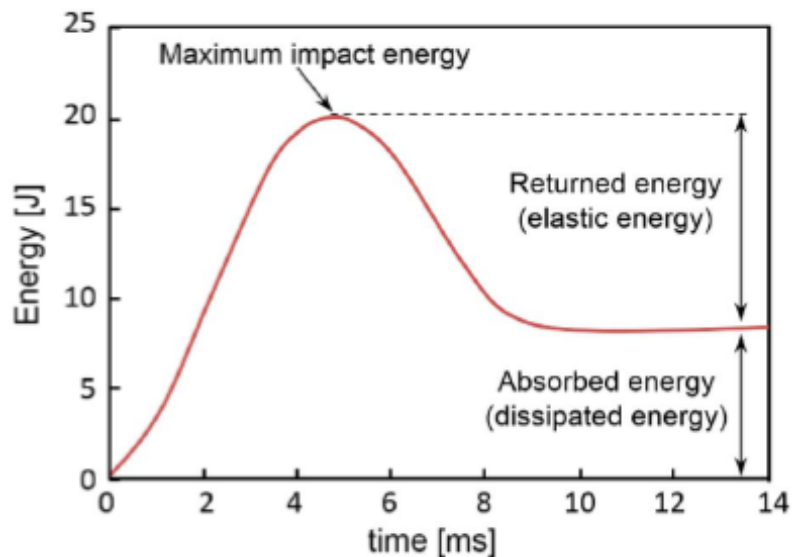


Figure 2.10 Typical energy-time curve of sandwich panel under impact [43]

Core deformation and facesheet failure are decisive factors for the energy absorption capability of sandwich structures. The failure mechanism a core can exhibit under impact loading can be noted as cell wall buckling, core crushing and traverse cracking. V. Crupi et al. [49] analysed the failure modes in aluminium honeycomb sandwich panels under bending and impact loading with different cell sizes. Tomographic investigation shows that the collapse of the honeycomb panels occurs for progressive crumpling of cell walls due to the phenomenon of buckling. Ugale et al. [50] compared the impact responses of glass fibre reinforced polymer (GFRP) thin sandwich panels and carbon fibre reinforced polymer (CFRP) thin sandwich panels with polyester foam Coremat XM. The CFRP thin sandwich panel was penetrated under the applied impact energy of 18J while the GFRP thin sandwich panel was not penetrated because of its higher elastic deflection and lower stress. A summary of facesheet failure modes during impact testing are illustrated in Figure 2.11.

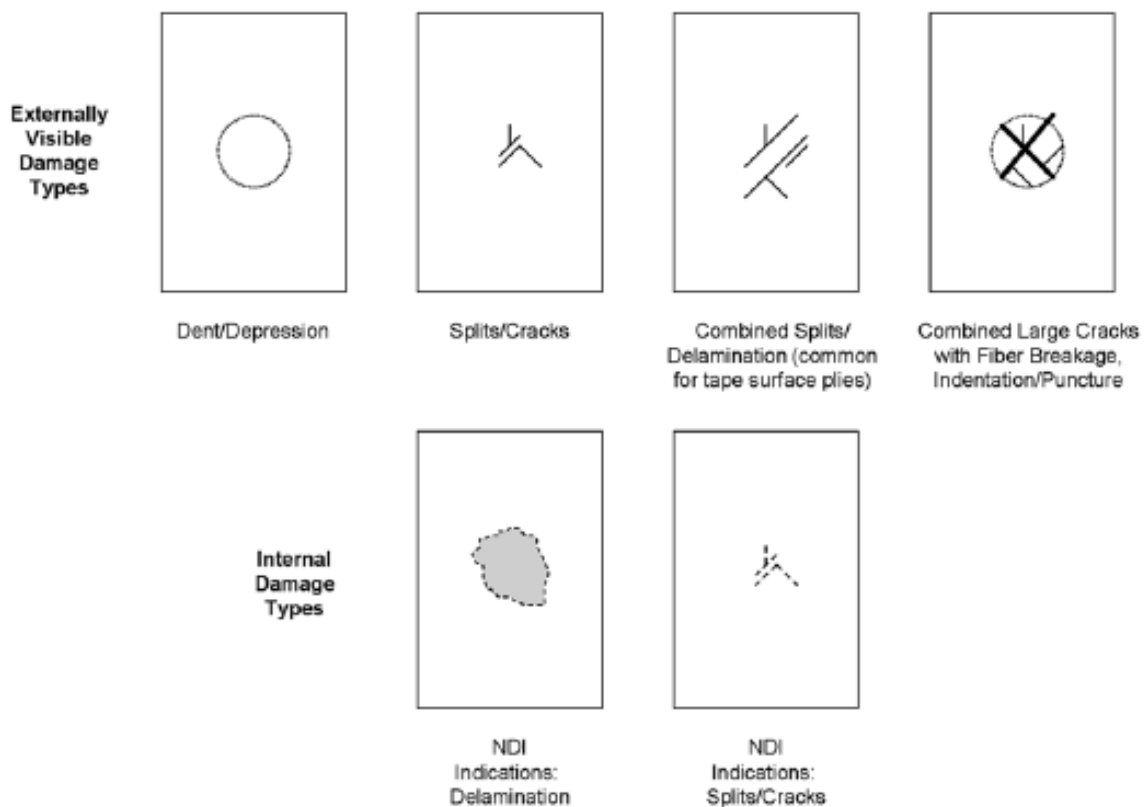


Figure 2.11 Commonly Observed Damage Modes during impact testing [47]

In summary, sandwich panel impact damage can occur during its production and life cycle. During an impact event, the density and material of the core have been reported to influence the energy absorption mechanisms of a panel. Core compression, buckling, facesheet penetration and barely visible damage are commonly observed failure modes under impact loading. Theoretical expressions have been developed to analyse the law of energy conservation and energy absorption during an impact event. It is therefore important to ensure suitable sandwich panel materials are selected to withstand impact damage according to its application.

2.5 Literature Summary and Gap

A recurring trend from previous literature reveal that carbon fibre reinforced composites (CFRP) tend to generally be stiffer and offer higher strengths than glass fibre reinforced composites (GFRP). New developments in the manufacturing techniques for both carbon and glass fibre have encouraged a diverse range of application and gradual adoption for their utilisation for the fabrication of sandwich panels. Growing concerns about the large amounts of fibre cut-off waste have led to innovative methods to producing recycled carbon fibre (RCF) and chopped strand matt glass fibres (CSMG). The configuration of a sandwich panel has been noted to be beneficial to the overall damage resistance of both fibres when

laminated as the core aids in absorbing the loads transferred unto the top facesheet. Experimental observations for both three-point bending, and impact damage reveal that sandwich panels fabricated with carbon and glass fibre exhibit failure modes that depend on the configuration used for the loaded facesheet and core.

Constant research effort has been put into the optimisation of fibre reinforced sandwich panels for better mechanical performance but their increased application, and adoption across industries translate to increased fibre cut off waste. With growing environmental concerns about fibre waste generation, it becomes important to investigate the mechanical behaviour of RCF and CSMG in sandwich panel configurations. This stems from a significant lack of information from previous literature for experimental data on randomly oriented fibre reinforced sandwich panels. This thesis aims to address this gap by experimentally testing recycled carbon fibre and chopped strand mat glass in a sandwich panel configuration under three-point bending and low-velocity impact.

CHAPTER 3: PANEL FABRICATION AND EXPERIMENTAL METHODS

3 PANEL FABRICATION AND EXPERIMENTAL METHODS

3.1 Materials

The facesheets used for the sandwich panels investigated in this paper were 300 gsm Carbiso™ M recycled carbon fibre (RCF) acquired from Gen2Carbon (formerly known as ELG), and 300 gsm chopped strand mat glass (CSMG) fibre acquired from EasyComposites. RAVATHERM extruded polystyrene (XPS) H LB foam was the material choice for the core. The resins that were used for fabrication were IN2 Epoxy infusion resin that was mixed with AT30 slow hardener. The properties of both fibres are presented in Table 3.1.

Table 3.1 CSMG and RCF properties

	Tensile strength (MPa)	Tensile modulus (GPa)	Flexural strength (MPa)	Flexural modulus (MPa)
CSMG	108	7.8	204	6770
RCF	300	30	300	-

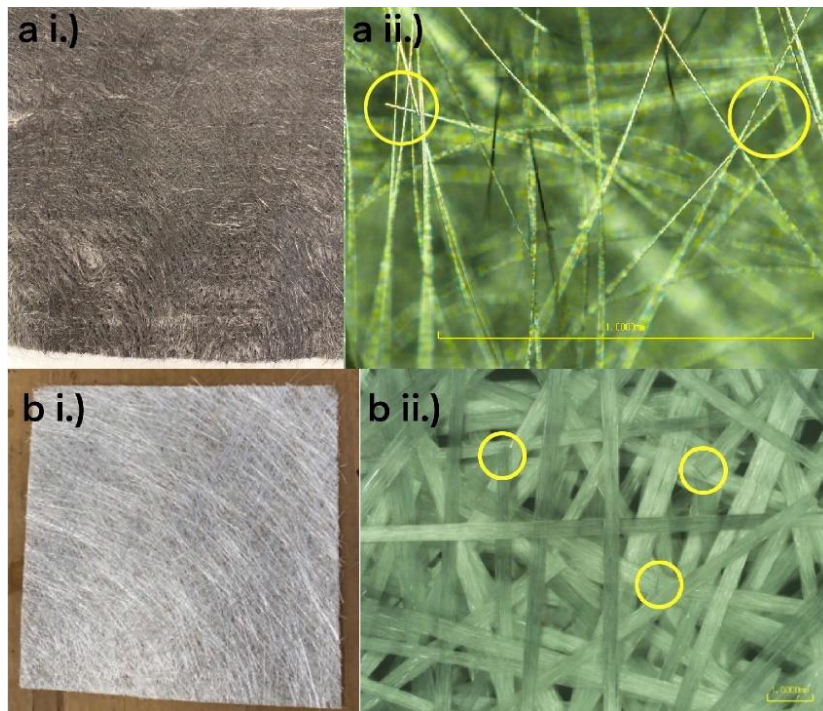


Figure 3.1 Image of both RCF (a i., a ii.) and CSMG (b i., b ii.) matts alongside their microscopic images

As shown in Figure 3.1, both fibres are random by design. CSMG facesheets have wider industrial application due to the fibres low cost. The RCF facesheet was chosen for comparative analysis to explore how a randomly oriented carbon composite would fare against a randomly oriented glass composite under three point and impact loading.

3.2 Panel Fabrication

Both RCF and CSMG panels were fabricated through Vacuum Assisted Resin Infusion (VARI). All infusion was carried out using just the vacuum bag as the mould. In doing so, the contents in the bag are held tightly together due to equal crumpling of the bag at the top and bottom under vacuum allowing for maximum pressure to be applied. This approach was adopted because it was observed to significantly reduce the time looking for of air leaks around the mould. It also allows for even surface finish of the panels and saves costs as it eliminates the need to apply a mould release agent or acetone for mould cleaning. This also meant easy removal of laminate after curing.

The materials used for laying-up the sandwich panels were vacuum bag as the mould, 2-flow media mesh sheets, 2 peel plies, two layers of breathers, two spiral tubes for the inlet and outlet pipes. As shown in Figure 3.2, The layup sequence was as follows: vacuum bag + 1 layer of flow media mesh + 1 layer of peel ply + 2 layers of facesheet + core. The reverse order of the peel ply, flow media mesh and vacuum bag was applied before sealing the mould with vacuum sealant tape, ensuring enough space for the inlet and outlet connectors. Before infusion, the epoxy resin and hardener are mixed in the ratio 100:30 as recommended by the manufacturer. The calculations below were used to determine the resin : hardener ratio.

$$W \div \left(\frac{100+30}{100}\right) = R \quad \text{Eq(3.1)}$$

$$W - R = H \quad \text{Eq(3.2)}$$

Where W is the amount of mixture required, R is the amount of resin and H is the amount of hardener.

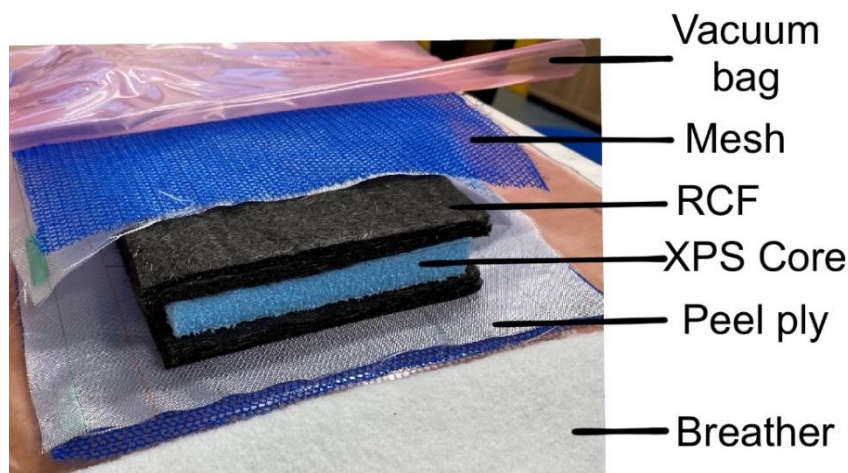


Figure 3.2 Sandwich panel layup sequence

Once the epoxy and hardener are mixed, they are then degassed for approximately 15 mins at 1 bar before infusing the mixture into the sandwich panels. Two sets of panels were fabricated using; 1.) non-standard ASTM C393 and 2.) ASTM D7136. Further explanation as to why is given in section 3.3. The amount resin required for both panels are presented in Table 3.2. For every infusion run, an extra 150 g was added into the mixture to account for resin that would be absorbed by the peel ply, flow media mesh and inlet / outlet pipes.

Table 3.2 Amount of resin used per panel. (ns: non – standard)

	Panel	Resin (g)	Hardener (g)	Total (g)
ASTM C393 (ns)	RCF	384.6	115.4	500
	CSMG	269.23	80.77	380
ASTM D7136	RCF	307.7	92.3	400
	CSMG	215.38	64.42	280

Once the mixture is degassed, the vacuum pump is used to apply a pressure of 1 bar through a catch pot before the inlet pipe is opened to draw resin into the bag as shown in Figure 3.3. Upon completion of the process, the laminate was cured at room temperature for 24 hrs as recommended by the technical data sheet provided for the Epoxy. Post curing of the laminate was done in a ThermoScientific oven at 60 °C for 30 mins as a compromise instead of 6 hrs to avoid heating up and melting of the core. Throughout each fabrication, two facesheets of both RCF and CSMG are used at the top and bottom.

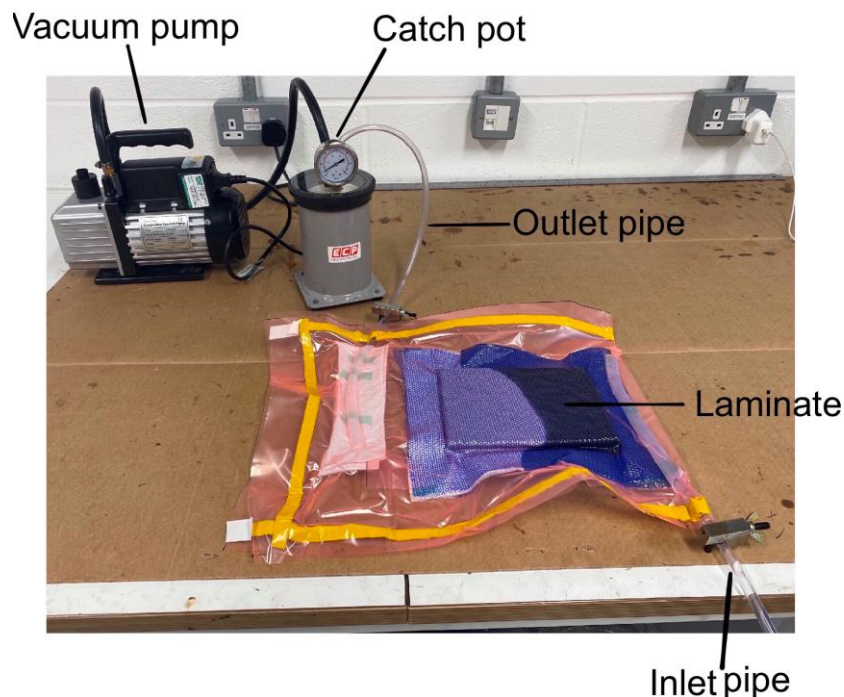


Figure 3.3 Sandwich panel undergoing infusion.

3.3 Experimental Methods

There are two ASTM standards used for panels dimensions. The first is the non-standard ASTM C393 which is used to fabricate the same size of panels for three-point bending and impact samples used to develop a fatigue guideline. The second is the ASTM D7136 standard. This standard was used to analyse the damage response of standard impact size samples under increasing impact energy. The samples are cut-out to required testing size from a large laminate using the Brilliant ATAI 420 machine displayed in Figure 3.4. The sample dimensions are presented in Table 3.3.

Table 3.3 Sample size of cut-out samples for tests

Standard	Sample size (mm)	No. of panels
	RCF	
Non-standard ASTM C393 (Bending / Impact)	150 x 30 x 22	5
ASTM D7136 (Impact)	150 x 100 x 22	3
	CSMG	
Non-standard ASTM C393 (Bending / Impact)	150 x 30 x 17	5
ASTM D7136 (Impact)	150 x 100 x 17	3

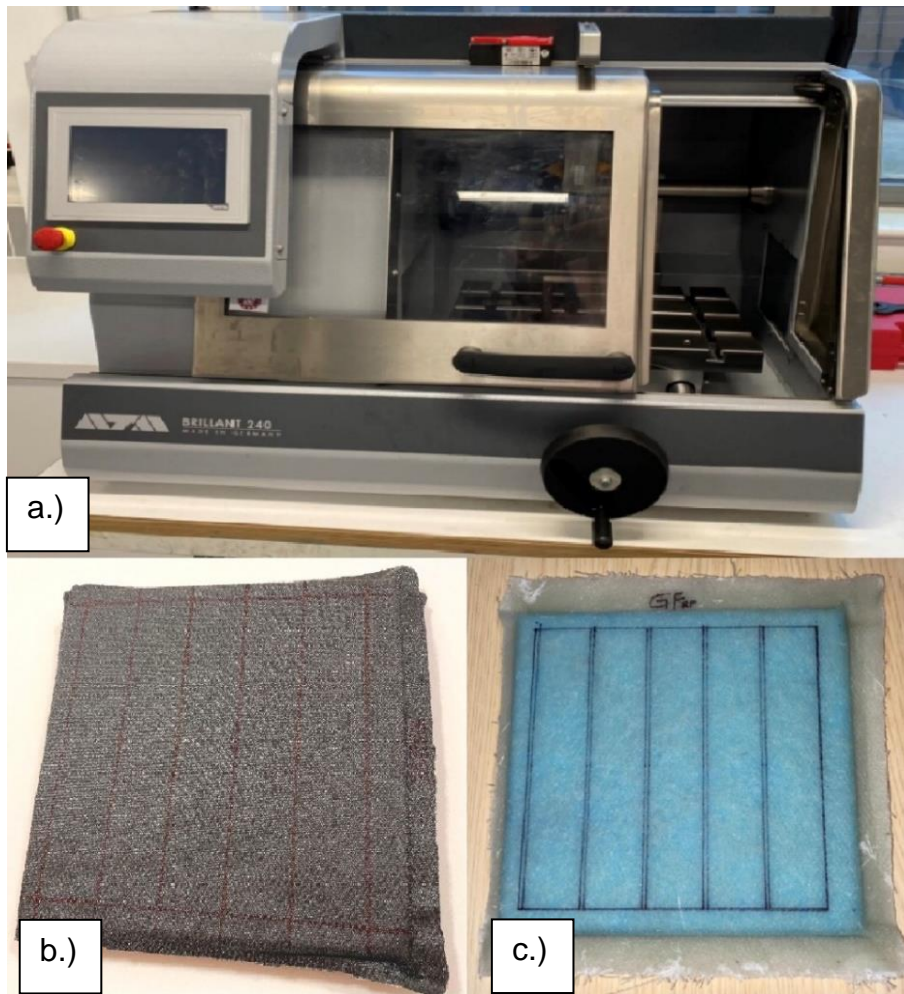


Figure 3.4 a.) Brilliant ATAI 420 cutting machine, b.) RCF, and c.) CSMG sandwich panels ready for cutting.

Sample ID is derived as F-X-N where F is either recycled carbon fibre or the chopped strand glass mat where applicable, X is the experimental test and N is the sample number. The side of the cores for the non-standard samples were marked with gridlines to help with positioning of the samples on the equipment fixtures to reduce reliance on eye positioning. Figure 3.5 shows the cut and marked out samples.

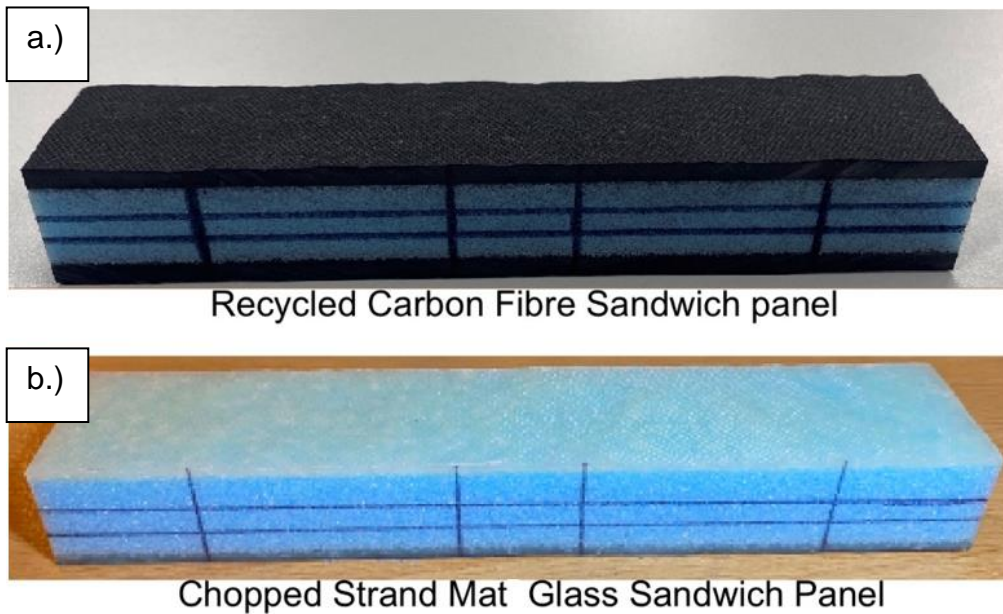


Figure 3.5 Gridlines on cores of a.) RCF and b.) CSMG sandwich panels

Microscopic images were taken using Nikon ShuttlePix P-MFSC stereoscopic microscope with a magnification range from 0.75x to 11. The experimental methods for each experiment are presented in sections 3.3.1, 3.3.2, and 3.3.3.

3.3.1 Fibre Content

The fibre volume fraction of fibres in a composite laminate is derived from the fibre to resin weight ratio. The properties of a composites are controlled by the relative volume of fibre and matrix. By the design of composite structures, volume fractions are used because they can enter directly in the computation of mechanical properties such as stiffness and Young's modulus [51]. The BS ISO 14127:2008 standard was used for the methodology for the fibre volume fraction.



Figure 3.6 a.) High performance microwave digestion system, b.) tubes containing samples.

Small cut-outs of the samples were put into the tubes in Figure 3.6b with Nitric acid, extra pure, 60% solution before putting them into a High-Performance Microwave Digestion System as shown in Figure 3.6a. As recommended by the standard, the specimens were placed in the microwave for 1hr 30 mins at 120 °C. Once the digestion cycle is complete the samples are then repeatedly washed in a conical flask until the acid has been removed as shown in Figure 3.7.

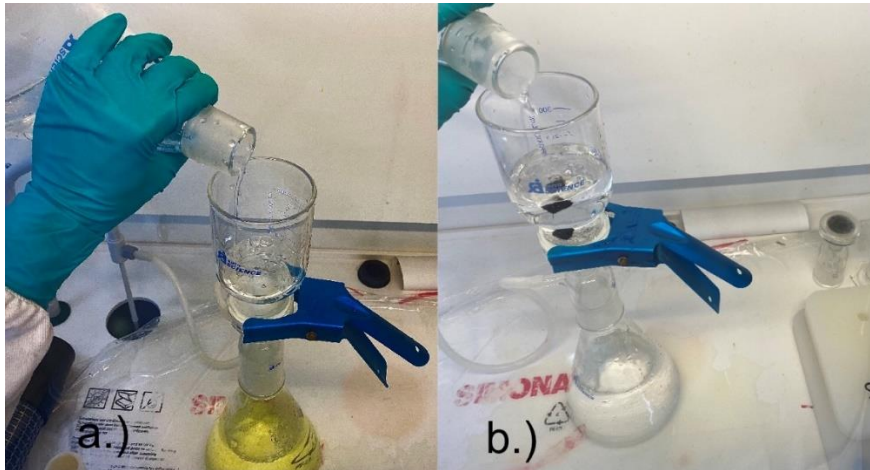


Figure 3.7 a.) Yellow liquid indicating the fibre requiring more washing, b.) clear liquid indicating the fibre is fully clean.

The following equations were used for the volume fraction calculations-

Fiber reinforcement (W_f):

$$W_f = (M_f / M_i) \times 100 \quad \text{Eq(3.3)}$$

Where M_i = initial mass of the specimen and M_f = final mass of the specimen after digestion.

Fibre Content (V_f):

$$V_f = (M_f / M_i) \times 100 \times \rho_c / \rho_r \quad \text{Eq(3.4)}$$

Where ρ_r = density of the reinforcement, g/cm^3 and ρ_c = density of the specimen, g/cm^3 .

Matrix Content (W_m)

$$W_m = (M_i - M_f) / M_i \times 100 \quad \text{Eq(3.5)}$$

Matrix Content, (V_m):

$$V_m = (M_i \times M_f) / M_i \times \rho_c / \rho_m \times 100 \quad \text{Eq(3.6)}$$

Where ρ_m = density of the matrix, g/cm^3

Void Volume, (V_v):

$$V_v = 100 - (V_r + V_m) \quad \text{Eq(3.7)}$$

For this test, specimens were obtained from different places from one panel. Results for the fibre volume fraction are discussed in section 4.1.

3.3.2 Three-Point Bending Tests

The samples tested under three-point bending were fabricated according to recommendations of the non-standard ASTM C393. The three-point bending tests were carried out using the Tinius Olsen H50KT Universal Testing Machine. As displayed in Figure 3.8 b, the sandwich panel is fixed on top of two roller supports that measure 35.06 mm in width and 9.95 mm in diameter. The machine is also equipped with a 5kN load cell which is used to apply force on the sandwich panels.

The machine can send data directly to the Tinius Olsen Horizon software located on a monitor that is connected to the machine. When the software collects data from the machine, it analyses it and displays results on a force deflection curve in real time whilst the sample is being loaded. The 'Method Editor' setting on the software was used to set a controlled displacement rate of 3 mm/min as recommended by ASTM C393. The setting was also used to alert the software to stop the machine loading sandwich panels once the specimens broke and there was a sudden drop from of the peak force. Prior to executing the tests, the force and deflection readings on the software were zeroed as the crosshead is manually lowered as accurately as possible unto each of the specimens using the control keys on the machine as shown in Figure 3.8 c. This is done to avoid adding any preload reading into the results.

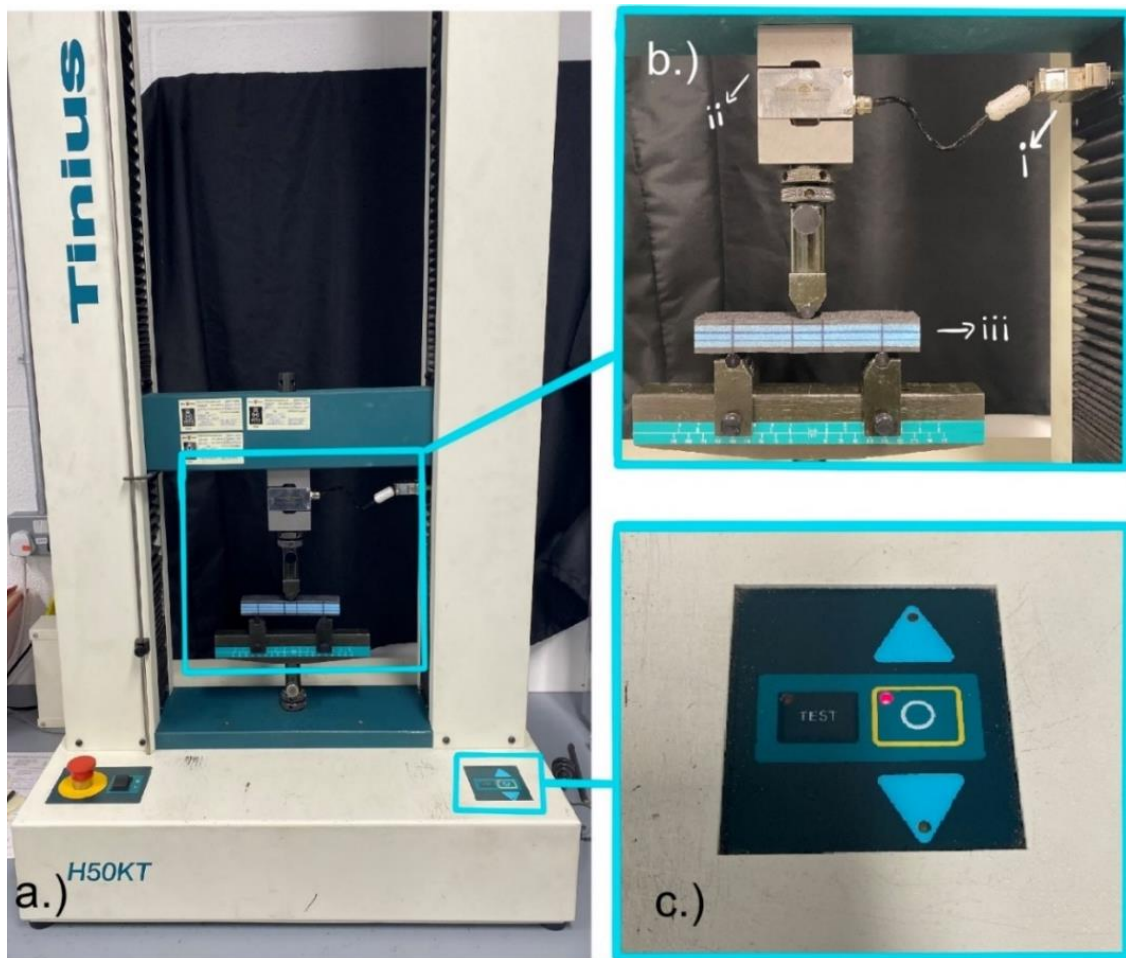


Figure 3.8 a.) Tinus Olsen H50KT Universal Testing Machine, b i.) Load Cell, b ii.) Crosshead b iii.) Sandwich panel placed on supports, c.) Control keys.

3.3.3 Low-velocity Impact Tests

There are two sets of panels fabricated for impact testing. The first set are fabricated using ASTM D7136. These will be tested at 10, 20 and 30 J to analyse the progression of impact damage in standard size samples. The second set are fabricated using the ASTM C393 standard and impacted at 4.5 J. These samples will be used to develop parameters for fatigue after impact test which is further discussed in section 5. The ASTM C393 standard was selected as it is commonly referenced when investigating sandwich panel fatigue in a bending configuration. Parameters such as drop height and impact velocity are automatically calculated by the machine software and have been verified using Eq(2.10) from section 2.4. Table 3.4 contains the input parameters used for the low-velocity impact tests for both non-standard and standard samples.

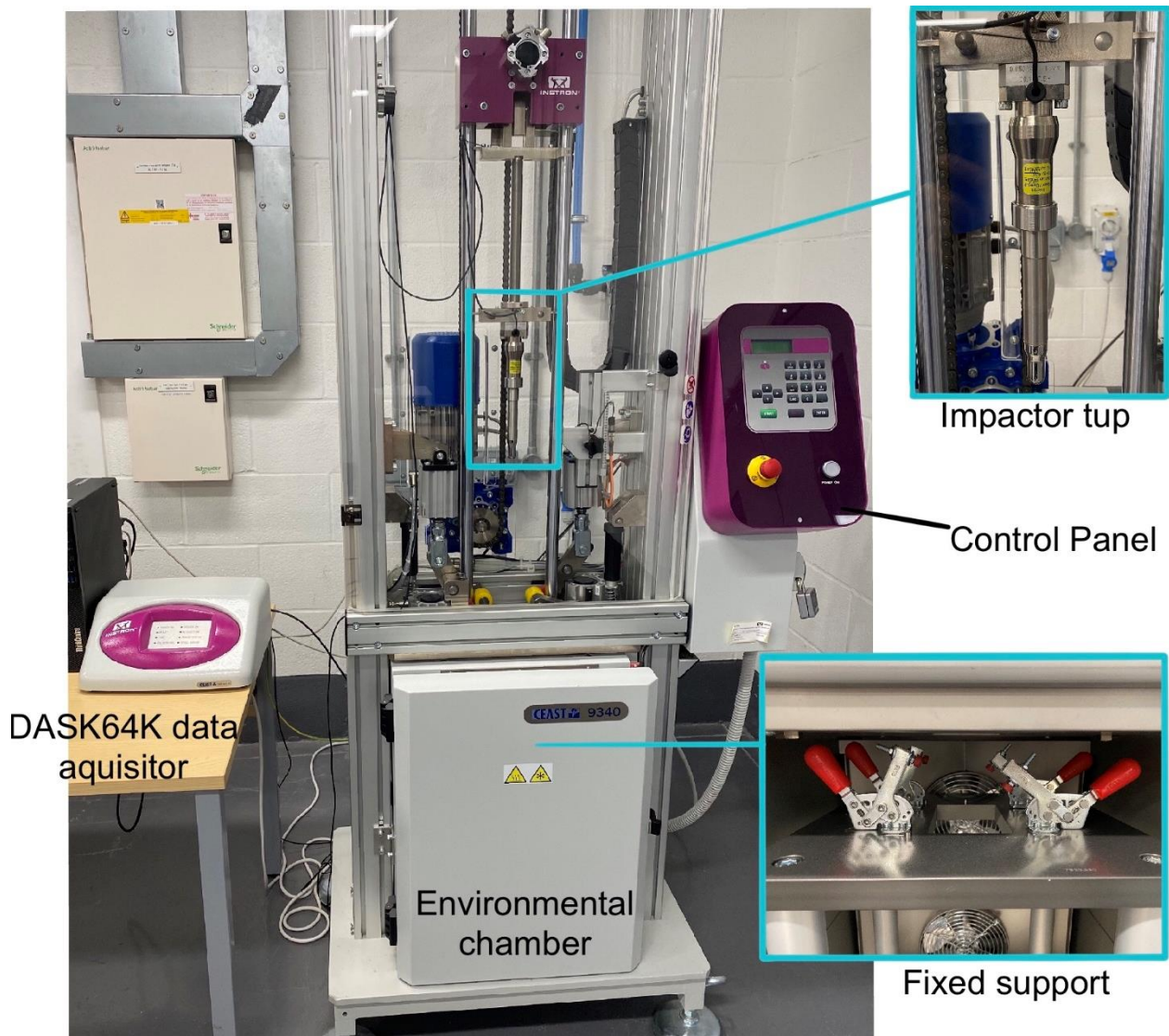


Figure 3.9 Instron CEAST 9340 drop tower impact system

Low-velocity impact tests are carried out at room temperature using the Instron CEAST 9340 drop tower. The impact machine is connected to a monitor where test data is recorded and analysed. Test results are acquired by a DASK64K data acquisition system which is connected in-between the monitor and impact machine. A hemispherical impactor of 16mm in diameter and nominal mass of 3.265 kg was used. The sandwich panels were placed on a fixed height specimen support with dimensions of 76 x 127 mm. The machine's software allows in obtaining impact characteristics of the test such as: total time of impact, the displacement of the impactor and the measurement for the peak force during impact. Hence, force-time, force-displacement and energy-time curves were easily obtained. An anti-rebound mechanism was applied through the software to avoid multiple impacts on the sample after the initial drop.

Table 3.4 Parameters used for low velocity impact tests.

Non-standard samples		
Impact velocity (m/s)	Impact energy (J)	Drop height (mm)
1.65	4.5	260
Standard samples		
2.48	10	312
3.50	20	625
4.29	30	937

CHAPTER 4: RESULTS AND ANALYSIS

4 RESULTS AND ANALYSIS

Due to the difference in thickness between the RCF and CSMG sample at 22 and 17 mm respectively, for comparative purposes, the difference in inertia of the panels is ignored. The experimental results obtained are discussed in this chapter. Firstly, the fibre content for both RCF and CSMG panels are presented and discussed. Secondly, three-point bending results for the RCF and CSMG panels are presented. Following this, results for the samples tested under low-velocity impact are presented.

4.1 Fibre Content

As the panel fabrication method was kept consistent for all the panels, five randomly selected RCF and CSMG specimens were cut out and tested for their fibre volume content. High fibre content in composite structures is usually desirable as it translates to good mechanical performance. The average fibre volume content that was achieved for the RCF and CSMG specimens at 300 gsm are presented in Table 4.1. The values for void content have not been included due to a high uncertainty of the theoretical values for laminate density used for calculation which led to error in final values.

Table 4.1 Average fibre volume content for RCF and CSMG panels

Panel	RCF	CSMG
Avg. fibre content (%)	32 ± 6	53.6 ± 7

As seen in Figure 4.1, the RCF specimens took up more resin than the CSMG specimens as they have a lower value for the fibre content. The values can be analysed using a theoretical expression “(R/r)” by M.E. Messiry on the effects of the ratio of fibre spacing (R) to fibre radius (r) on fibre volume fraction in a laminate [52].

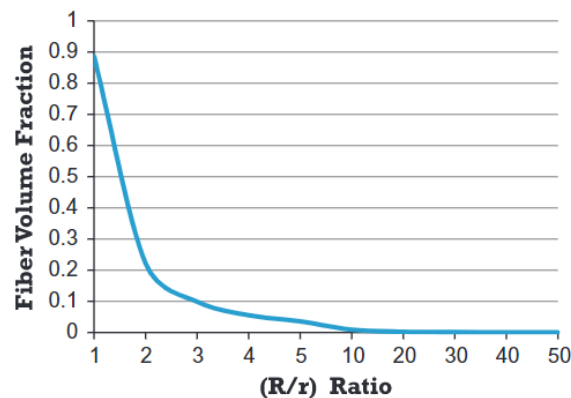


Figure 4.1 fibre volume fraction VS spacing ratio (R/r) [52]

As shown in Figure 4.1, an increase in spacing ratio causes a decrease in the fibre volume fraction. Therefore, it can be assumed that the spacing ratio in the RCF samples are higher than the CSMG samples.

Due to the difference in the fibre volume fraction of the RCF and CSMG specimens, data obtained for three-point bending and impact will be normalised at 50% of the fibre volume fraction for comparison.

4.2 Three-point Bending Tests

The RCF and CSMG samples tested under three-point bending all share the same span length of 100 mm. The failure modes and experimental results for the RCF and CSMG samples are presented and discussed in section 4.2.1 and 4.2.2. A comparative summary is then presented in 4.2.3. During three-point bending, the stresses experienced in a panel causes the core to exhibit shear failure as this component typically has a significantly lower modulus than the facesheet. Hence, the stresses for the facesheet and core are calculated separately. An illustration for the parameters required for calculating facesheet and core stress are presented in Figure 4.2.

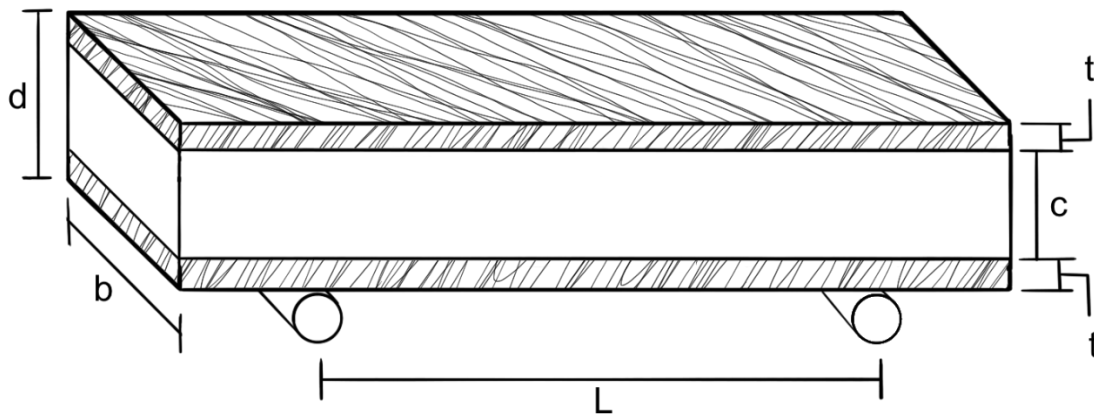


Figure 4.2 Parameters required for calculating sandwich panel stress.

The equations for both are outlined in ASTM D7249 and ASTM C393 respectively and are described as:

Facesheet stress (ASTM D7249) [53]:

$$F_1^u = \frac{P_{max}L}{2(d+c)bt_1} \quad \text{Eq(4.1)}$$

$$F_2^u = \frac{P_{max}L}{2(d+c)bt_2} \quad \text{Eq(4.2)}$$

Where F_1^u is the upper facesheet ultimate stress, F_2^u is the bottom facesheet ultimate stress, P_{max} is the maximum force before failure, L is the panel span length, d is the sandwich thickness, c is the core thickness, b is the width, t_1 is the thickness of the top facesheet and t_2 is the thickness of the bottom facesheet.

Core shear stress (ASTM C393) [54]:

$$\tau_{max} = \frac{P}{(d + c)b} \quad \text{Eq(4.3)}$$

Where τ_{max} is the maximum core shear stress.

4.2.1 RCF Panels

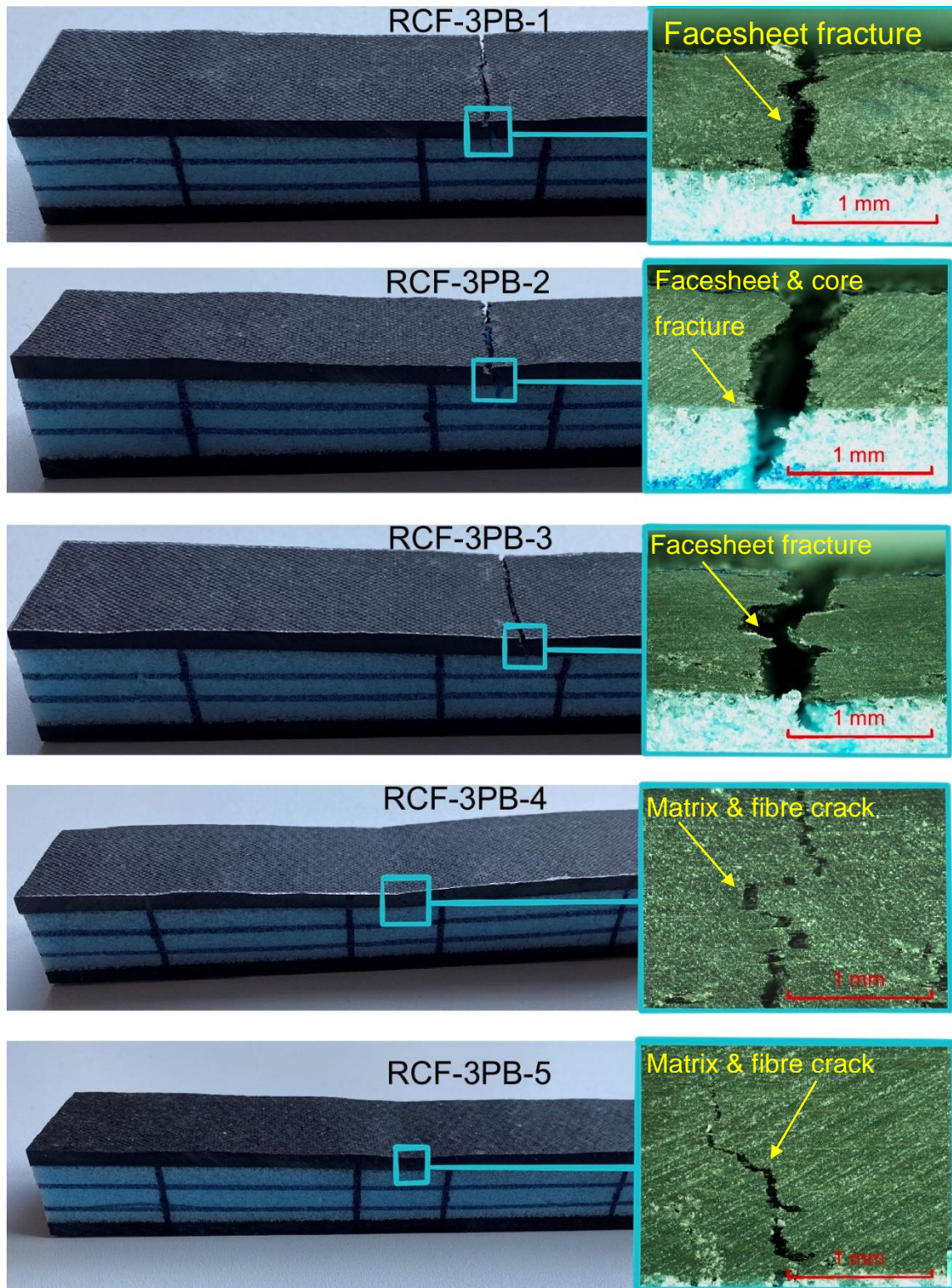


Figure 4.3 RCF samples post-loading.

As seen in Figure 4.3 sample RCF-3PB-1 up to samples RCF-3PB-3 display visible top facesheet indentation and fracture failure. Although sample RCF-3PB-4 and RCF-3PB-5 appear to exhibit only indentation of the top facesheet, microscopic imaging reveals matrix

and fibre crack at the centre of the panels. Minimal core crushing is also observed for all the RCF panels.

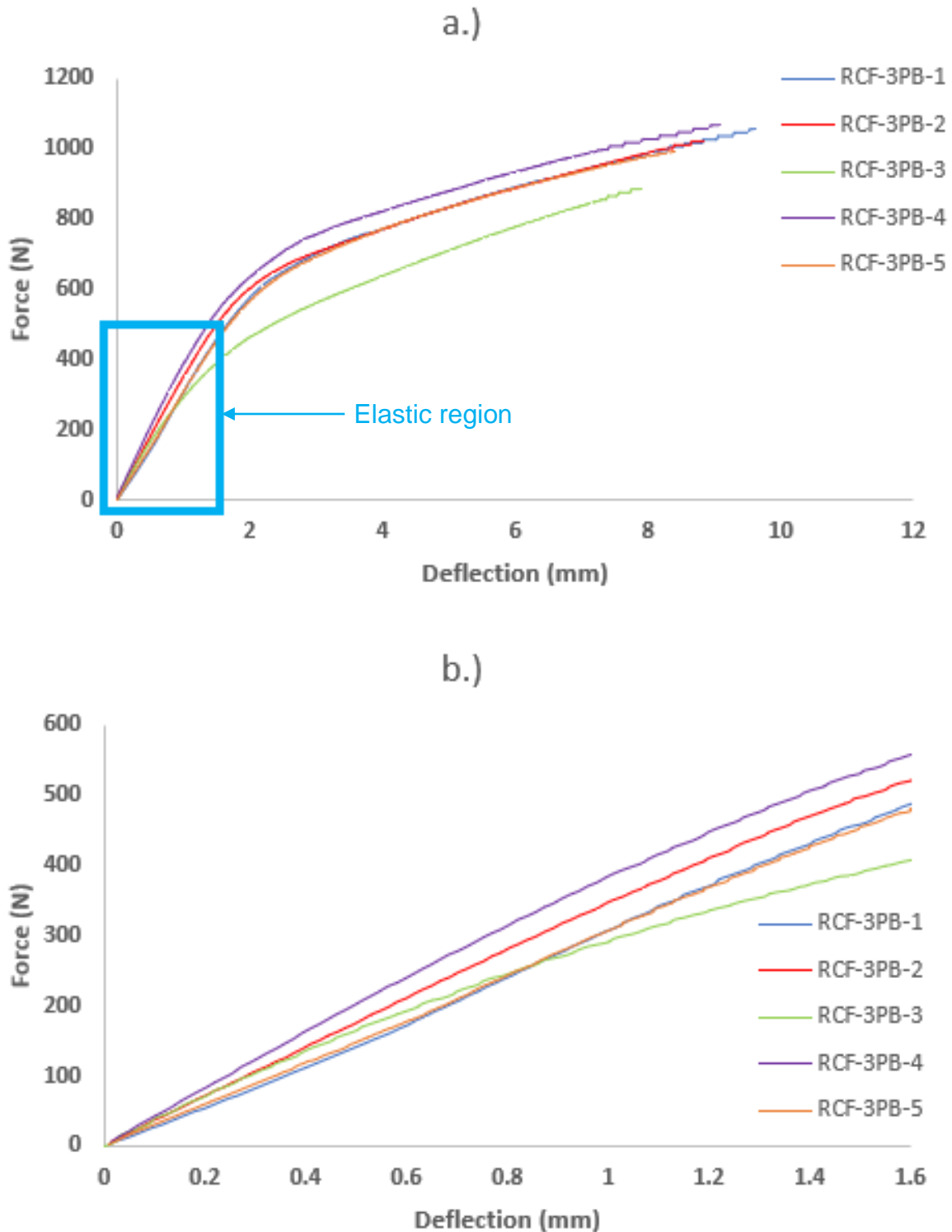


Figure 4.4 a.) Force-deflection curves for RCF samples, b.) Elastic region of RCF panels

As seen in Figure 4.4a, when the load is initially applied onto the RCF specimens, their force-displacement curves appear to display an almost non-linear start. At 100 mm span-

length, an observable specimen failure mode during each test was notably the sound of crack propagation initiating at the top facesheet within 440 N – 600 N of loading. This continues until the ultimate failure force within 1070 N – 1130 N for the RCF. At this point, the top facesheet of the RCF samples are observed to fail by fracture into the core. Throughout each test the bottom face sheet remained slightly indented but still intact. The results for the ultimate force and maximum deflection of the samples are presented in Table 4.2.

Table 4.2 Results for: maximum deflection (δ_{max}), ultimate force (F_{ult}), facesheet stress (F_1^u & F_2^u) and core shear stress (τ_{max}) for RCF panels

	Panel	δ_{max} (mm)	F_{ult} (N)	F_1^u & F_2^u (MPa)	Core τ_{max} (MPa)
	RCF-3PB-1	10	1070	11.9	1
	RCF-3PB-2	10	1070	11.5	0.9
	RCF-3PB-3	10	1130	10	0.8
	RCF-3PB-4	8.96	1110	12	1
	RCF-3PB-5	9.52	1108	11.2	0.9
Average		9.70 ± 0.5	1097.6 ± 26	11.32 ± 0.8	0.92 ± 0.08

An estimate of the elastic region in Figure 4.4b of the RCF samples is obtained from the region highlighted by the blue box in Figure 4.4a. The samples reach their limit of elasticity after which they move into plastic deformation and eventually fracture.

4.2.2 CSMG Panels

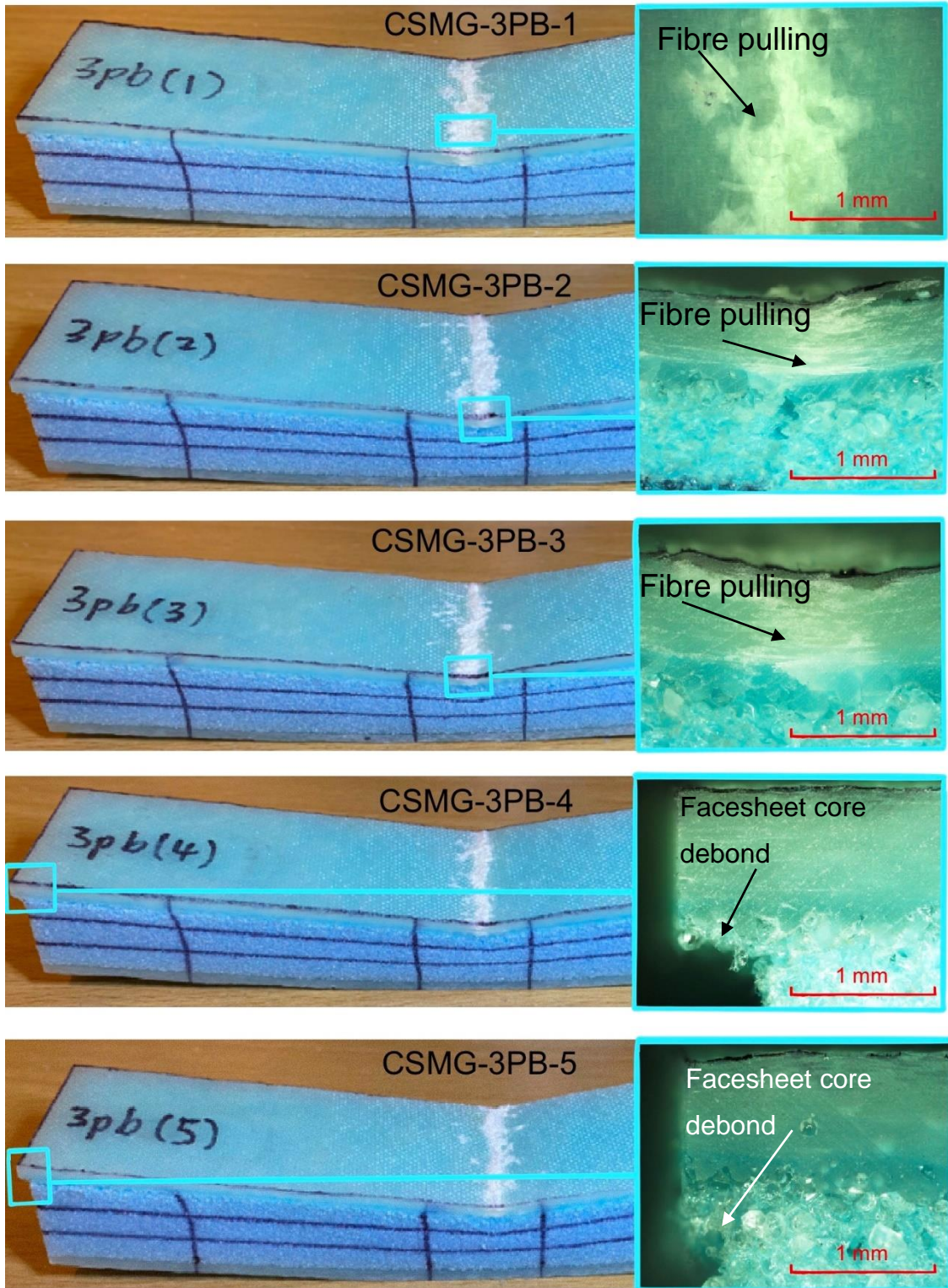


Figure 4.5 CSMG samples post bending

The failure modes observed for samples CSMG-3PB-1 to CSMG-3PB-5 are indentation and fibre pulling of the top facesheet, core crushing, bottom facesheet indentation and core facesheet debonding as highlighted for the microscopic images for CSMG-3PB-4 and CSMG-3PB-5.

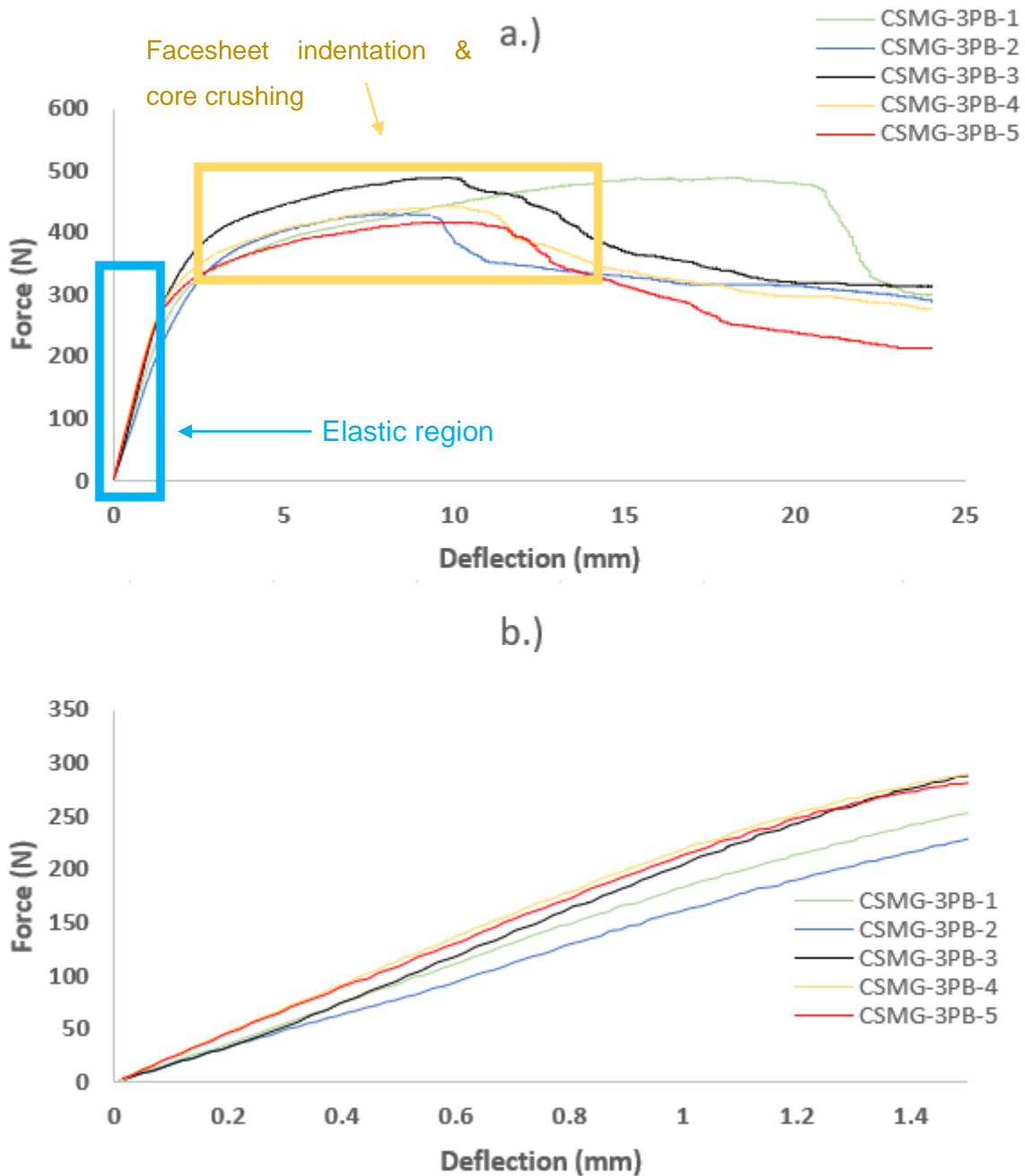


Figure 4.6 a.) Force-deflection curves for CSMG samples, b.) Elastic region of CSMG panels

In Figure 4.6a, the initiation of facesheet fracture in the CSMG panels start after 258 - 305N of loading. Following this is plastic deformation in the form of indentation of the top face sheet and crushing of the core in the region highlighted in yellow. The tests for the CSMG samples were programmed to stop loading just before 25 mm deflection as the ductile nature of the CSMG fibre would allow for continuous deformation of the panels. The results for the ultimate force and maximum deflection of the samples are presented in Table 4.3.

Table 4.3 Results for: maximum deflection (δ_{max}), ultimate force (F_{ult}), facesheet stress (F_1^u & F_2^u) and core shear stress (τ_{max}) for CSMG panels.

	Panel	δ_{max} (mm)	F_{ult} (N)	F_1^u & F_2^u (MPa)	Core τ_{max} (MPa)
	CSMG-3PB-1	24	476	15	0.3
	CSMG-3PB-2	24	420	15	0.3
	CSMG-3PB-3	23.7	482	16.3	0.3
	CSMG-3PB-4	23.5	398	14.4	0.3
	CSMG-3PB-5	24	395	11.2	0.2
Average		23.8 ± 0.2	434.2 ± 42	14.38 ± 1.9	0.28 ± 0.04

On average the ultimate force for the RCF samples is about twice that of the CSMG samples. on the other hand, the maximum deflection of the CSMG panels is about twice that of the RCF panels.

4.2.3 Comparative Summary

A graphical comparison for the average force, deflection, and stress values for both the RCF and CSMG panels can be found in Figure 4.7. From this, a few points can be drawn:

- The RCF panels can withstand double the applied force of the CSMG panels in Figure 4.7a. However, due to the ductile nature of glass fire, the CSMG panels can bear the applied force at twice the deflection of the RCF panels in Figure 4.7b.
- The CSMG panels having greater value for deflection also mean that their facesheets would undergo higher stress than the RCF panels as shown in Figure 4.7c.

In Figure 4.7d the average core shear stress for both panel groups can be explained using the visual observations in Figure 4.3 and Figure 4.5:

- The high stiffness in of the RCF facesheet mean that it is likely to slide over the core causing it to shear than crush it as seen in Figure 4.7d. This is highlighted in Figure 4.3 where the vertical lines on the core appear slanted at an angle.
- The stiffness of the CSMG facesheets are so low that during three point loading the core crushing becomes the dominant failure mode of the CSMG panels. Hence a low value for the core shear stress. This is evident throughout Figure 4.5 as the horizontal gridlines curve upwards.

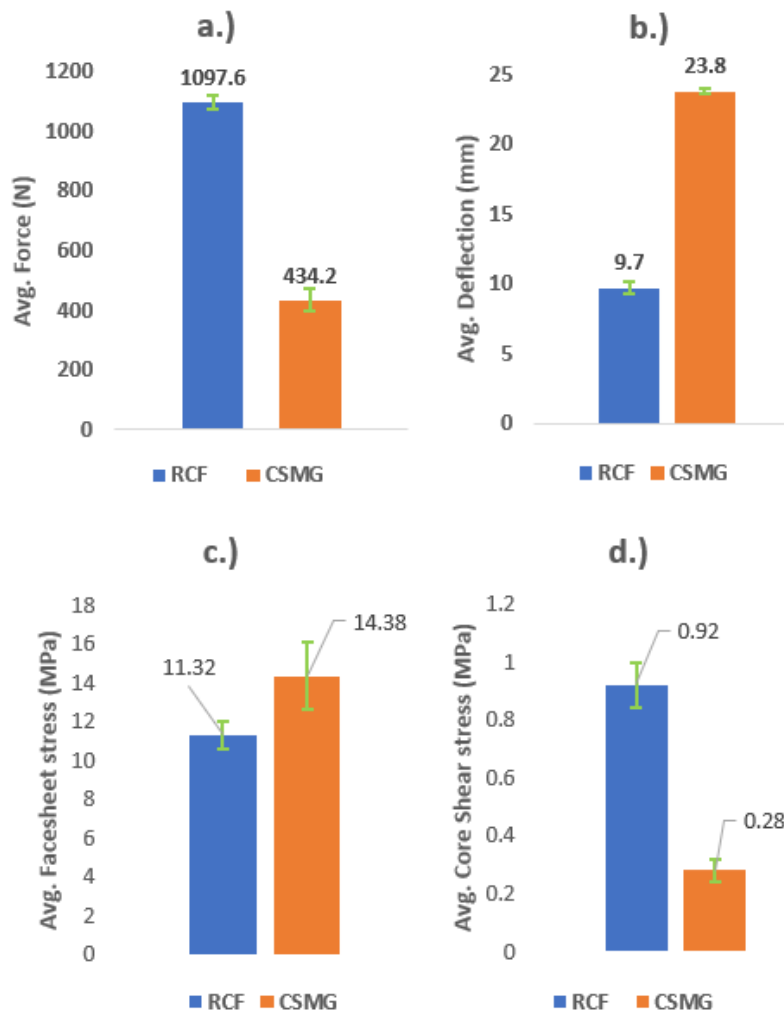


Figure 4.7 Average comparison of a.) force and b.) deflection c.) facesheet stress and d.) core shear stress

The normalised values for the average ultimate force, average facesheet stress and average core shear are presented in Table 4.4. As shown in Table 4.4, at 50% normalised fibre volume fraction, the RCF panels still have higher strengths and core shear than the CSMG panels.

Table 4.4 normalised three-point bending data.

Panel	F_{ult} (N) @ 50% FVF	F_1^u and F_2^u (MPa) @ 50% FVF	Core τ_{max} (MPa) @ 50% FVF
RCF	1715 ± 20	17.7 ± 0.7	1.43 ± 0.07
CSMG	405 ± 37	13.4 ± 1.7	0.26 ± 0.04

4.3 Impact Tests

As mentioned previously in section 3.3.3, the samples in this section are fabricated to assess the impact damage progression of RCF and CSMG panels at 10, 20 and 30 J of impact energy. Three samples of RCF and CSMG were fabricated with total thickness of 22 and 17 mm respectively and cut to measure 150 x 100 mm as recommended by ASTM D7136. The failure modes and experimental results per impact energy for each sample are presented and discussed in section 4.3.1 through to section 4.3.4. (Note: the SI in the specimen ID in section 4.3.1 to 4.3.4 means Standard size Impact panels.)

4.3.1 Samples Tested at 10 J

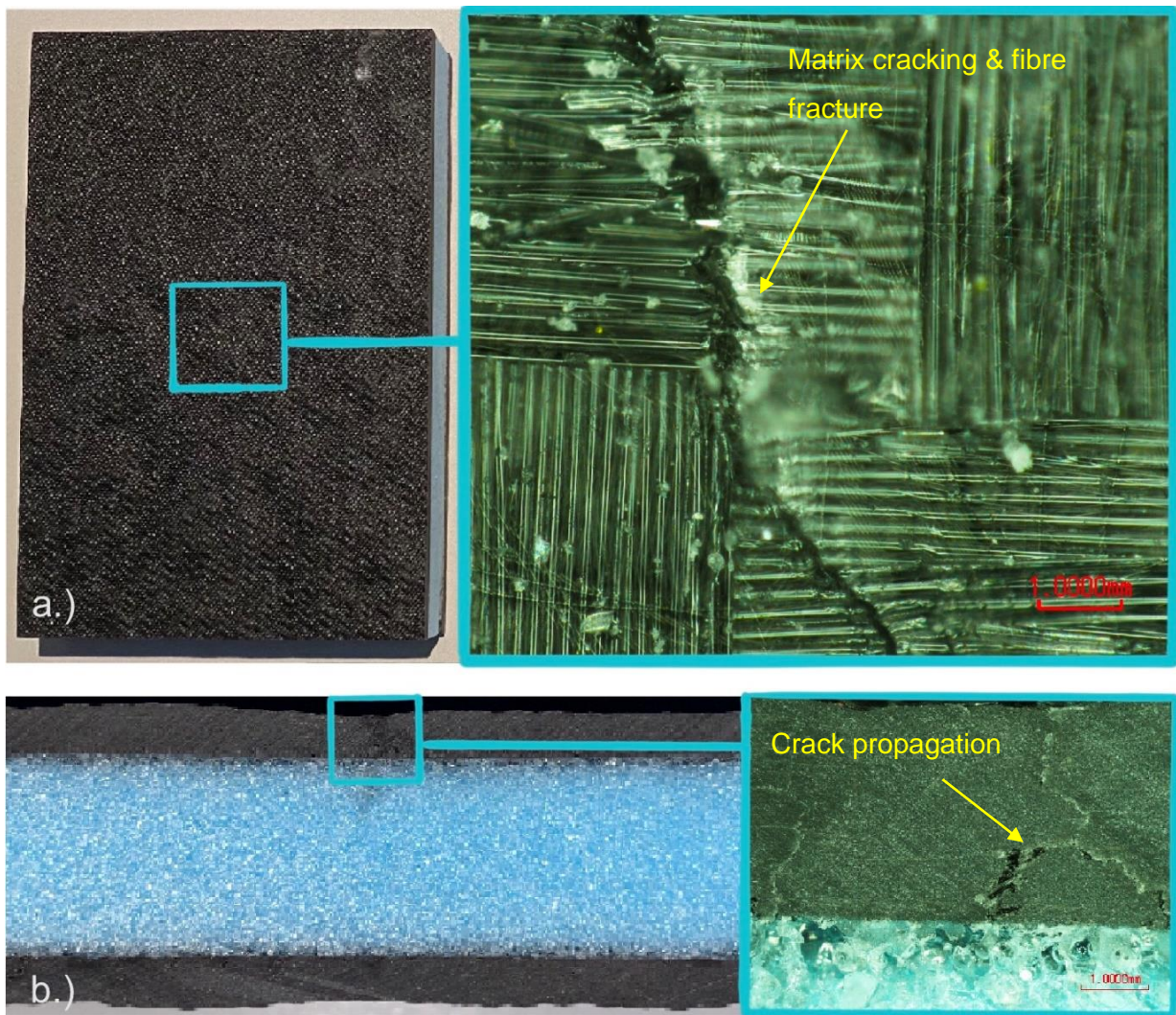


Figure 4.8 a.) Top facesheet view with microscopic image and b.) cross sectional view with microscopic image of impacted RCF panel at 10 J

As shown in Figure 4.8a, RCF-SI-1 panel exhibits barely visible damage at 10 J. Closer observation in the microscopic image reveals matrix cracking and fibre fracture at the area of impact. The crack also propagates through RCF-SI-1 facesheet as shown in the cross-

sectional view and microscopic image in Figure 4.8 b. Both core and facesheet also appear to be intact.

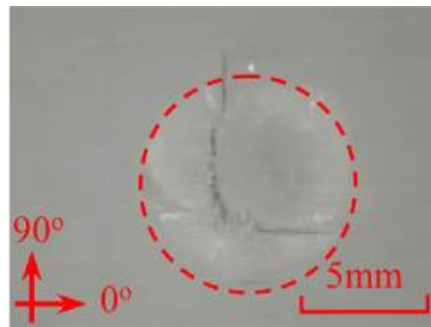


Figure 4.9 Impacted CFRP sample exhibiting fibre fracture at 10 J[55]

Similar observations for the top facesheets impacted at 10 J have been made by W. He et al in Figure 4.9, on CFRP sandwich structures of similar dimensions with aluminium honeycomb cores [55].

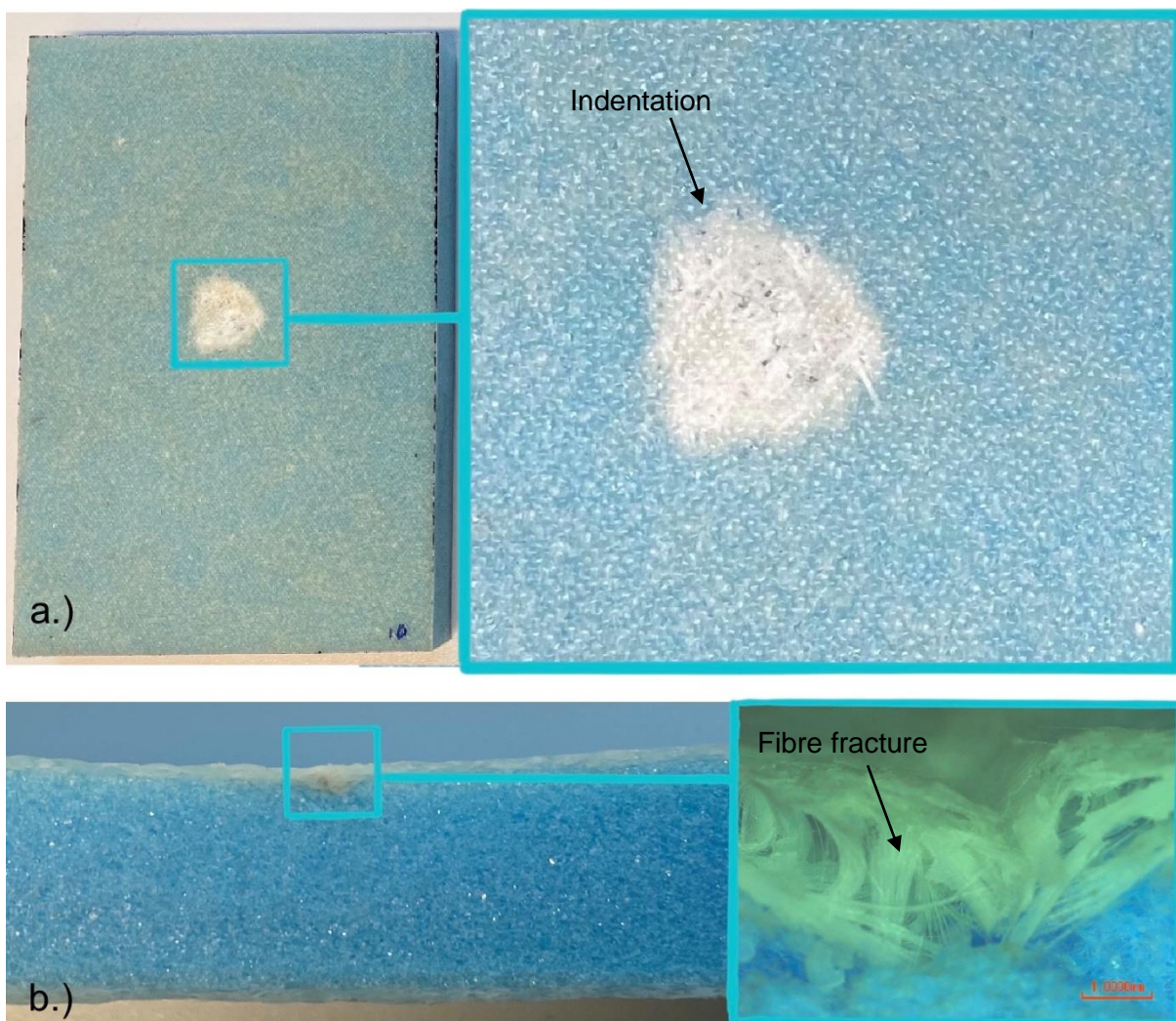


Figure 4.10 Top facesheet view with microscopic image and b.) cross sectional view with microscopic image of impacted CSMG panel at 10 J

At 10 J, the CSMG damage area and fibre fracture is more apparent on the top facesheet in Figure 4.10a. The cross-sectional view of the top facesheet in Figure 4.10b exhibits indentation along with fibre fracture and matrix cracking highlighted by the microscopic image. Just like the FRP panels, both core and facesheet for the CSMG panels remain intact. RCF-SI-1 generally Force-displacement, Force-time, and Energy-time curves of follow similar profile of tested CFRP samples by H. We et al [55].

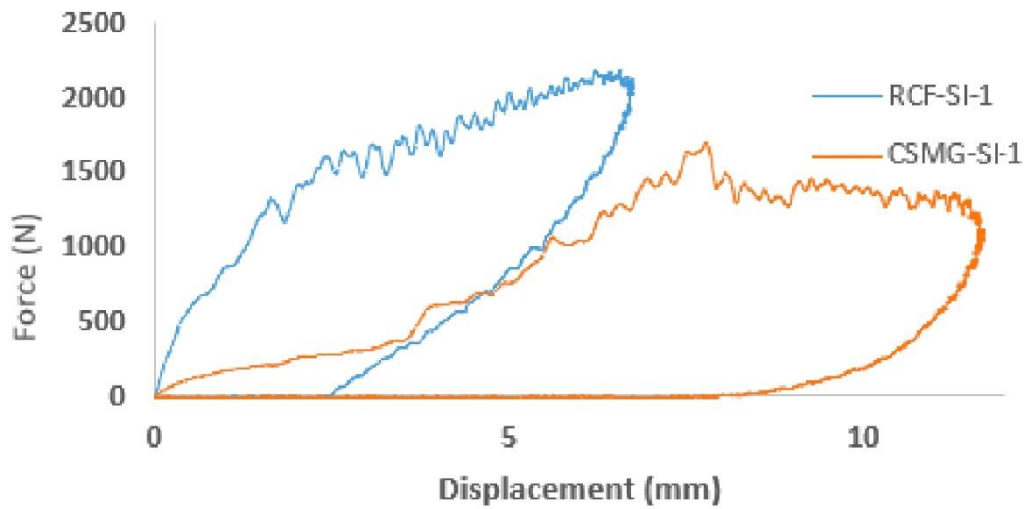


Figure 4.11 Force-displacement curve for RCF-SI-1 and CSMG-SI-1 at 10 J

Figure 4.11 shows the combined force-displacement curve for RCF-SI-1 and CSMG-SI-1. At 10 J, CSMG-SI-1 is impacted at almost twice the displacement than RCF-SI-1 but at a lower force. The impact force for the RCF-SI-1 rises much quicker than for CSMG-SI-1 at approximately 600 N.

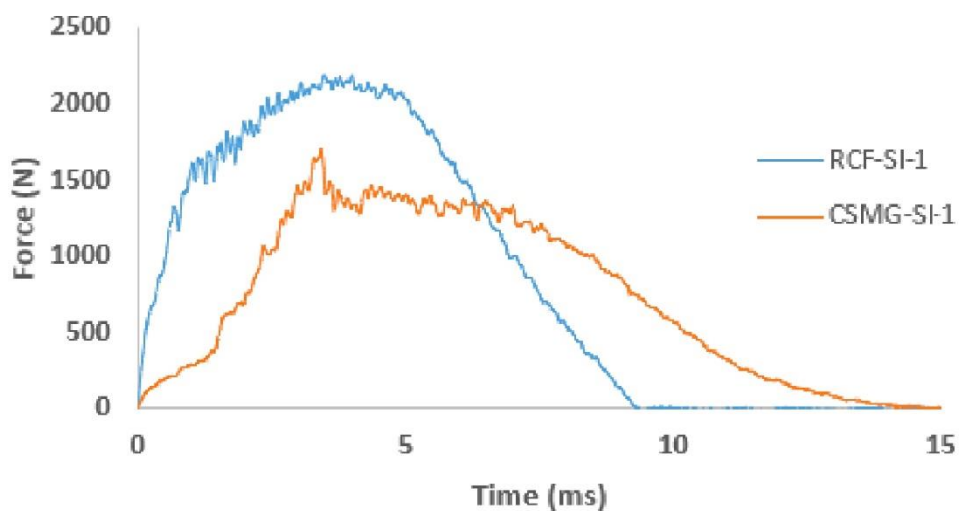


Figure 4.12 Force-time curve for RCF-SI-1 and CSMG-SI-1 at 10 J

Similarly, in Figure 4.12 RCF-SI-1 reaches its peak displacement quicker than its force-time history is smaller than that of CSMG-SI-1. The loading during the impact event also happens for a shorter time for RCF-SI-1 than CSMG-SI-1.

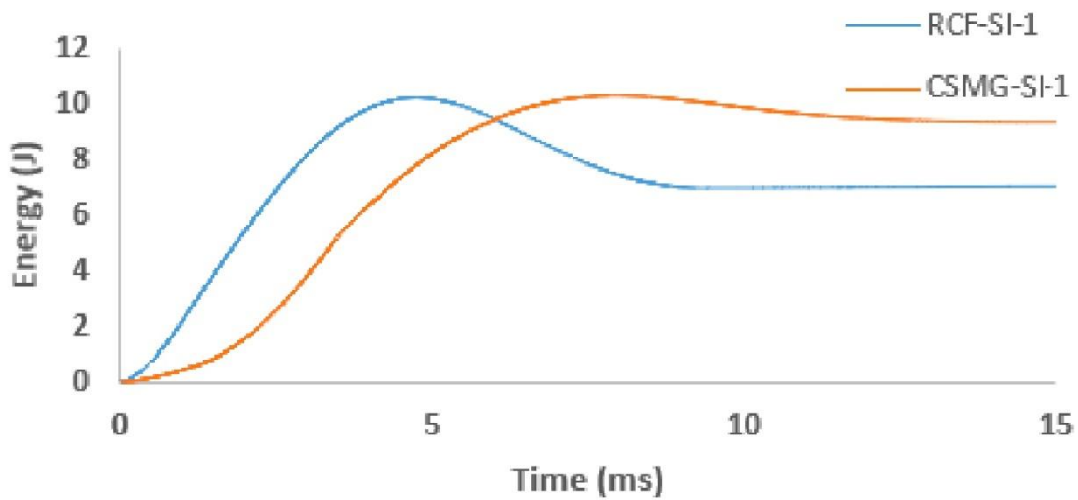


Figure 4.13 Energy-time curve for RCF-SI-1 and CSMG-SI-1 samples at 10 J

During testing for RCF-SI-1 and CSMG-SI-1, the impactor rebounded before the anti-rebound system in the machine kicks in to stop it. As seen in Figure 4.13 the overall energy appears to be absorbed and the prolonged plateau for CSMG-SI-1 is related to further expansion of fibre breakage and matrix cracking for the top facesheet. Hence, it absorbed more energy than the RCF-SI-1.

4.3.2 Samples Tested at 20 J

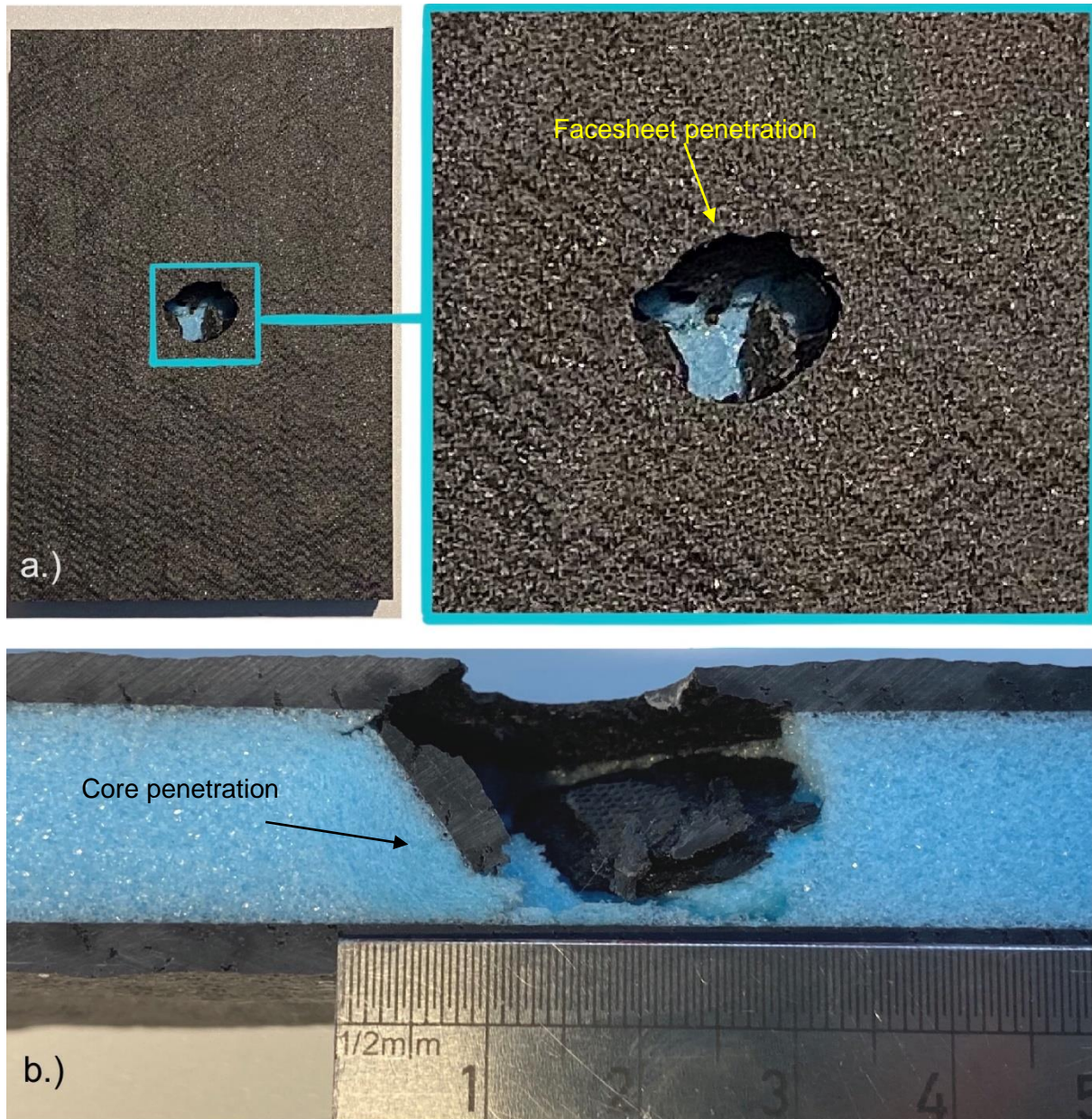


Figure 4.14 Top facesheet view and b.) cross sectional view of impacted RCF specimen at 20 J
At 20 J the top facesheet of the RCF-SI-2 in Figure 4.14a gets penetrated by the impactor with the damage area almost having the same diameter as the impactor at 17 mm. In the process of impactor penetration, the core also gets crushed with internal damage of approximately 33mm in Figure 4.14b.

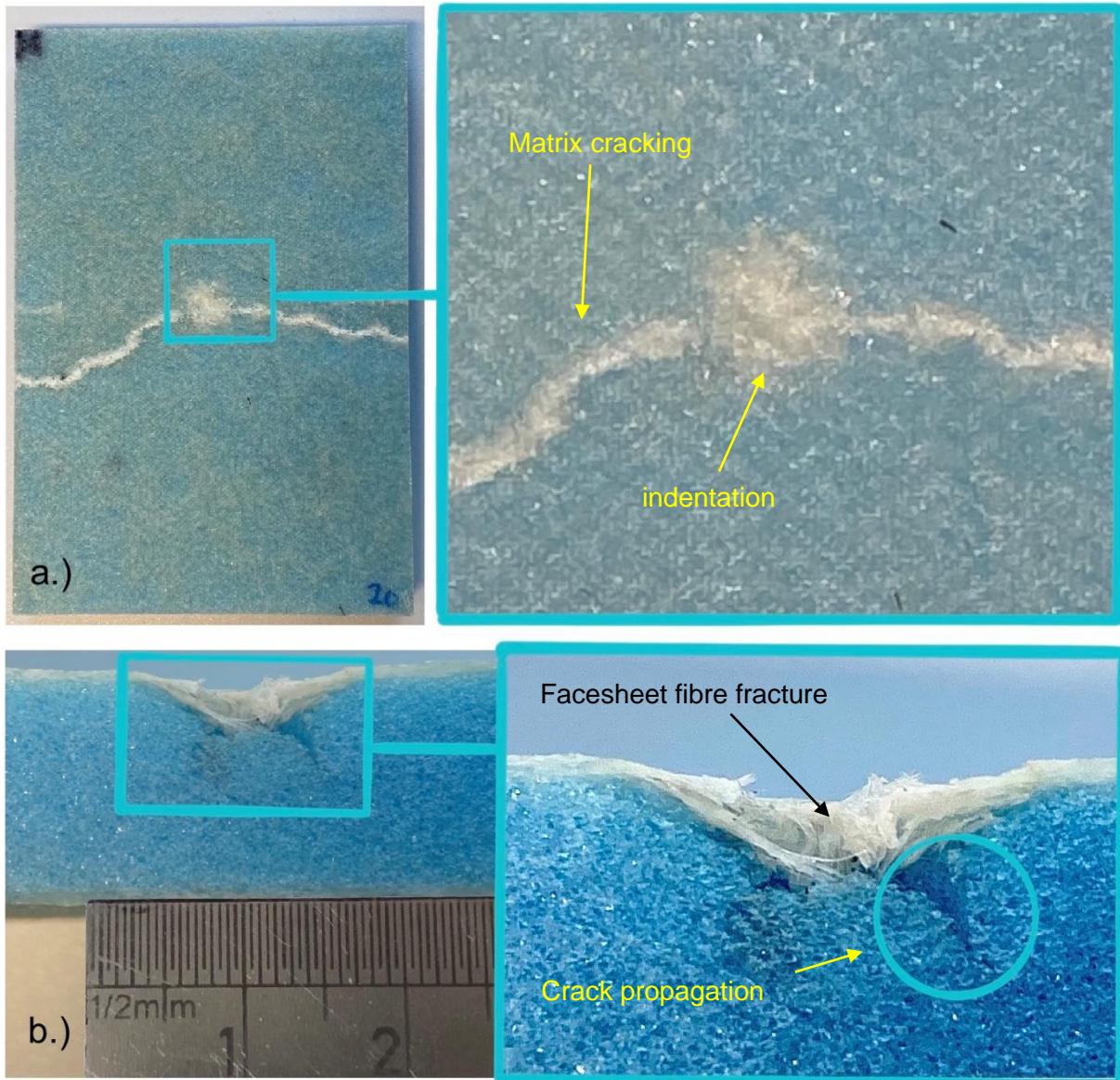


Figure 4.15 a.) Top facesheet view and b.) cross sectional view of impacted CSMG specimen at 20J

The top facesheet of sample CSMG-SI-2 in Figure 4.15a at 20 J disperses the energy across its surface through matrix cracking which results in the crack propagation extended from the impact area. Unlike sample RCF-SI-2, sample CSMG-SI-2 in Figure 4.15b appears to be able to absorb the impact energy better at 20 J as the facesheet exhibited indentation failure with little crack propagation into the core as highlighted by the circle. The fibre fracture is also more apparent in the highlighted cross-sectional view in Figure 4.15b.

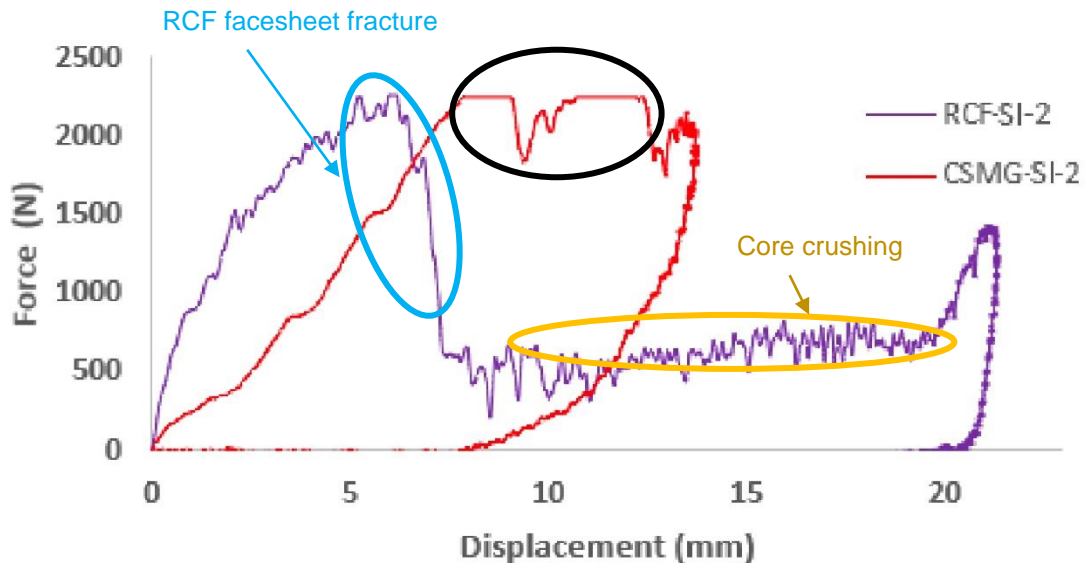


Figure 4.16 Force-displacement curve for RCF-SI-2 and CSMG-SI-2 at 20 J

The force-displacement curve for RCF-SI-2 and CSMG-SI-2 is presented in Figure 4.16. The top facesheet fracture that RCF-SI-2 undergoes is highlighted by the blue oval which is then followed by core crushing highlighted by the yellow oval. This is followed by impactor rebound. A unique situation for CSMG-SI-2 is highlighted by the black oval. The first plateau suggests that the facesheet has reached a critical point in bearing load. The delay before the drop in force is where the matrix begins to crack across the surface of the facesheet as seen in Figure 4.15a. This then leads to the fibre fracture observed in Figure 4.15b. The increase in force up to the second plateau is a result of the core and bottom facesheet stiffness and the drop in force occurs when cracks start to propagate in the core as seen in Figure 4.15b. The impactor eventually rebounds, and the force drops to zero.

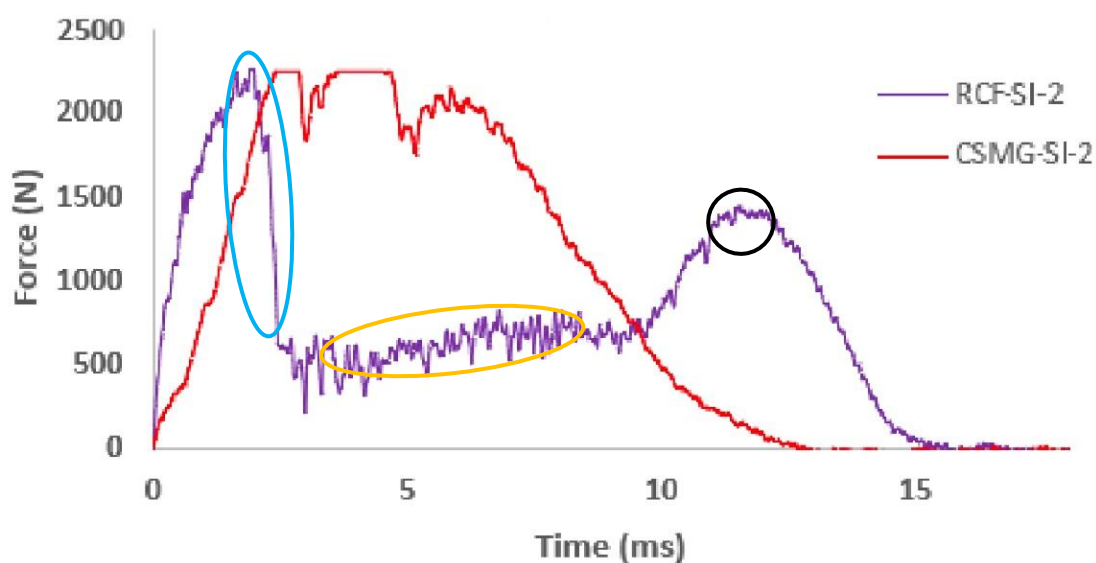


Figure 4.17 Force-time curve for RCF-SI-2 and CSMG-SI-2 at 20 J

The force-time curve for RCF-SI-2 and CSMG-SI-2 is presented in Figure 4.17. The blue oval highlights that sample RFC-SI-2 undergoes penetration of its top facesheet and eventually core crushing in the yellow oval. The black circle suggests the residual kinetic energy is transferred unto the bottom facesheet for RCF-SI-2 hence a second force peak increases. The CSMG-SI-2 panel reaches a point of maximum load bearing capability twice before eventually being unloaded.

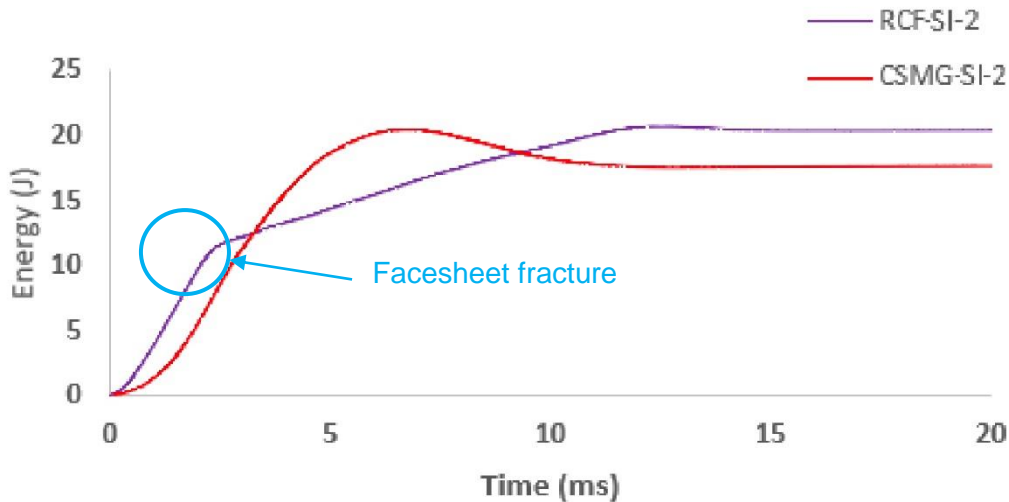


Figure 4.18 Energy-time curve for RCF-SI-2 and CSMG-SI-2 at 20 J

The energy-time curve for RCF-SI-2 and CSMG-SI-2 is presented in Figure 4.18. The sharp upward linear inclination in the blue circle corresponds to the top facesheet fracture of RCF-SI-2 and the core crushing. The second slope corresponds to the energy absorption of the bottom facesheet of RCF-SI-2. As for CSMG-SI-2, the energy-time curve shows a steady increase to the maximum force and eventually a prolonged plateau which corresponds to its overall better energy absorption.

4.3.3 Samples Tested at 30 J

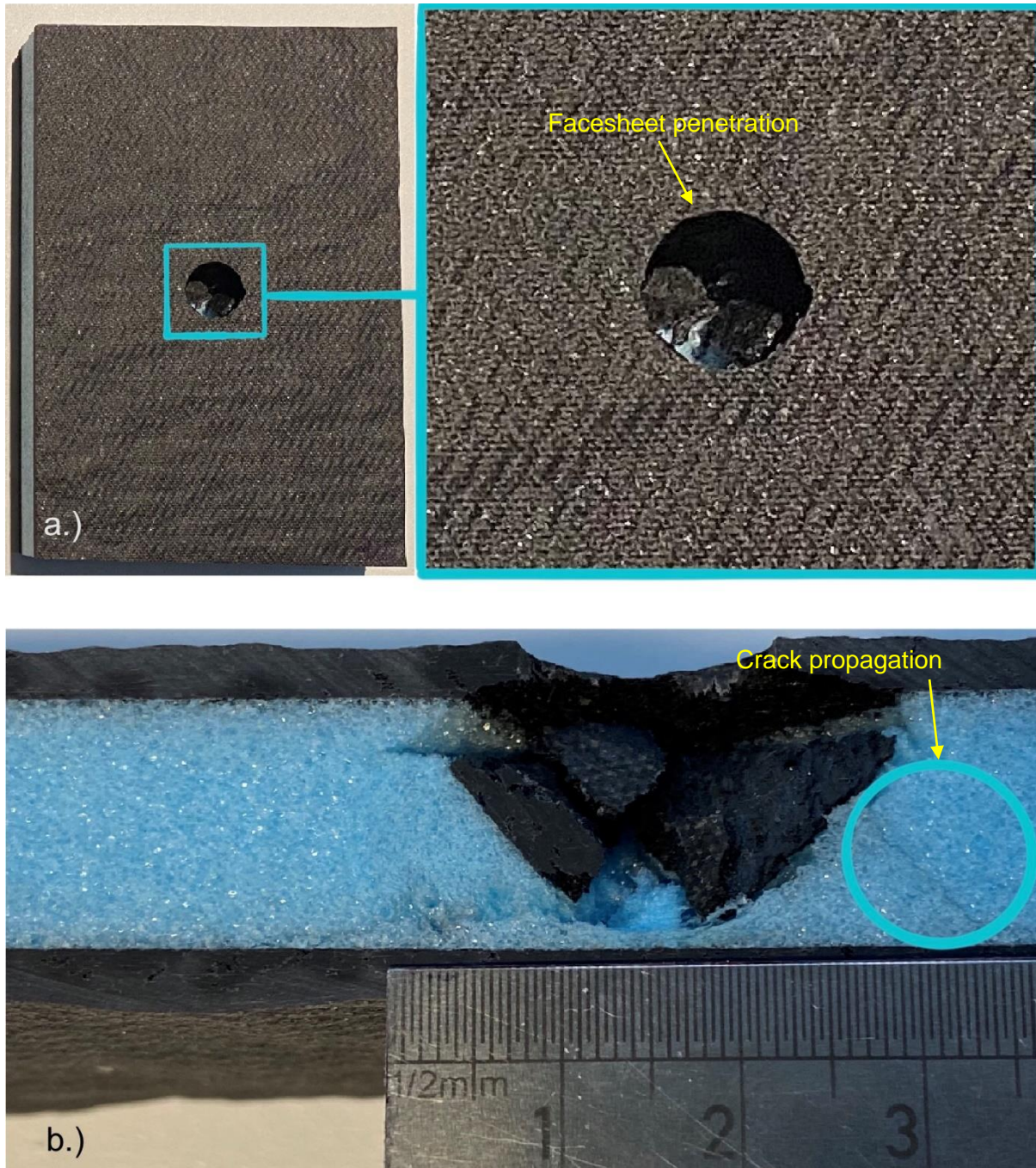


Figure 4.19 Top facesheet view and b.) cross sectional view of impacted RCF specimen at 30 J. At 30 J the same top sheet fracture failure is repeated sample RCF-SI-3 in Figure 4.19a in an almost similar manner to sample RCF-SI-2 in Figure 4.14a. The same can be said for the core crushing after the facesheet fractures. Crack propagation through the thickness of the core highlighted by the circle in Figure 4.19b. The internal damage width came to be approximately 30 mm. the bottom facesheet remained intact.

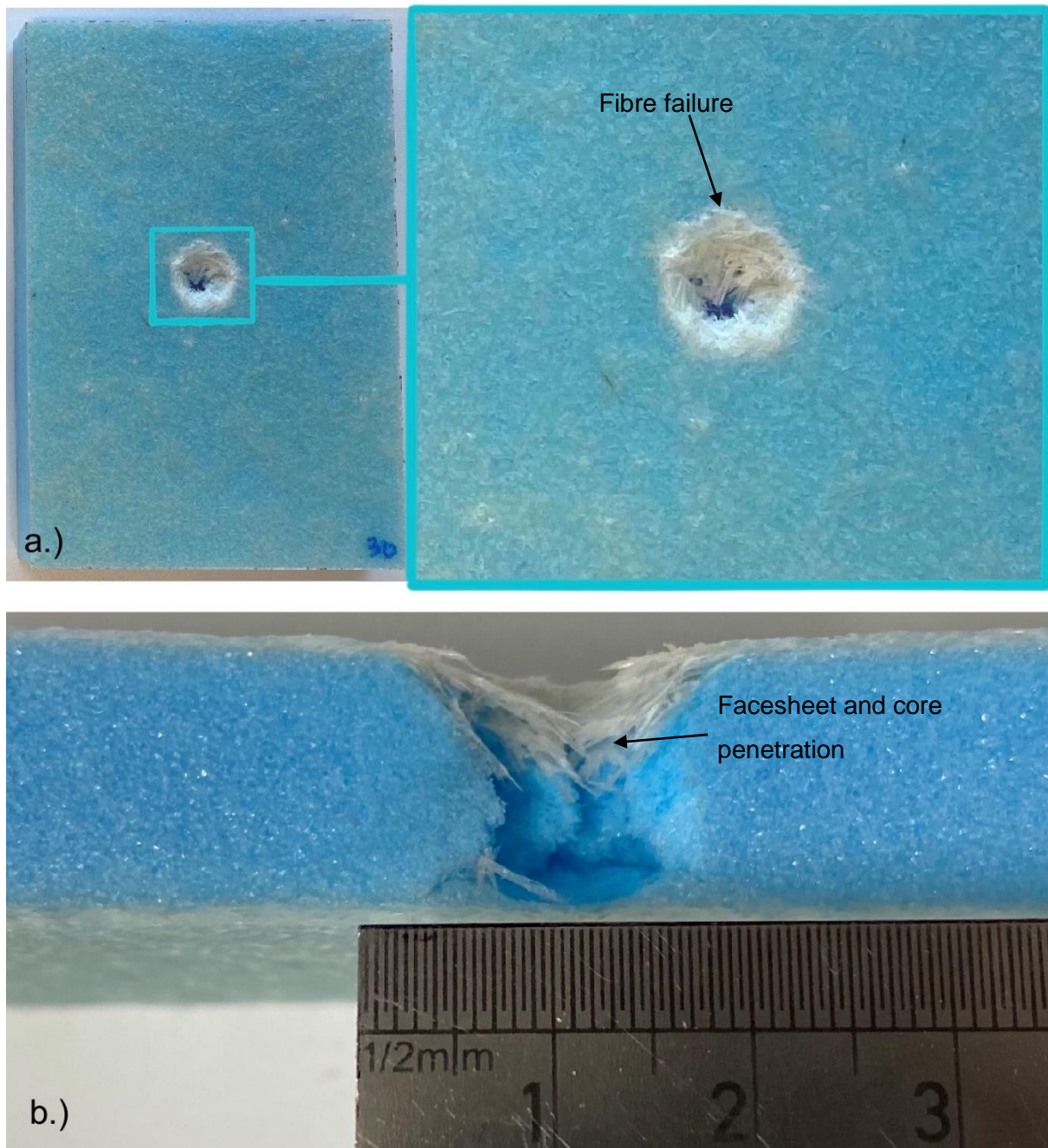


Figure 4.20 Top facesheet view and b.) cross sectional view of impacted CSMG specimen at 30 J. In Figure 4.20, At 30 J the GSMG-SI-3 exhibited facesheet and core penetration. However, the damage area of the impact zone appears smaller than that of the RCF panels at 20 J and 30 J as it came out to be approximately 16 mm. The bottom facesheet exhibited slight indentation failure. The force-displacement curve for RCF-SI-3 and CSMG-SI-3 are presented in Figure 4.21. Similar penetration damage has been reported by H. Wang et al [56] experimentally and analytically investigating low-velocity impact penetration of the fully clamped foam-core composite sandwich panels.

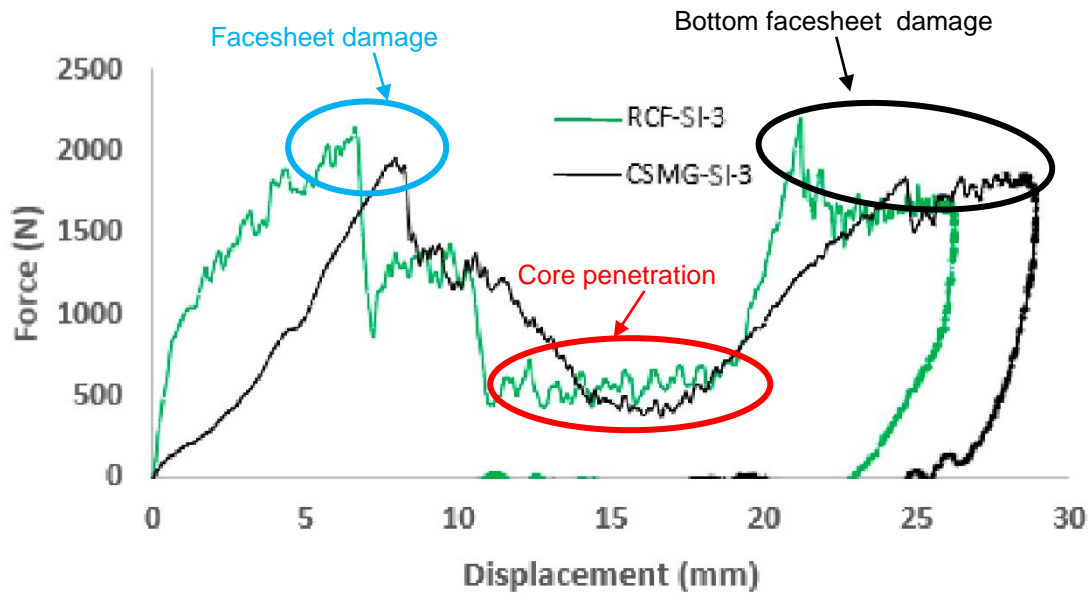


Figure 4.21 Force-displacement curve for RCF-SI-3 and CSMG-SI-3 samples at 30 J

In Figure 4.21 both RCF-SI-3 and CSMG-SI-3 initially undergo top facesheet damage as highlighted by the blue oval. This is then followed by core penetration in the region highlighted by the red oval. The damage then progresses further into the bottom facesheet, in the black oval. This is then followed by the impactor rebounding. The pattern of the curves closely matches the damage profile of typical force deflection responses of foam core sandwich panels reported by Castellanos & Prabhakar [57]. They are presented in Figure 4.22.

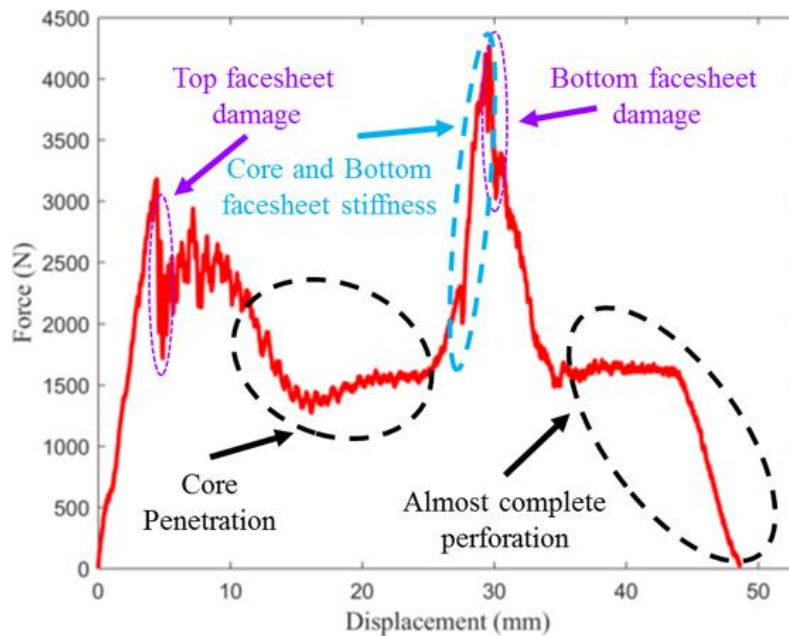


Figure 4.22 Typical force deflection responses of foam core sandwich composites under low-velocity impact loading [57].

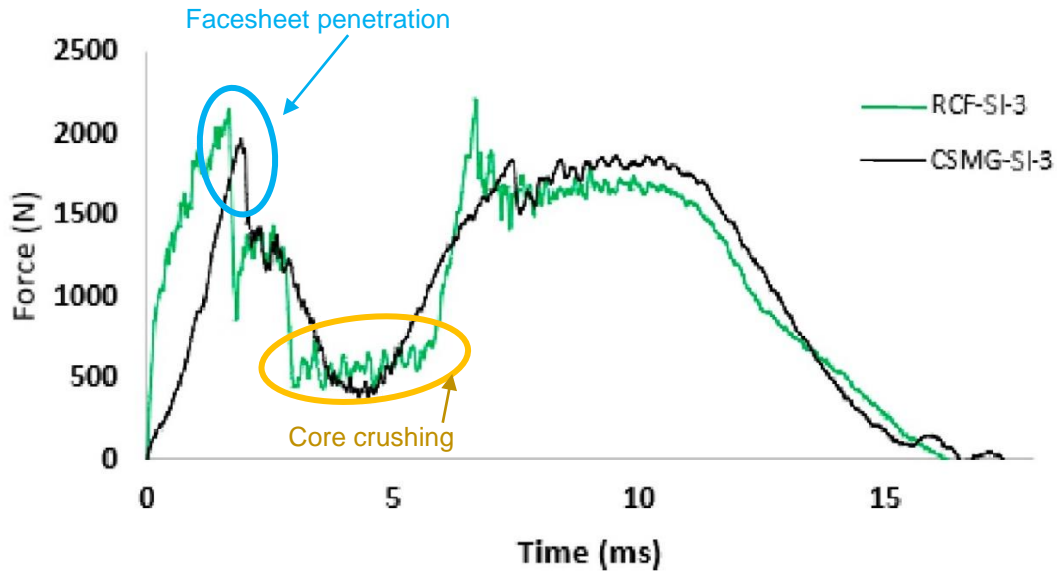


Figure 4.23 Force-time curve for RCF-SI-3 and CSMG-SI-3 samples at 30 J

The force-time histories for RCF-SI-3 and CSMG-SI-3 are presented in Figure 4.23. The facesheet penetration for both panels are observed in the drop in the peak force highlighted by the blue oval. The yellow oval shows that after the drop in peak force, the crack propagation of the top facesheet of RCF-SI-3 leads to the prolonged crushing of the core in comparison to the CSMG-SI-3 panel. For both panels, the residual kinetic energy is transferred to the bending of their bottom facesheets. This is represented by the second peak right after the core is crushed. The force first increases due to the bending resistance of both face sheets which is continued the bottom facesheets. Throughout the process, the force values for RCF-SI-3 are relatively higher than those of CSMG-SI-3. The force-time histories for both panels closely match that of the load – time history for sandwich panel penetration documented by H. Wang et al in Figure 4.24 [56].

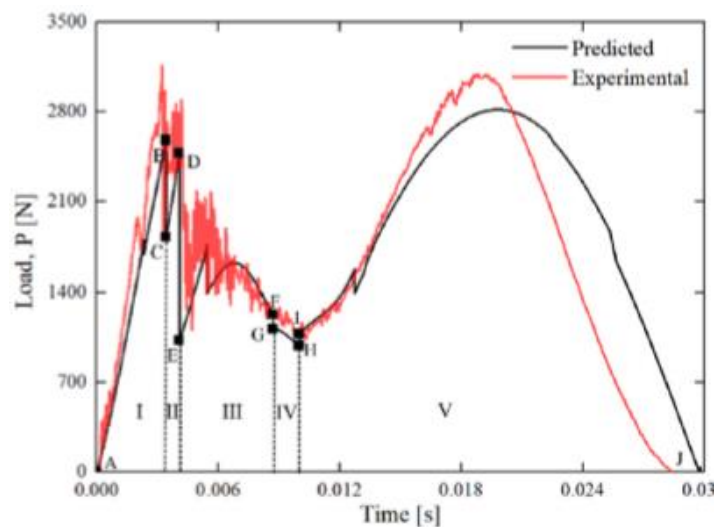


Figure 4.24 Comparison of experimental and analytical load-time curve for penetrated panel [56]

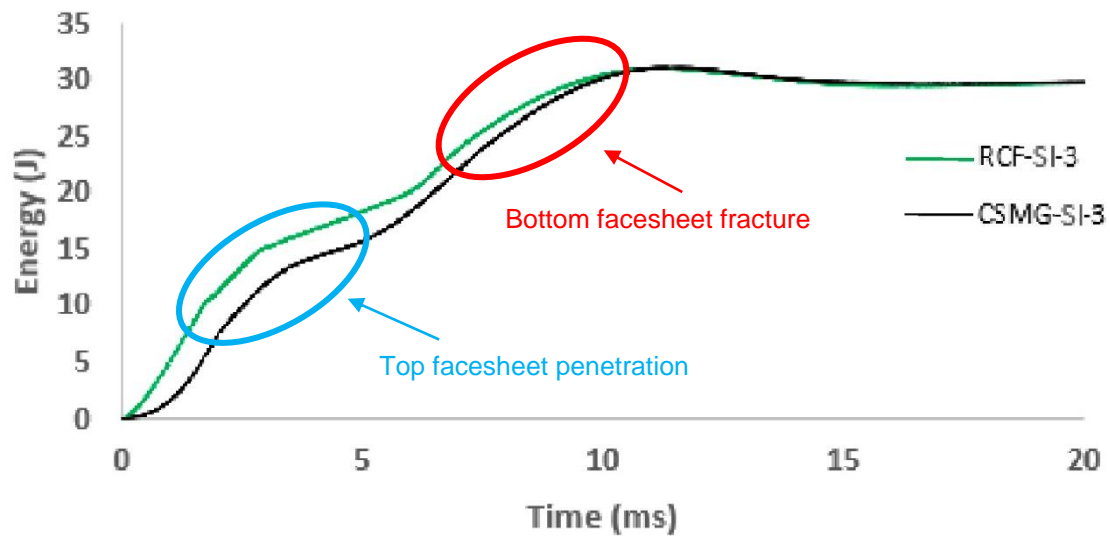


Figure 4.25 Energy-time curve for RCF-SI-3 and CSMG-SI-3 samples at 30 J

The energy-time curve for RCF-SI-3 and CSMG-SI-3 is presented in Figure 4.25. The two peak forces observed in the force-displacement curve in for both panels in Figure 4.23 are due to damage in the top facesheet, core and bottom facesheet for both panels. Hence, in Figure 4.25 the first regime with the reduced slope, highlighted by the blue circle, corresponds with the perforation of the top facesheets and penetration of the core. The second reduced slope highlighted by the red circle in Figure 4.25 corresponds to the fibre fracture of the bottom facesheet. Similar observations for the energy-time curve of penetrated sandwich panels have been presented by Castellanos & Prabhakar and O. A. Mocian et al [57], [58]. The data obtained for both RCF and CSMG standard size samples are presented in Table 4.5.

Table 4.5 Impact data for standard size RCF and CSMG panels

Specimen ID	Applied Energy (J)	Peak Force (N)	Peak Displacement (mm)	Absorbed energy (J)
RCF-SI-1	10	2183.7	6.55	6.98
RCF-SI-2	20	2256.35	20.54	20.4
RCF-SI-3	30	2205.17	22.9	29.4
Average	-	2215 ±37	16.66 ±8.8	18.92 ±11
Specimen ID	Applied Energy (J)	Peak Force (N)	Peak Displacement (mm)	Absorbed energy (J)
CSMG-SI-1	10	1704.9	8.3	9.38
CSMG-SI-2	20	2243.4	8.2	17.53
CSMG-SI-3	30	1961.13	25.5	29.6
Average	-	1969 ± 270	14 ±9.9	18.8 ±10

4.3.4 Comparative Summary

Experimental findings for the progression of damage can be summarised in the following:

- At 10 J of impact energy, fibre fracture is evident for both RCF-SI-1 and CSMG-SI-1. RCF-SI-1 initially appears to have barely visible damage but microscopic image reveals cracks on its facesheet. The CSMG-SI-1 panel displays the area of damage due to the fibre's transparent nature.
- At 20 J of impact energy, CSMG-SI-2 can withstand the applied energy better than RCF-SI-2 as the top face sheet fractures into the core. As for RCF-SI-2, the top facesheets gets penetrated and the core gets crushed.
- At 30 J of impact energy, both RCF-SI-3 and CSMG-SI-3 fail through top facesheet penetration and core crushing.

Summary of observed damage per energy is presented in Table 4.6.

Table 4.6 Observable failure per energy level for standard RCF and CSMG samples

Panel	Energy (J)	Observed failure
RCF-SI-1	10	Barely visible damage, fibre fracture
RCF-SI-2	20	Top facesheet penetration, core crushing
RCF-SI-3	30	Top facesheet penetration, core crushing
CSMG-SI-1	10	Visible damage area, fibre fracture
CSMG-SI-2	20	Visible cracks along surface, fibre fracture, slight core crushing
CSMG-SI-3	30	Top facesheet fracture, core crushing

The average experimental data shown in Figure 4.26a reveal the RCF samples can withstand higher forces than the CSMG samples. The average displacement is also higher for the RCF panels as shown by the average peak displacement in Figure 4.26b than for the CSMG panels which is evident of facesheet penetration. Again, in similar manner, the RCF and CSMG have almost similar energy absorption as shown in Figure 4.26c. Overall, even though the RCF samples have higher values for peak force, the CSMG panels can better resist damage at applied impact energy of 10, 20 and 30 J.

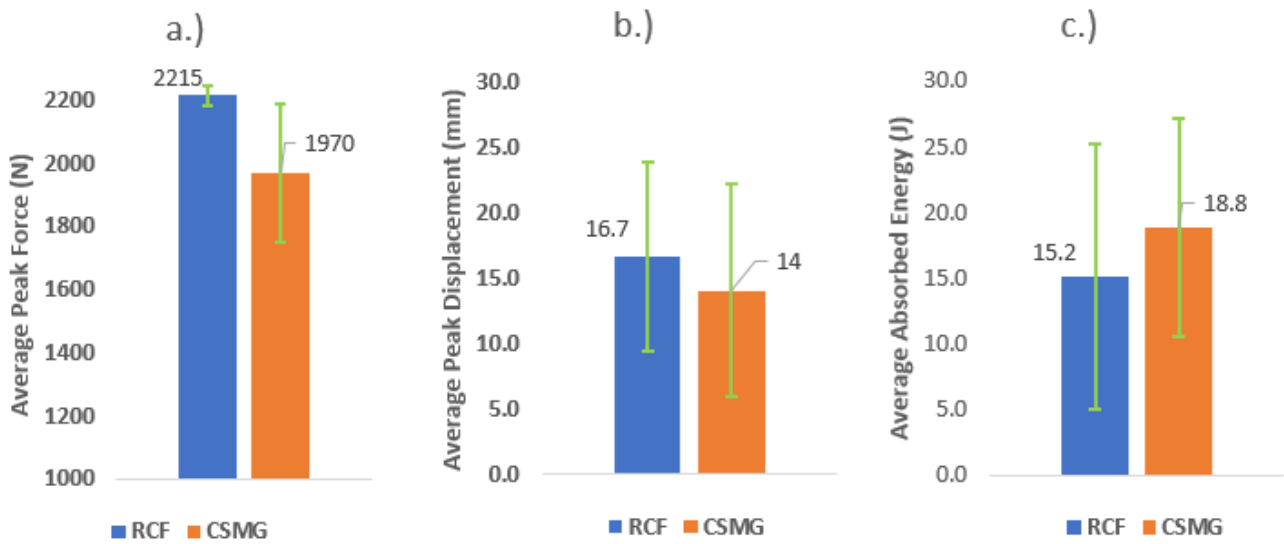


Figure 4.26 Comparison between a.) average peak force, b.) average displacement c.) average absorbed energy of standard impact RCF and CSMG panels

Values for the average peak force, and average absorbed energy have been normalised at 50% fibre volume fraction and presented in Table 4.7. As shown in Table 4.7, at 50% normalised fibre volume fraction, the RCF panels still have higher strengths than the CSMG panels.

Table 4.7 Normalised impact data F_{peak} - peak force, E_a - absorbed energy

Panel	F_{peak} (N) @ 50% FVF	E_a (J) @ 50% FVF
RCF	3460.9 ± 30	29.5 ± 9.2
CSMG	1837.2 ± 219	17.5 ± 8.3

4.4 Chapter Summary

Experimental work has been carried out on RCF and CSMG panels using the same areal density and core thickness. The fibre content analysis reveals that the CSMG panels have a higher fibre volume content than the RCF panels. Under three-point bending, the RCF and CSMG panels both exhibited failure modes such as facesheet indentation, facesheet fracture and core crushing. Experimental data revealed the CSMG panels were more ductile in behaviour as they underwent twice the deflection of the RCF panels during loading.

Visual analysis for the damage progression for the standard size panels revealed that the RCF panels were more brittle than the CSMG panels. 10 J of energy was significant to initiate top facesheet damage for both panels. At 20 J both core and facesheet of the RCF panel were penetrated but the CSMG facesheet dispersed the damage across its surface. At 30 J both panels were penetrated. In summary, the chapter was able to achieve the objectives laid out in Chapter 1. A guideline for carrying out fatigue after impact tests is presented in Chapter 5.

CHAPTER 5: GUIDELINE FOR FATIGUE AFTER IMPACT TEST

5 GUIDELINE FOR FATIGUE AFTER IMPACT TEST

A panel undergoes minor to major forms of damage throughout its service life which varies according to their application. For example, panels in the body of a car are exposed to impact damage from road debris. Simultaneously, a second phenomenon known as fatigue has been observed to contribute to panel damage after impact i.e., vibrations from the car engine leading to fatigue damage of the panel. Although fatigue tests are not performed in this thesis, this chapter aims to provide parameters that can be used to carry out a fatigue after impact tests on RCF and CSMG panels. Firstly, samples are fabricated using the ASTM C393 guideline as mentioned in section 3.3.3 and tested at a low impact energy of 4.5 J. Secondly, as a requirement for fatigue tests, load levels for the test will be taken at 25%, 50% and 75% of the maximum mid-span deflection and force values from the three-point bending tests in section 4.2. These are presented in section 5.2.

5.1 Impact Tests at 4.5 J

5.1.1 RCF Panels

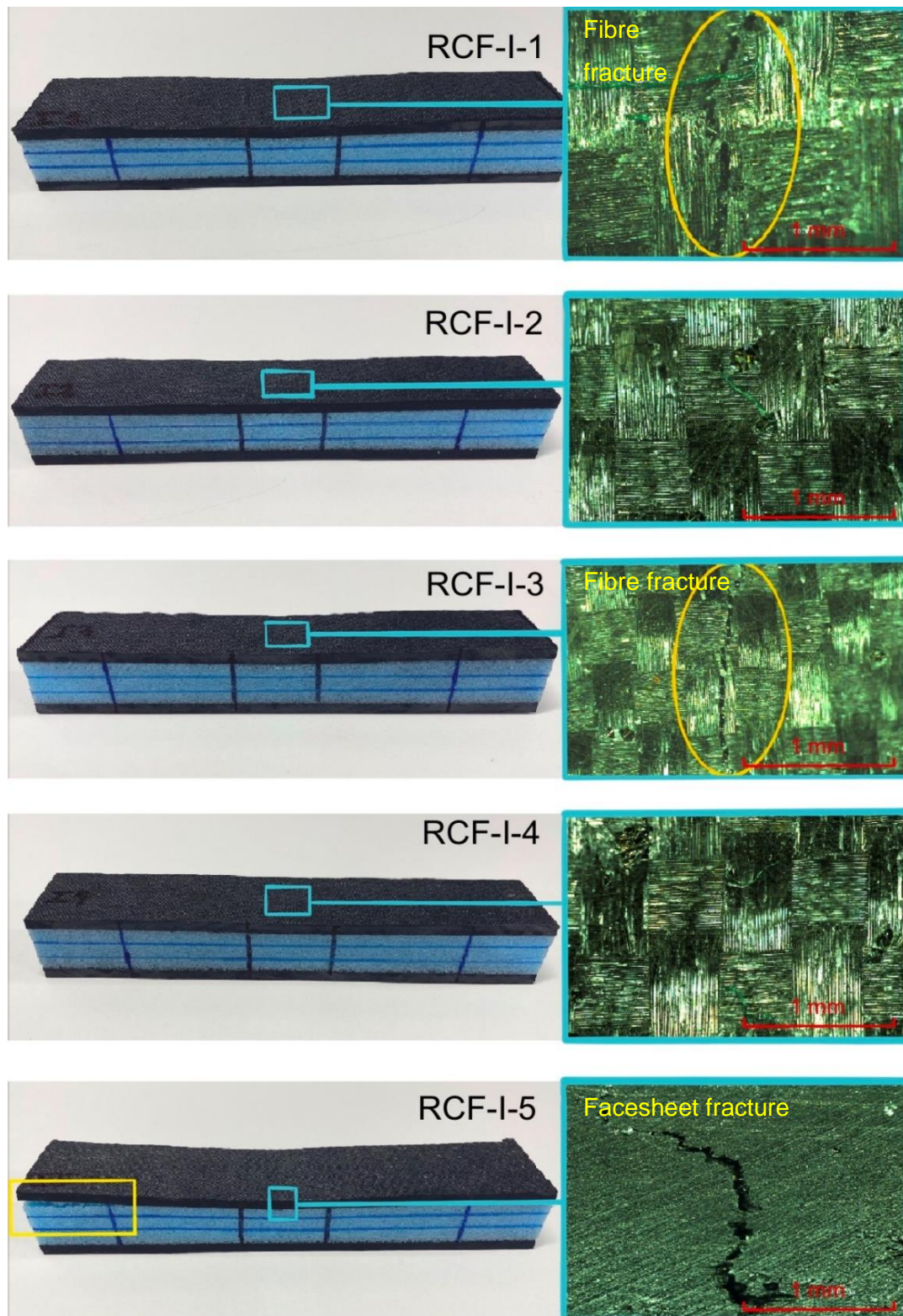


Figure 5.1 Impacted RCF specimens alongside microscopic images.

At first glance, in Figure 5.1, all RCF specimens impacted appear to display barely visible damage and only facesheet indentation. Microscopic imaging reveals fibre fracture in RCF-

I-1, RCF-I-3, and RCF-I-5. RCF-I-5 also exhibits facesheet-core delamination as highlighted in Figure 5.1. RCF-I-2 and RCF-I-4 remain relatively undamaged at the area of impact but still have slight top facesheet indentation. There is also a good correlation between the damage observed and characteristics displayed by the force-displacements curves as shown in Figure 5.2.

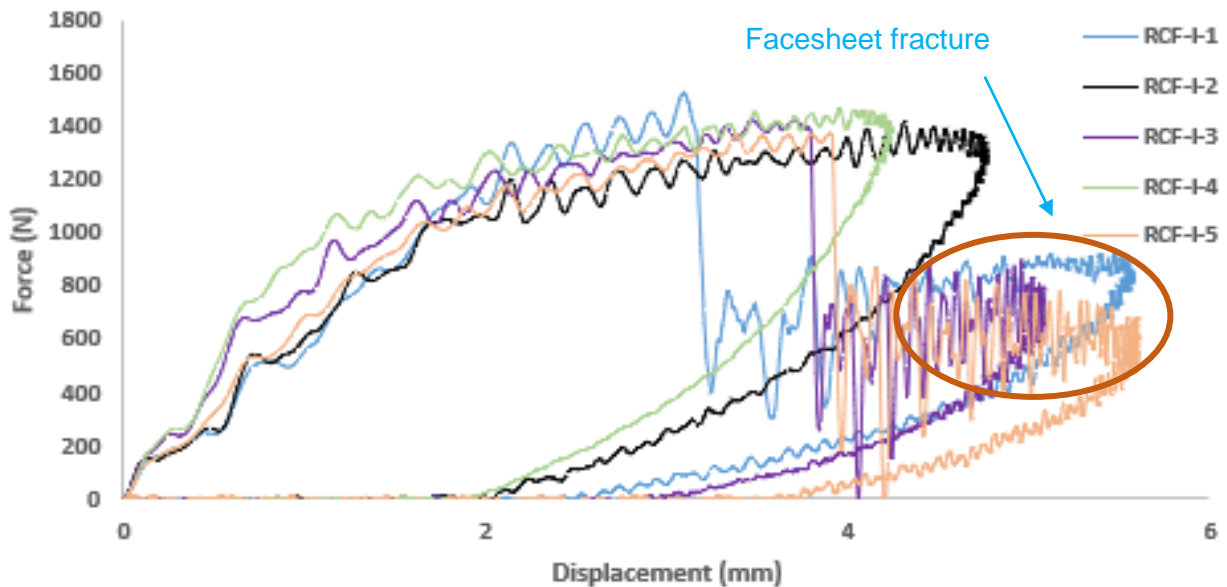


Figure 5.2 Force-displacement curve for RCF samples at 4.5 J

In the force-displacement curve presented in Figure 5.2, the facesheet for RCF-I-1, RCF-I-3 and RCF-I-5 fracture in a brittle manner as there is a sudden drop in the applied force. After this the core continues to bear the impact force until the impactor rebounds as highlighted by the brown oval. As for RCF-I-2 and RCF-I-4, the facesheet remains intact so the peak force is reached then followed by the impactor rebound.

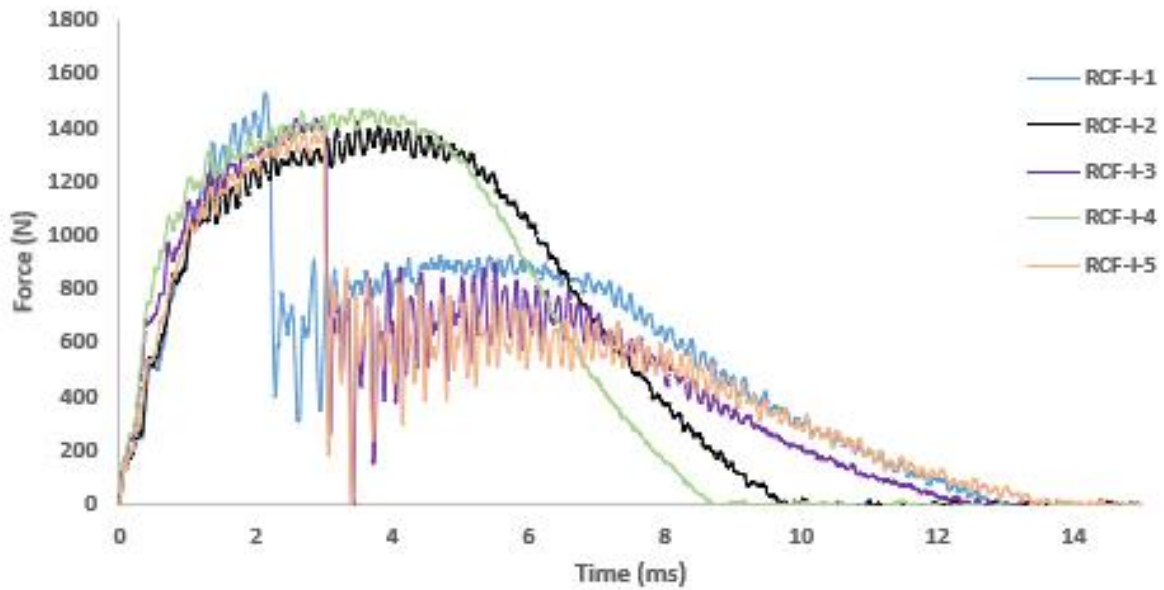


Figure 5.3 Force-time curve for RCF samples at 4.5 J

The shape of the force-time curve for RCF-I-2 and RCF-I-4 in Figure 5.3 are similar to a sine function with almost a nearly smooth process whereas the shape for RCF-I-1, RCF-I-3 and RCF-I-5 are not. At the beginning of impact for all the RCF samples the contact force increases to more than 200 N over a short period of time which both facesheet and core remain in an elastic stage. The force then rises at a slower rate to the peak force eventually dropping towards the end of the event.

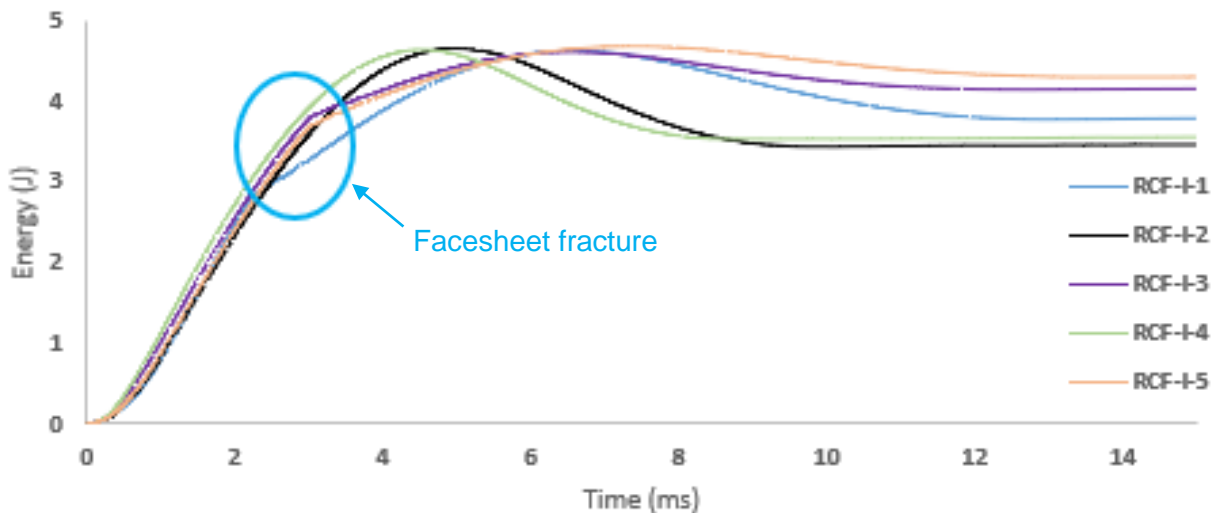


Figure 5.4 Energy-time curve for RCF samples at 4.5 J

In Figure 5.4, the sharp upward inclination highlighted in the blue oval for the energy-time curves of RCF-I-1, RCF-I-3 and RCF-I-5 is a result of their top facesheet fracture which is then prolonged due to the core absorbing the remaining energy. The force-displacement, force-time and energy-time curves for the RCF panels display similar pattern to ones noted

by X.Zhang et al [59] whilst investigating the low-velocity impact behaviour of CRFP honeycomb structures at energy levels ranging between 3 to 10 J. They are presented in Figure 5.5.

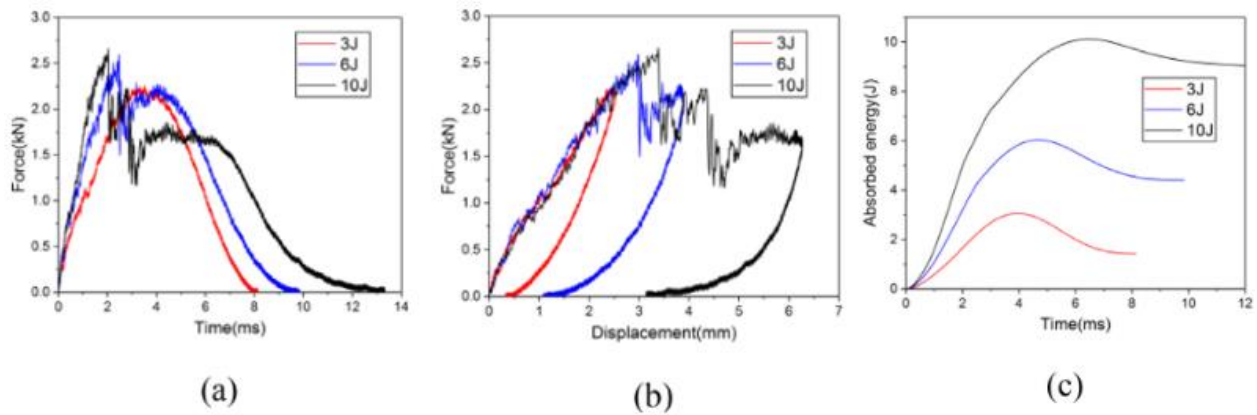


Figure 5.5 a.) impact force history, b.) impact force-displacement curve and c.) energy absorption [59]

The data for the peak force, peak displacement and absorbed energy are presented in Table 5.1.

Table 5.1 Obtained RCF data form impact tests.

	Specimen ID	Peak Force (N)	Peak displacement (mm)	Absorbed energy (J)
	RCF-I-1	1529.73	3.09	2.67
	RCF-I-2	1423.53	4.32	4.05
	RCF-I-3	1430.13	3.70	3.66
	RCF-I-4	1474.15	3.95	4.24
	RCF-I-5	1379.51	3.90	3.66
Average		1447.4 ± 57	3.79 ± 0.45	3.65 ± 0.6

5.1.2 CSMG Panels

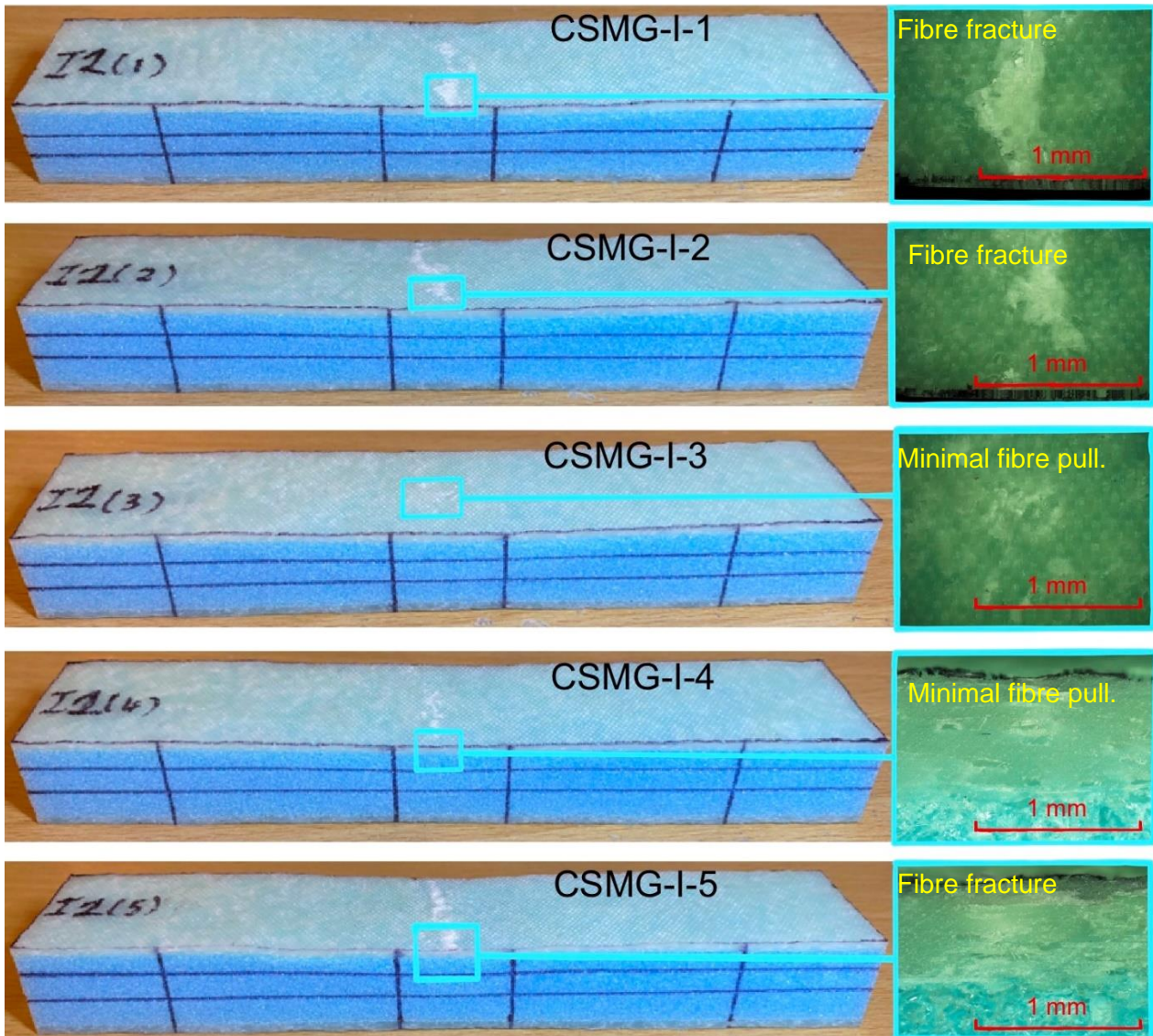


Figure 5.6 Impacted RCF specimens alongside microscopic images.

For the same applied impact energy, in Figure 5.6, the CSMG panels performed better than the RCF panels as the only observable damage was just top facesheet indentation. Samples CSMG-I-1, CSMG-I-2, and CSMG-I-5 are observed to show the most fibre fracture on the top facesheet. Very minimal fibre pulling is recorded on samples CSMG-I-3 and CSMG-I-4. Microscopic image also revealed slight damage to the fibres post-test.

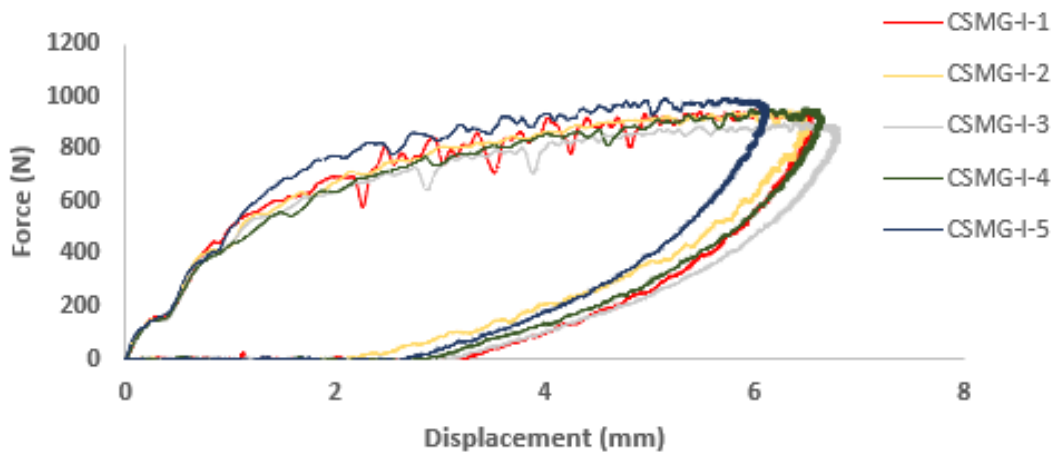


Figure 5.7 Force-displacement curve for CSMG samples at 4.5 J

Figure 5.7 shows that there is no sudden force drop in the CSMG panels during loading which is indicated by the barely visible indentation in top facesheets and relatively intact core in the panels.

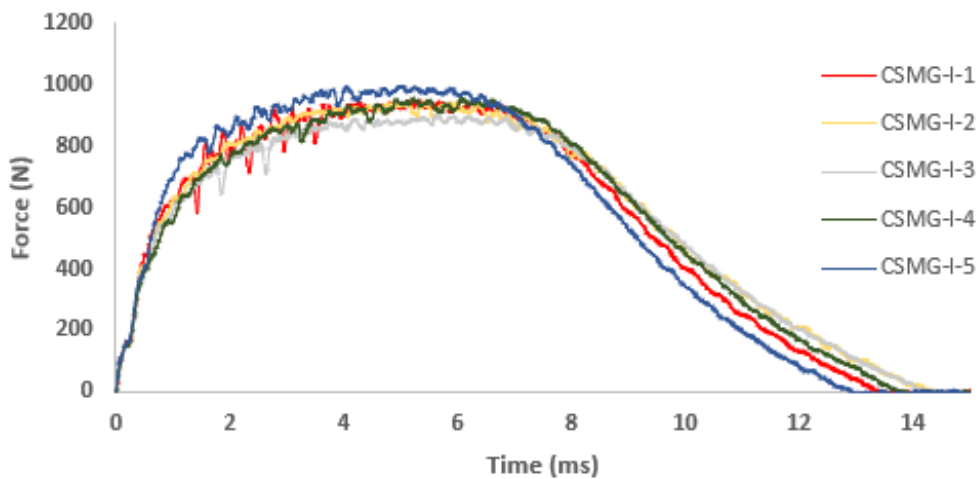


Figure 5.8 Force-Time curve for CSMG samples at 4.5 J

The force-time history in Figure 5.8 show that the impact force for all the samples rise quickly to approximately 180 N. The impact force continues to rise at a lower rate and continues to increase up to the peak force. The CSMG facesheets and the core remain in an elastic stage before reaching the peak force. The force time history also shows a gradual and relatively smooth unloading on the samples as the force reduces.

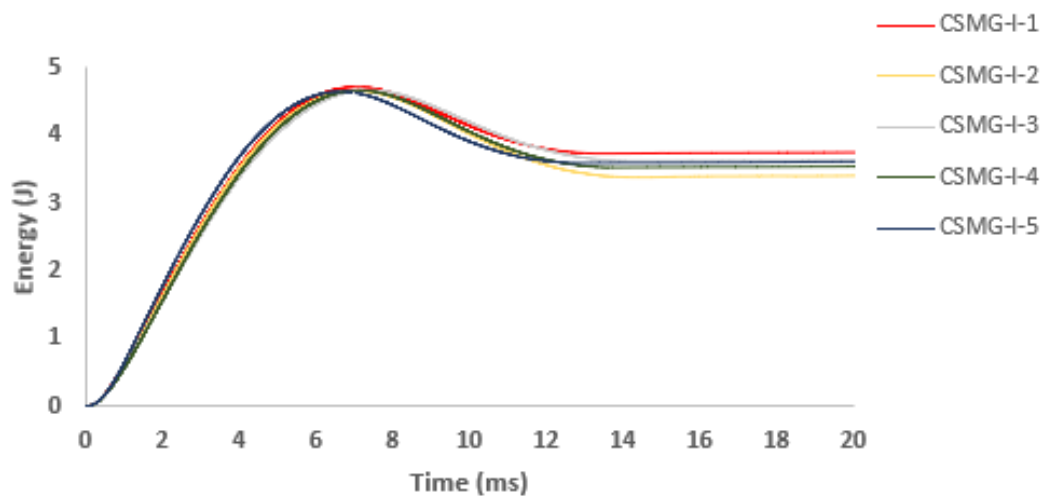


Figure 5.9 Force-time curve for CSMG samples at 4.5 J

All CSMG samples follow the same energy absorption trend in Figure 5.9, and this is to be expected as there was very little damage on all their top facesheets. The peak force, peak displacement and absorbed energy for the CSMG panels are presented in Table 5.2.

Table 5.2 Obtained CSMG data form impact tests.

	Specimen iD	Peak Force (N)	Peak displacement (mm)	Absorbed energy (J)
	CSMG-I-1	946.17	3.26	3.73
	CSMG-I-2	947	2.21	3.37
	CSMG-I-3	899.7	3.14	3.62
	CSMG-I-4	953.3	2.9	3.52
	CSMG-I-5	994.6	2.7	3.58
Average		948.15 ± 33	2.84 ± 0.41	3.56 ± 0.13

5.1.3 Comparative Summary

For the same applied energy of 4.5 J, visual observation shows that the CSMG panels performed significantly better than the non-standard RCF panels. Observable damage from visual analysis of the CSMG panels are top facesheet indentation and minimum fibre breakage. As for the RCF panels, top facesheet fracture was a common observable failure mode. This is given by the lower average displacement in Figure 5.10b. In contrast, the average data for the peak force presented in Figure 5.10a shows that the RCF panel take higher forces that the CSMG panels. Both groups of panels are closely matched for absorbed energy in Figure 5.10c.

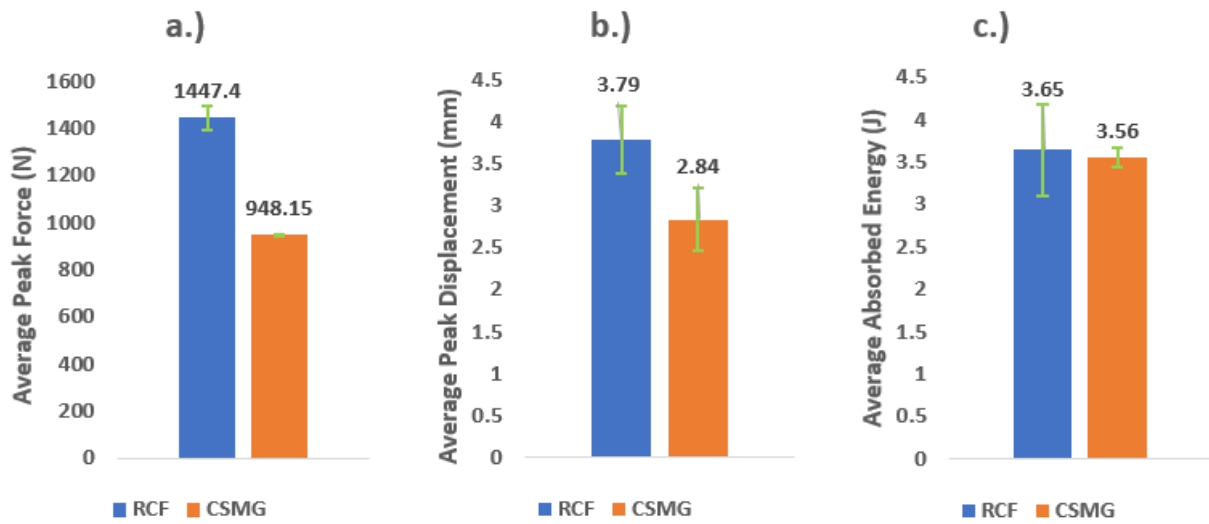


Figure 5.10 Comparison between a.) average peak force, b.) average displacement c.) average absorbed energy of non-standard impact RCF and CSMG panels

Values for the average peak force, and average absorbed energy have been normalised at 50% fibre volume fraction and presented in Table 5.3. As shown in Table 5.3, at 50% normalised fibre volume fraction, the RCF panels still have higher strengths than the CSMG panels.

Table 5.3 Normalised impact data F_{peak} - peak force, E_a - absorbed energy

Panel	F_{peak} (N) @ 50% FVF	E_a (J) @ 50% FVF
RCF	2261.5 ± 50.9	5.7 ± 3.66
CSMG	884.4 ± 30.1	3.3 ± 0.11

5.2 Load Levels for Fatigue Test

A requirement for testing sandwich panels under fatigue is to derive load levels from the specimens three-point bending force-deflection curve. This is done by taking percentages of the maximum value in the elastic region of the specimen's force-deflection curve. The load levels are used to control the test to avoid immediate specimen failure when placed under fatigue loading. Therefore, using data from the elastic region for the RCF and CSGM panels, load levels have been taken at 25%, 50%, 75% and presented in Table 5.4. The data presented in Figure 5.11a and Figure 5.11c can be used to generate a strain vs no. of cycle curve while the data presented in Figure 5.11b and Figure 5.11d can be used to generate a stress vs no. of cycle curve.

Table 5.4 Three-point bending data for RCF and CSGM specimen's elastic region. (F – force, D – deflection, Avg. Average, S.D – Standard deviation)

Load level %	Elastic limit for RCF specimens						Avg.	S.D
	Specimen iD	RCF-3PB-1	RCF-3PB-2	RCF-3PB-3	RCF-3PB-4	RCF-3PB-5		
100	F (N)	531	565	440	600	523	532	59.7
	D (mm)	1.8	1.44	1.25	1.48	1.8	1.6	0.2
75	F (N)	398.25	423.75	330	450	392.25	399	44.8
	D (mm)	1.35	1.08	0.94	1.11	1.35	1.2	0.2
50	F (N)	265.5	282.5	220	300	261.5	266	29.9
	D (mm)	0.9	0.72	0.63	0.74	0.9	0.8	0.1
25	F (N)	132.75	141.25	110	150	130.75	133	14.9
	D (mm)	0.45	0.36	0.31	0.37	0.45	0.4	0.1
Load level %	Elastic limit for CSGM specimens						Avg.	S.D
	Specimen iD	CSGM-3PB-1	CSGM-3PB-2	CSGM-3PB-3	CSGM-3PB-4	CSGM-3PB-5		
100	F (N)	258	305	290	283	278	283	17.2
	D (mm)	1.55	2.26	1	1.43	1	1.4	0.5
75	F (N)	193.5	228.75	217.5	212.25	208.5	212	12.9
	D (mm)	1.16	1.70	0.75	1.07	0.75	1.1	0.4
50	F (N)	129	152.5	145	141.5	139	141	8.6
	D (mm)	0.78	1.13	0.5	0.72	0.5	0.7	0.3
25	F (N)	64.5	76.25	72.5	70.75	69.5	71	4.3
	D (mm)	0.39	0.57	0.25	0.36	0.25	0.4	0.13

A standard deviation for the load levels at 25%, 50% and 75% is taken to ensure that the values for the average deflection does do not overlap. This to account for variation in the load-deflection curves shown in Figure 4.4 and Figure 4.6. As shown in Figure 5.11, values for the average deflection (blue dots) will be used as they do not overlap each other.

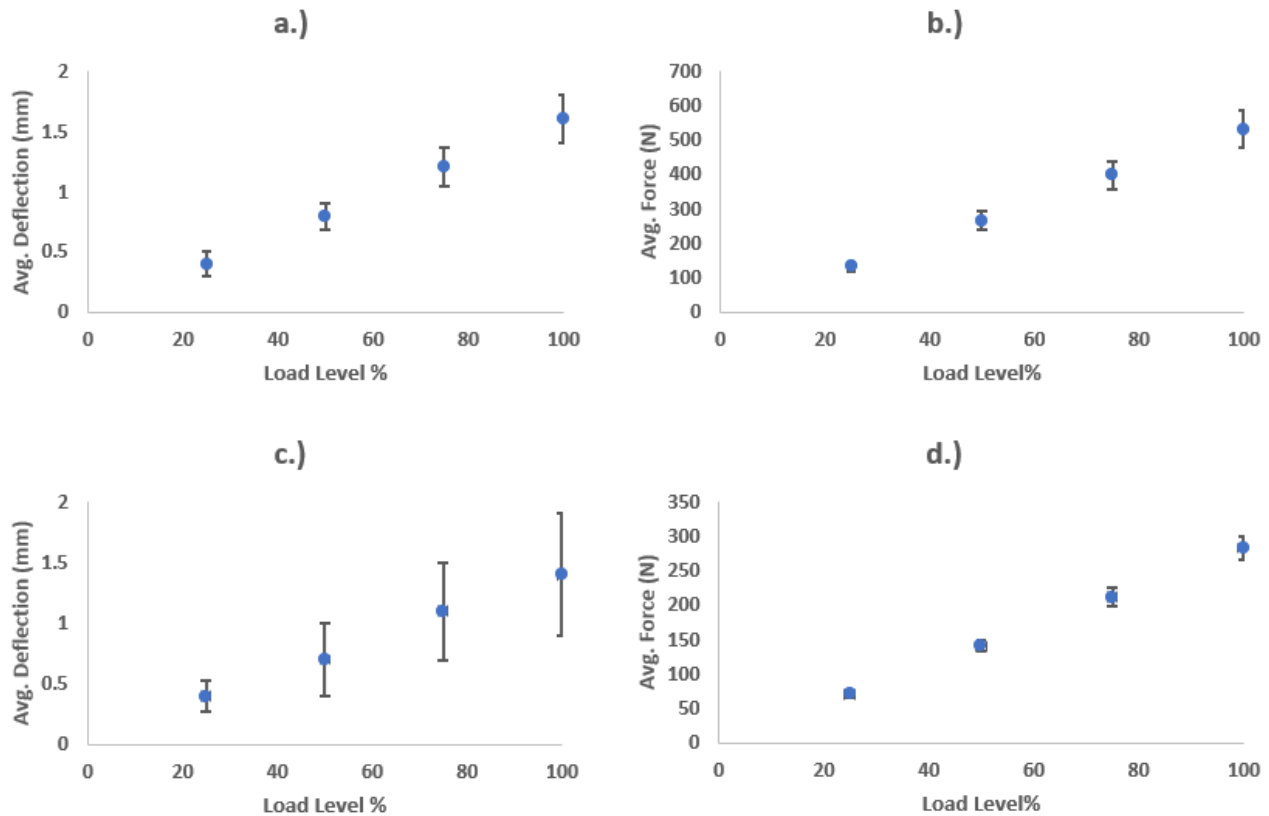


Figure 5.11 Deflection and Force standard deviation for RCF (a, b) and CSMG (c, d) panels.

5.3 Chapter Summary

In this chapter, samples for a fatigue after impact test were fabricated and impacted at 4.5J. Load levels for a fatigue test were derived from the three-point bending data. Based on work done, a guideline for a fatigue after impact tests on RCF and CSMG panels is as follows:

- The maximum applied impact energy should be 4.5 J as visual analysis reveal it does not cause significant panel damage.
- As a requirement for fatigue tests, load levels will be derived at 25%, 50% and 75% of the maximum mid-span deflection values of three-point bending tests.
- The fatigue test should be performed using loading frequency between 1 - 5 Hz. Higher values are reported to contributes towards thermal softening of the core [60].

- Specimen size would be guided by the non-standard ASTM C393 guideline for sample compatibility.

CHAPTER 6: CONCLUSION AND RECOMMENDATIONS

6 CONCLUSION AND RECOMMENDATIONS

In this thesis the mechanical behaviour of sandwich panels fabricated with recycled carbon fibre and chopped strand matt fibre are experimentally investigated and compared under three-point bending and low-velocity impact tests. The sandwich panels featured two layers of top and bottom facesheet, same fibre density of 300 gsm and fabricated using vacuum assisted resin infusion. A guideline for testing RCF and CSMG panels under fatigue after impact test was developed using experimental data that was obtained from each test carried out. By comparing the RCF and CSMG panels, this thesis can contribute to the knowledge of the mechanical behaviour of such panels under three-point bending and impact loading. Furthermore, the experimental work presented highlights how the RCF facesheet can be an alternate material to the commonly used CSMG facesheets.

Based on experimental work carried out, the following key points can be drawn:

- During three-point bending, the failure modes of the RCF panels were dominated by fracture of the top facesheets. Under microscopic imaging, the facesheets that showed no visible damage were fractured at the centre of indentation.
- The CSMG facesheets were able to resist three-point loading better by exhibiting fibre pulling and indentation. However, this was achieved at much lower forces than the RCF panels. The increased deflection of the CSMG panels resulted in indentation of both the core and bottom facesheet.
- During the standard impact tests, 10 J of applied energy was enough to initiate crack propagation for the top facesheet of the RCF panel. The CSMG panel underwent fibre fracture and matrix cracking.
- The damage observed on the panels became more evident with increasing applied energy, the, however, the CSMG panels were able to resist damage better than the RCF panels.
- At 4.5 J, the non-standard impact RCF and CSMG panels exhibited facesheet fracture and facesheet indentation respectively. The RCF panels still withstood higher load bearing capabilities than the CSMG panels.
- The normalised data for each test still highlights the RCF panels are stronger than the CSMG panels.

Although the thesis was able to achieve all the aims and objectives laid out, it was faced with two limitations. Firstly, there is no ASTM standard which explicitly defines how to test sandwich panels under low velocity impact. Secondly, there was very little literature

information on sandwich panels made with randomly oriented fibres that could be used for comparison against the experimental work presented.

Recommendations for future works are listed as follows:

- For a much fairer comparison, the same fibre content and facesheet thickness should be used for both RCF and CSMG panels.
- To minimise the time spent carrying out experimental trials, simulation work can be employed.
- The optimisation of the core in a panel made of RCF and CSMG under bending and impact should be considered for investigation.
- Use of Scanning electron microscopy (SEM) for more in-depth visual analysis .

7 REFERENCES

- [1] N. Sharma, R. F. Gibson, and E. O. Ayorinde, "Fatigue of foam and honeycomb core composite sandwich structures: A tutorial," *Journal of Sandwich Structures and Materials*, vol. 8, no. 4, pp. 263–319, Jul. 2006, doi: 10.1177/1099636206063337.
- [2] D. Hara and G. O. Özgen, "Investigation of Weight Reduction of Automotive Body Structures with the Use of Sandwich Materials," in *Transportation Research Procedia*, Elsevier B.V., 2016, pp. 1013–1020. doi: 10.1016/j.trpro.2016.05.081.
- [3] A. Pavlović, D. Sintoni, G. Minak, and C. Fragassa, "On the modal behaviour of ultralight composite sandwich automotive panels," *Compos Struct*, vol. 248, Sep. 2020, doi: 10.1016/j.compstruct.2020.112523.
- [4] Weijermars Wouter, "Mechanical behaviour of composite sandwich panels in bending after impact."
- [5] G. Zhou, M. Hill, and N. Hookham, "Investigation of Parameters Governing the Damage and Energy Absorption Characteristics of Honeycomb Sandwich Panels," *Journal of Sandwich Structures & Materials*, vol. 9, no. 4, pp. 309–342, Jul. 2007.
- [6] C. A. Steeves and N. A. Fleck, "Collapse mechanisms of sandwich beams with composite faces and a foam core, loaded in three-point bending. Part II: experimental investigation and numerical modelling," *Int J Mech Sci*, vol. 46, no. 4, pp. 585–608, Apr. 2004, doi: 10.1016/j.ijmecsci.2004.04.004.
- [7] J. Li, Y. Durandet, X. Huang, G. Sun, and D. Ruan, "Additively manufactured fiber-reinforced composites: A review of mechanical behavior and opportunities," *J Mater Sci Technol*, vol. 119, pp. 219–244, Aug. 2022, doi: 10.1016/j.jmst.2021.11.063.
- [8] C. E. Duty, T. Drye, and A. Franc, "Material Development for Tooling Applications Using Big Area Additive Manufacturing (BAAM)," 2015. [Online]. Available: <http://www.osti.gov/scitech/>

- [9] H. L. Tekinalp *et al.*, “Highly oriented carbon fiber-polymer composites via additive manufacturing,” *Compos Sci Technol*, vol. 105, pp. 144–150, Dec. 2014, doi: 10.1016/j.compscitech.2014.10.009.
- [10] Charles Hill, Kyle Rowe, Robert Bedsole, James Earle, and Vlastmil kunc, “Materials and Process Development for Direct Digital Manufacturing of Vehicles,” 2016.
- [11] Philippe Boisse, “Materials for reinforcements in composites,” in *Composite Reinforcements For Optimum Performance*, P. Boisse, Ed., 2nd ed. Matthew Deans , 2021, pp. 18–24.
- [12] W. D. Callister, *Material Science and Engineering: An introduction*, 7th ed. New York: John Wiley and Sons, 2007.
- [13] Frazer Barnes, “Recycled carbon fiber: Its time has come.”
- [14] Gen2Carbon, “G-TEX TM.”
- [15] Sigmex, “Recycled fabrics.” <https://www.sigmatex.com/recycled-fabrics> (accessed May 12, 2022).
- [16] F. R. Jones and N. T. Huff, “The structure and properties of glass fibers,” in *Handbook of Properties of Textile and Technical Fibres*, Elsevier, 2018, pp. 757–803. doi: 10.1016/B978-0-08-101272-7.00019-5.
- [17] S. S. Heckadka, S. Y. Nayak, K. Narang, and K. Vardhan Pant, “Chopped Strand/Plain Weave E-Glass as Reinforcement in Vacuum Bagged Epoxy Composites,” *J Mater*, vol. 2015, pp. 1–7, Sep. 2015, doi: 10.1155/2015/957043.
- [18] Fibreglass ware house, “Choosing between fibre glass cloth and chopped strand mat,” Mar. 01, 2022. <https://fiberglasswarehouse.com/blogs/news/choosing-between-fiberglass-cloth-and-chopped-strand-mat-fiberglass-mat> (accessed May 12, 2022).
- [19] M. C. Serna Moreno and J. L. Martínez Vicente, “In-plane shear failure properties of a chopped glass-reinforced polyester by means of traction-compression biaxial testing,” *Compos Struct*, vol. 122, pp. 440–444, Apr. 2015, doi: 10.1016/j.compstruct.2014.12.018.

- [20] S. Dolati, A. Fereidoon, and A. R. Sabet, "Experimental investigation into glass fiber/epoxy composite laminates subjected to single and repeated high-velocity impacts of ice," *Iranian Polymer Journal*, vol. 23, no. 6, pp. 477–486, Jun. 2014, doi: 10.1007/s13726-014-0242-y.
- [21] I. Daniel, "Fabrication, testing and analysis of composite sandwich beams," *Compos Sci Technol*, vol. 60, no. 12–13, pp. 2455–2463, Sep. 2000, doi: 10.1016/S0266-3538(00)00039-7.
- [22] G. Kalaprasad, P. Pradeep, G. Mathew, C. Pavithran, and S. Thomas, "Thermal conductivity and thermal diffusivity analyses of low-density polyethylene composites reinforced with sisal, glass and intimately mixed sisal/glass fibres," *Compos Sci Technol*, vol. 60, no. 16, pp. 2967–2977, Dec. 2000, doi: 10.1016/S0266-3538(00)00162-7.
- [23] S. Sahraoui, E. Mariez, and M. Etchessahar, "Mechanical testing of polymeric foams at low frequency," *Polym Test*, vol. 20, no. 1, pp. 93–96, Sep. 2000, doi: 10.1016/S0142-9418(00)00006-4.
- [24] Allard Jean F. and Atalla Nouredine, *Propagation of Sound in Porous Media: Modelling of Sound Absorbing Materials, Second Edition*.
- [25] A. Petras, "Design of Sandwich Structures," 1998.
- [26] A. Mostafa, K. Shankar, and E. v. Morozov, "Independent analytical technique for analysis of the flexural behaviour of the composite sandwich panels incorporated with shear keys concept," *Materials and Structures/Materiaux et Constructions*, vol. 48, no. 8, pp. 2455–2474, Aug. 2015, doi: 10.1617/s11527-014-0331-6.
- [27] M. Burman and D. Zenkert, "Fatigue of foam core sandwich beams-1: undamaged specimens," 1997.
- [28] Y. M. Jen and L. Y. Chang, "Effect of thickness of face sheet on the bending fatigue strength of aluminum honeycomb sandwich beams," *Eng Fail Anal*, vol. 16, no. 4, pp. 1282–1293, Jun. 2009, doi: 10.1016/j.engfailanal.2008.08.004.
- [29] G. Sun, E. Wang, H. Wang, Z. Xiao, and Q. Li, "Low-velocity impact behaviour of sandwich panels with homogeneous and stepwise graded foam cores," *Mater Des*, vol. 160, pp. 1117–1136, Dec. 2018, doi: 10.1016/j.matdes.2018.10.047.

- [30] H. Fan, L. Yang, F. Sun, and D. Fang, "Compression and bending performances of carbon fiber reinforced lattice-core sandwich composites," *Compos Part A Appl Sci Manuf*, vol. 52, pp. 118–125, 2013, doi: 10.1016/j.compositesa.2013.04.013.
- [31] H. E. Balcioğlu, "FLEXURAL BEHAVIORS OF SANDWICH COMPOSITES PRODUCED USING RECYCLED AND NATURAL MATERIAL," *Mugla Journal of Science and Technology*, pp. 64–73, Jun. 2018, doi: 10.22531/muglajsci.421813.
- [32] B. Wang, Y. Shi, C. Zhou, and T. Li, "Failure mechanism of PMI foam core sandwich beam in bending," *International Journal for Simulation and Multidisciplinary Design Optimization*, vol. 6, p. A8, 2015, doi: 10.1051/smdo/2015008.
- [33] K. P. Toradmal, P. M. Waghmare, and S. B. Sollapur, "Three Point Bending Analysis of Honeycomb Sandwich Panels: Experimental Approach," *International Journal of Engineering and Techniques*, vol. 3, [Online]. Available: <http://www.ijetjournal.org>
- [34] C. Kaboglu, L. Yu, I. Mohagheghian, B. R. K. Blackman, A. J. Kinloch, and J. P. Dear, "Effects of the core density on the quasi-static flexural and ballistic performance of fibre-composite skin/foam-core sandwich structures," *J Mater Sci*, vol. 53, no. 24, pp. 16393–16414, Dec. 2018, doi: 10.1007/s10853-018-2799-x.
- [35] I. M. Daniel, J. L. Abot, K. A. Wang, and W. P. Murphy, "TESTING AND ANALYSIS OF COMPOSITE SANDWICH BEAMS."
- [36] C. A. Steeves and N. A. Fleck, "Collapse mechanisms of sandwich beams with composite faces and a foam core, loaded in three-point bending. Part II: Experimental investigation and numerical modelling," *Int J Mech Sci*, vol. 46, no. 4, pp. 585–608, Apr. 2004, doi: 10.1016/j.ijmecsci.2004.04.004.
- [37] J. Arbaoui, Y. Schmitt, J. L. Pierrot, and F. X. Royer, "Effect of core thickness and intermediate layers on mechanical properties of polypropylene honeycomb multi-layer sandwich structures," *Archives of Metallurgy and Materials*, vol. 59, no. 1, pp. 11–16, 2014, doi: 10.2478/amm-2014-0002.

- [38] J. Mei, J. Liu, and W. Huang, "Three-point bending behaviors of the foam-filled CFRP X-core sandwich panel: Experimental investigation and analytical modelling," *Compos Struct*, vol. 284, Mar. 2022, doi: 10.1016/j.compstruct.2022.115206.
- [39] G. Caprino and R. Teti, "Impact and post-impact behavior of foam core sandwich structures," *Compos Struct*, vol. 29, no. 1, pp. 47–55, 1994, doi: [https://doi.org/10.1016/0263-8223\(94\)90035-3](https://doi.org/10.1016/0263-8223(94)90035-3).
- [40] M. S. H. Fatt and K. S. Park, "Dynamic models for low-velocity impact damage of composite sandwich panels ± Part B: Damage initiation." [Online]. Available: www.elsevier.com/locate/compstruct
- [41] G. Li and V. D. Muthyala, "Impact characterization of sandwich structures with an integrated orthogrid stiffened syntactic foam core," *Compos Sci Technol*, vol. 68, no. 9, pp. 2078–2084, Jul. 2008, doi: 10.1016/j.compscitech.2008.03.014.
- [42] C.-G. Kim and E.-J. Jun, "Impact Resistance of Composite Laminated Sandwich Plates," *J Compos Mater*, vol. 26, no. 15, pp. 2247–2261, Dec. 1992, doi: 10.1177/002199839202601504.
- [43] R. Ouadday, A. Marouene, G. Morada, A. Kaabi, R. Boukhili, and A. Vadean, "Experimental and numerical investigation on the impact behavior of dual-core composite sandwich panels designed for hydraulic turbine applications," *Composite Structures*, vol. 185. Elsevier Ltd, pp. 254–263, Feb. 01, 2018. doi: 10.1016/j.compstruct.2017.11.007.
- [44] Y. Zhang, Y. Li, K. Guo, and L. Zhu, "Dynamic mechanical behaviour and energy absorption of aluminium honeycomb sandwich panels under repeated impact loads," *Ocean Engineering*, vol. 219, p. 108344, 2021, doi: <https://doi.org/10.1016/j.oceaneng.2020.108344>.
- [45] K. B. Shin, J. Y. Lee, and S. H. Cho, "An experimental study of low-velocity impact responses of sandwich panels for Korean low floor bus," *Compos Struct*, vol. 84, no. 3, pp. 228–240, Jul. 2008, doi: 10.1016/j.compstruct.2007.08.002.
- [46] J. A. Artero-Guerrero, J. Pernas-Sánchez, J. López-Puente, and D. Varas, "Experimental study of the impactor mass effect on the low velocity impact of carbon/epoxy woven laminates," *Compos Struct*, vol. 133, pp. 774–781, Dec. 2015, doi: 10.1016/j.compstruct.2015.08.027.

- [47] ASTM-D7136/7136M-12, "Standard Test Method for Measuring the Damage Resistance of a Fiber-Reinforced Polymer Matrix Composite to a Drop-Weight Impact Event 1", doi: 10.1520/D7136_D7136M-12.
- [48] D. Zhang, Q. Fei, and P. Zhang, "Drop-weight impact behavior of honeycomb sandwich panels under a spherical impactor," *Compos Struct*, vol. 168, pp. 633–645, May 2017, doi: 10.1016/j.compstruct.2017.02.053.
- [49] V. Crupi, G. Epasto, and E. Guglielmino, "Collapse modes in aluminium honeycomb sandwich panels under bending and impact loading," *Int J Impact Eng*, vol. 43, pp. 6–15, May 2012, doi: 10.1016/j.ijimpeng.2011.12.002.
- [50] V. B. Ugale, K. K. Singh, N. M. Mishra, and P. Kumar, "Comparative study of carbon fabric reinforced and glass fabric reinforced thin sandwich panels under impact and static loading," *J Compos Mater*, vol. 49, no. 1, pp. 99–112, Jan. 2015, doi: 10.1177/0021998313514874.
- [51] R. Frassine and V. Carvelli, "POLITECNICO DI MILANO School of Industrial and Information Engineering EFFECTS OF RESIN AND PROCESSING ON MECHANICAL PROPERTIES OF CARBON FIBER COMPOSITES," 2014.
- [52] M. el Messiry, "Theoretical analysis of natural fiber volume fraction of reinforced composites," *Alexandria Engineering Journal*, vol. 52, no. 3, pp. 301–306, Sep. 2013, doi: 10.1016/j.aej.2013.01.006.
- [53] ASTM D7249/D7249M - 12, "Standard Test Method for Facing Properties of Sandwich Constructions by Long Beam Flexure 1", doi: 10.1520/D7249_D7249M-12.
- [54] ASTM-C393/C393 M, "Standard Test Method for flexural Properties of Sandwich Constructions".
- [55] W. He, S. Lu, K. Yi, S. Wang, G. Sun, and Z. Hu, "Residual flexural properties of CFRP sandwich structures with aluminum honeycomb cores after low-velocity impact," *Int J Mech Sci*, vol. 161–162, Oct. 2019, doi: 10.1016/j.ijmecsci.2019.105026.
- [56] H. Wang, S. Long, X. Yao, G. Lu, X. Zhang, and Q. Han, "Analytical study on the low-velocity impact penetration of the fully-clamped foam-core composite

sandwich panels,” *Compos B Eng*, vol. 224, Nov. 2021, doi: 10.1016/j.compositesb.2021.109214.

- [57] A. Castellanos and P. Prabhakar, “Elucidating the Mechanisms of Damage in Foam Core Sandwich Composites under Impact Loading and Low Temperatures,” Apr. 2021, doi: 10.1177/1099636221993848.
- [58] O. A. Mocian, D. M. Constantinescu, Ş. Sorohan, and M. Sandu, “Low velocity failure and integrity assessment of foam core sandwich panels,” *Frattura ed Integrita Strutturale*, vol. 13, no. 48, pp. 230–241, Apr. 2019, doi: 10.3221/IGF-ESIS.48.24.
- [59] X. Zhang, F. Xu, Y. Zang, and W. Feng, “Experimental and numerical investigation on damage behavior of honeycomb sandwich panel subjected to low-velocity impact,” *Compos Struct*, vol. 236, Mar. 2020, doi: 10.1016/j.compstruct.2020.111882.
- [60] N. Kulkarni, H. Mahfuz, S. Jeelani, and L. A. Carlsson, “Fatigue crack growth and life prediction of foam core sandwich composites under flexural loading,” 2003. doi: [https://doi.org/10.1016/S0263-8223\(02\)00249-0](https://doi.org/10.1016/S0263-8223(02)00249-0).